DISTRIBUTION OF THE PHOSPHORYLATED HIGH MOLECULAR WEIGHT NEUROFILAMENT PROTEIN [PNF-H] IN NEURAL TRACTS OF THE RAT BRAIN FROM THE NINTH TO THE FIFTEENTH POSTNATAL DAY.

by

Bradford K. Poulos

A dissertation submitted to the Graduate Faculty in Biology in partial fulfillment of the requirements for the degree of Doctor of Philosophy, The City University of New York

1995

This manuscript has been read and accepted for the Graduate Faculty in Biology in satisfaction of the dissertation requirements for the degree of Doctor of Philosophy.

Sept. 14, 1995
Date

Chair of Examining Committee

September 18, 1995
Date

Executive Officer

Supervisory Committee

THE CITY UNIVERSITY OF NEW YORK

Abstract

THE DISTRIBUTION OF THE PHOSPHORYLATED HIGH MOLECULAR WEIGHT NEUROFILAMENT PROTEIN [PNF-H] IN NEURAL TRACTS OF THE RAT BRAIN FROM THE NINTH TO THE FIFTEENTH POSTNATAL DAY

by

Bradford K. Poulos

Adviser: Professor David Soifer

The onset of synthesis and processing of individual cytoskeletal proteins can serve as an index of the maturation of specific groups of neurons. Analysis of Western blots of neurofilament proteins extracted from the developing brain had suggested that the appearance of the highly phosphorylated form of the highest molecular weight neurofilament protein, pNF-H, was both spatially and temporally regulated (eg (Fischer and Shea, 1991)). The present investigation increases the spatial and temporal resolution of those analyses. Serial sections of developing rat brains were immunohistochemical stained. RMO24.9, a NF-H - specific, phosphate-dependent monoclonal antibody, was chosen as the primary antibody. A seven-day window including postnatal days nine [P9] through postnatal day fifteen [P15] was investigated because previous studies demonstrated that the highest rate of increase in amount of pNF-H occurred during this period. The results of the present study were then correlated with studies that described

the ontogeny of behaviors, and others that described onset of synaptogenesis, electrophysiological maturation, myelinogenesis and changes in rates of neurofilament protein transport. Of these, onset of pNF-H specific immunohistochemical staining was most highly correlated with onset of decreased neurofilament transport and onset of myelination - specifically onset of appearance of the nodes of Ranvier. With the pattern of onset of pNF-H immunoreactivity established for tracts in the normal rat brain, an attempt was made to alter the pattern of appearance of pNF-H in the brains of pups by exposing rat dams to aluminum lactate during gestation and lactation. Aluminum had been shown to cause changes in NF-H phosphorylation in adult rats (eg (Johnson and Jope, 1988)) and behavioral deficits in the pups of aluminum-exposed rat dams (eg (Muller *et al.* 1990)). However, the present study demonstrates that chronic exposure to large doses of aluminum lactate cause renal and gastric lesions. These lesions compromise the ability of dams to nurture their pups and make it impossible to ascribe any delay in CNS development or changes in levels of pNF-H directly to aluminum in this or any other developmental study.

Acknowledgements:

I thank my wife, Maggie, and our children, Saskia, Heather and Benjamin for the patience and the understanding they demonstrated. Without their encouragement, my quest, to understand the workings of the mind through study of the developing brain, would have been a lost dream. I also thank my parents, Vera and Leo, for guiding the family discussions that led me to appreciate the importance of early development in shaping the adult mind. Finally, I thank my mentor, David Soifer for opening up his lab and the resources of the New York Institute for Basic Research in Developmental Disabilities to me.

I would also like to thank Diane Cocozza, Katherine Mack, Richard Weed, Dr. Julia Currie, Dr. David Miller, Dr. Judy Shek, Dr. Eugene Sersen, Lawrence Black, Marie Fittipaldi and Nicholas Gnazzo and the rest of the IBR Staff for sharing their knowledge and resources and Dr. Henry M. Wisniewski for inspiring me with his seminal work on aluminum toxicity.

Table of Contents:

Abbreviations:

3	oculomotor nucleus
^{3}H	tritium
3n	oculomotor nerve
4	trochlear nucleus
5	Trigeminal ganglion, [Vieussens,Gasser]
5n	trigeminal nerve
aci	Anterior commissure, intrabulbar part
ad lib.	free access [*ad libitum*]
AF	amygdaloid fissure
alv	Alveus of the hippocampus
APT	Anterior pretectal nucleus
APTV	Anterior pretectal nucleus,ventral par
BAC	Bed nucleus of the anterior commissure
BCIP/NBT	substrate/chromogen mixture for staining
bic	Brachium of the inferior colliculus
BIC	Nucleus of the brachium of the inferior colliculus
BSA	bovine serum albumin
bsc	Brachium of the superior colliculus
CA3p	Field CA3 of Ammon's horn, pyramidal layer
CA3pc	Field CA3 of Ammon's horn, pyramidal layer,area
CA3r	Field CA3 of Ammon's horn, radiatum layer

Abbreviations (continued)

Cb	Cerebellum
CbIII	3rd cerebellar lobule
CbIV	4th cerebellar lobule
CbV	5th cerebellar lobule
CbVI	6th cerebellar lobule
cg	Cingulum
cic	Commissure of the inferior colliculus
CIC	Central nucleus of the inferior colliculus
cp	Cerebral peduncle, basal part
CPu	Caudate putamen (striatum)
d	day
DG	Dentate gyrus
dhc	Dorsal hippocampal commissure
DLG	Dorsal lateral geniculate nucleus
dpNF-H	dephosphorylated heavy neurofilament protein
dpNF-M	dephosphorylated middle MW neurofilament protein
DpWh	Deep white layer of the superior colliculus
DTT	DL-dithiothreitol
E-face	outer leaflet of the plasma membrane bilayer
E0	the day of conception
ec	External capsule
ECIC	External cortex of the inferior colliculus
EGTA	Ethylenediamine tetracetic acid
eml	External medullary lamina

Abbreviations (continued)

Ent	Entorhinal cortex
EPl	External plexiform layer of the olfactory bulb
ESP	glutamate-serine-proline oligopeptide
fi	Fimbria of the hippocampus
fr	Fasciculus retroflexus
Gl	Granular insular cortex
hbc	Habenular commissure
ic	Internal capsule
icp	Inferior cerebellar peduncle (restiform body)
IGr	Internal granular layer of the olfactory bulb
InWh	Intermediate white layer of the superior colliculus
IPl	Internal plexiform layer of the olfactory bulb
KSD	lysine-serine-aspartate oligopeptide
KSP	lysine-serine-proline oligopeptide
KSPXK	lysine-serine-proline-(any amino acid)-lysine oligopeptide
ll	Lateral lemniscus
LLF	Lateral lemniscal fields
lo	Lateral olfactory tract
LVe	Lateral vestibular nucleus
MAP2	one of many microtubule-associated proteins
mcp	Middle cerebellar peduncle (brachium pontis)
MCPC	Magnocelluclar nucleus of the posterior commissure
MES	2-[N-Morpolino] ethanesulfonic acid (butter)
Mi	Mitral cell layer of the olfactory bulb

Abbreviations (continued)

ml	Medial lemniscus
mlf	Medial longitudinal fasciculus
MME	homogenate buffer solution
MME-T	MME with detergent (triton X-100) added
mp	Mammillary peduncle
M_r	molecular weight relative to standard proteins
mt	Mammillothalamic tract
MW	molecular weight
NF-H	heavy MW neurofilament protein (native)
NF-L	low [light] MW neurofilament protein (native)
NF-M	middle MW neurofilament protein (native)
ON	Olfactory nerve layer
opt	Optic tract
ox	Optic chiasm
P0	the day of birth
P1-P...	the day after the birthdate and subsequent days
Par1	Parietal cortex,area 1
pc	Posterior commissure
Pir	Piriform cortex
PMSF	Phenylmethylsulfonyl fluoride
pNF-H	phosphorylated heavy neurofilament protein
PRh	Perirhinal cortex
R	Red nucleus
RMC	Red nucleus, magnocellular part

Abbreviations (continued)

RMO	monoclonal antibodies, mouse anti rat NF-M {996}
rpm	revolutions per minute
S	Subiculum
s5	Sensory root of the trigeminal nerve
SB	sample buffer
scp	Superior cerebellar peduncle (brachium conjunctivum)
SDS	sodium dodecyl sulfate (a non-ionic detergent)
sm	Stria medullaris of the thalamus
SM	Nucleus of the stria medullaris
SNC	Substantia nigra, compact part
str	Superior thalamic radiation
TA	monoclonal antibodies, rat anti bovine NF-H
Tf	transferrin
TfR	transferrin receptor
TS	Triangular septal nucleus
Tu	Olfactory tubercle
v/v	volume to volume
vhc	Ventral hippocampal commissure
vn	Vomeronasal nerve
VPM	Ventral posteromedial thalamic nucleus
vsc	Ventral spinocerebellar tract
w/w	weight to weight
w/v	weight to volume
xscp	Decussation of the superior cerebellar peduncle
ZIV	Zona incerta, ventral part

List of Tables:

List of Figures:

Introduction:

The onset of phosphorylated heavy neurofilament protein [pNF-H] immunoreactivity can be used as a marker of postnatal development of the CNS. The present report describes the normal temporal an :patial distribution of this marker during development of rat pup brains then relates this pattern to the pattern of other markers of CNS development. The normal developmental sequence of pNF-H appearance was then challenged by a treatment already used by the scientific community - oral exposure of the dams to aluminum lactate during gestation and lactation. As has been pointed out to the scientific community (Poulos *et al.* 1995), and as is explained here, oral aluminum treatment causes gross pathological changes in the dams. These changes in the dams have ramifications on the development of their pups that make interpretation of any alterations in CNS development of the dams' pups difficult. The value of this form of aluminum treatment is therefore challenged.

Neurofilament structure

Neurofilaments are long thread-like structures, found singly or collected into bundles running parallel to the long axis of axons and dendrites and within the soma of vertebrate neurons (Peters *et al.* 1976). This report describes the topographic and temporal emergence of one constituent of the neurofilament, the phosphorylated heavy neurofilament protein [pNF-H], during early postnatal development of the rat brain. In

the adult nervous system, neurofilaments are primarily found in myelinated neurons with large caliber neurites (Wuerker and Palay, 1969; Shaw *et al.* 1981). During early postnatal development, as neurofilaments begin to be expressed in the rat optic nerve, the diameter of the nerve increases (Peters and Vaughn, 1967; Cuenca *et al.* 1987; Foster *et al.* 1982). Since other cytoskeletal elements, such as microtubules, are present before the increase in diameter of the nerve, its structural maturation seems to be correlated with neurofilament appearance rather than the appearance of any other cytoskeletal element.

a. The neurofilament triplet: NF-H, NF-M and NF-L

Although neurofilaments had long been described in light eg (Cajal, 1911) and electron microscopic eg (Schmitt and Geren, 1950; Palay and Palade, 1955) studies, Hoffman and Lasek were first to correctly define their biochemical composition. Weiss and Hiscoe (Weiss and Hiscoe, 1948) had suggested that structural elements of the neuron flowed down the axon at 1-2 mm per day, the slowest rate of axonal transport. After injecting [^{3}H] leucine and [^{3}H] lysine into the spinal cord of rats, Hoffman and Lasek (Hoffman and Lasek, 19[illegible]) found five proteins that incorporated the radioactive amino acids and moved along the sciatic nerve at the slow rate suggested by Weiss and Hiscoe. Separated by SDS gel electrophoresis, two of these proteins were found to have an R_f value similar to that of purified tubulin - and were therefore identified as tubulin. Hoffman and Lasek reasoned that the remaining proteins did not belong to membranous elements such as mitochondria, because these organelles were known to migrate along

the sciatic nerve at rates faster than those of the structural elements. By exclusion, Hoffman and Lasek tentatively identified the three remaining proteins as proteins composing the neurofilament and the "matrices associated with the linear polymers" of the cytoskeleton. Immunohistofluorescence studies using polyclonal antibodies made against the contents of the axoplasm and adsorbed to the tentatively identified proteins suggested that the distribution of these structural proteins was limited to nerves (Schlaepfer and Lynch, 1977; Liem *et al.* 1978). The inadequacies of polyclonal antibodies became evident in biochemical studies. Selection of polyclonal antibodies by adsorption required that the protein to which the antisera was adsorbed was both pure and antigenically unique. The uniqueness was suggested by the exclusive binding of the absorbed polyclonal antibodies to neurons. The criterion for purity was often defined as the formation of one band after one-dimensional gel electrophoresis (Willard *et al.* 1980; Willard and Simon, 1981; Schlaepfer, 1977; Liem *et al.* 1978). Several proteins traveling with the same or similar R_f values could be mistaken as the same protein (Liem *et al.* 1978; Schlaepfer, 1977). To avoid these problems, Soifer and colleagues took another approach (Soifer *et al.* 1981).Transection of a nerve leads to the degeneration of the fibers on the side of the cut distal to the cell body (Waller, 1850). Studies monitoring proteins from central (Dahl *et al.* 1981) and peripheral (Schlaepfer and Micko, 1978) nerves undergoing this Wallerian degeneration suggested that specific proteins were lost. Electron micrographs of the sciatic nerve showed neurofilament loss and neural degradation but no decomposition of the myelin sheath (Schlaepfer and Micko, 1978). The protein loss seemed to be of neural rather than of glial origin. Soifer and associates

correlated electron micrographic evidence of the degeneration of optic nerves and the loss of neurofilaments after axotomy to the loss of four proteins. Three of these proteins had been identified by two-dimensional gel electrophoresis as components of neurofilament preparations (Czosnek *et al.* 1980; Czosnek and Soifer, 1980).They also found the loss of the same four proteins in the degenerating sciatic nerve. One of the components of the neurofilament prepared from the sciatic nerve would have been obscured in one dimensional gels by a protein of the same molecular weight. However, the separation of these two proteins by two-dimensional gel electrophoresis allowed them to confirm that neurofilaments of the peripheral nervous system, as well as neurofilaments of the central nervous system were composed of the same triplet of proteins.

b. Neurofilament protein phosphorylation

Of the attributes of the neurofilament in different compartments of the neuron, perhaps the most striking is the high degree of phosphorylation of the neurofilament in the axon compared to that in the somatodendritic compartment. When denatured and then separated by SDS gel electrophoresis, the neurofilament, purified from the brain or spinal cord of all the higher vertebrate that have been studied (Shaw *et al.* 1984; Phillips *et al.* 1983), is resolved into at least three constitutive intermediate filament proteins. Based on their relative electrophoretic mobilities, these subunits were designated the heavy, middle and light molecular weight neurofilament proteins (NF-H, NF-M, and NF-

L respectively). In the rat, the relative molecular weights [M_r] were found to be approximately 200,000 Daltons, 160,000 Daltons and 68,000 Daltons (Shaw and Weber, 1982; Hoffman and Lasek, 1975). Dephosphorylation of neurofilaments greatly increases the electrophoretic mobility of NF-H, increases the mobility of NF-M, although to a lesser extent, and causes no change the mobility of NF-L (Glicksman and Willard, 1985). Dephosphorylation of the neurofilament also changes its affinity for some antibodies. Monoclonal antibodies with affinities based on the degree of phosphorylation of the neurofilament have been produced (Carden *et al.* 1985; Sternberger and Sternberger, 1983). Those specific for phosphorylated epitopes of NF-H and NF-M were found to bind to axons; those specific for epitopes apparent after dephosphorylation of NF-H and NF-M were found to bind to dendrites and the soma of neurons (Sternberger and Sternberger, 1983). These results demonstrate that phosphorylated epitopes are differentially distributed to axons, suggesting that neurofilament proteins are more highly phosphorylated in the axon than in other neuronal compartments.

The segregation of phosphorylated epitopes has been linked to the alteration of a specific neurofilament protein domain. As with other intermediate filament proteins, secondary structural domains have been predicted from the primary structure of the neurofilament proteins (Steinert and Liem, 1990) (see figure 1). The globular amino-terminal 'head' and adjacent helical 'rod' domains are thought to be involved in the polymerization of the neurofilament proteins to form the core of the neurofilament (Steinert and Roop, 1988; Lieberburg *et al.* 1989; Lees *et al.* 1988). These domains can be

Figure 1: The triplet of rat neurofilament proteins. This diagram demonstrates the relative length of the tail domains of three neurofilament proteins: NF-H (accession number: P16884), NF-M (accession number: P12839) and NF-L (accession number: P19527). The length of the proteins are based on the consensus sequence listed in the OWL protein sequence database (http://www.gdb.org/Dan/proteins/owl.html) release 23 (last annotation update August 1, 1992). Only the NF-M sequence is complete; the N-terminal half of the rod domains and the head domains of NF-H and NF-L are unavailable for *Rattus norvigicus*. However, these domains have been included in the diagram because their peptide sequence, which has been highly conserved during evolution, defines the intermediate protein family - the family of proteins to which the neurofilament proteins are members (Steinert and Roop, 1988; Fliegner and Liem, 1991). The rod domain ends with the sequence YRKLLEGEE (Lees *et al.* 1988) and is followed by the tail domain. The tail domain includes a glutamate rich region (solid bar) in all three proteins and, in NF-H and NF-M only, an extended region containing KSP (or ESP or KSD) phosphorylation sites (open bar). The density of phosphorylation sites in NF-H (52 sites within a 364 peptide region) is much higher than in NF-M (6 sites within a 222 peptide region).

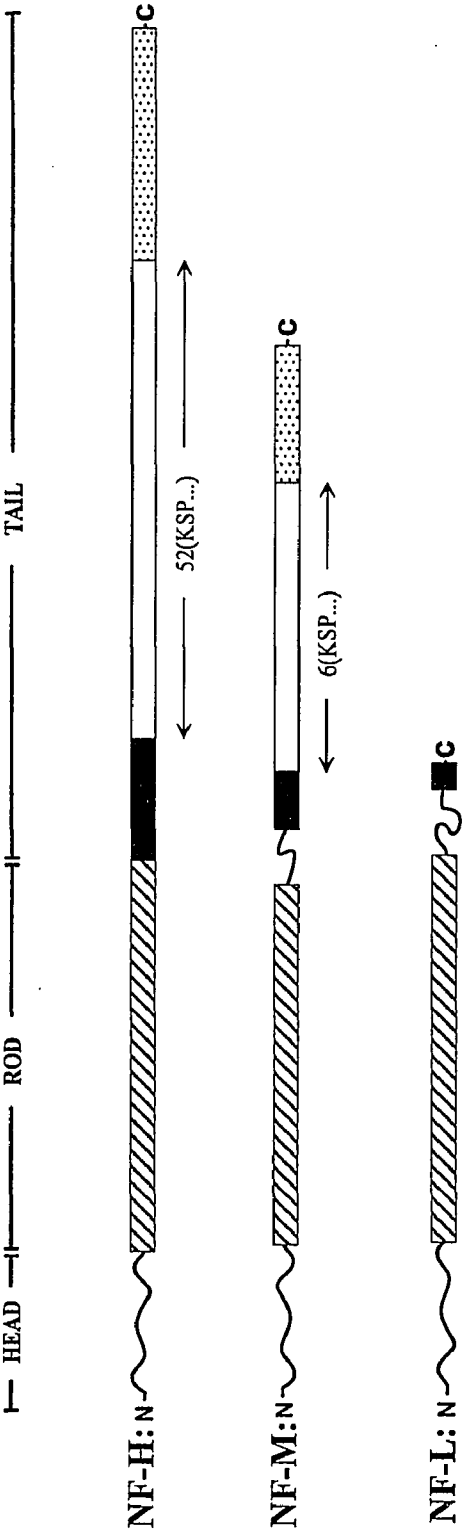
HEAD
ROD
TAIL
NF-H: N
C
52(KSP...)
NF-M: N
C
6(KSP...)
NF-L: N
C

phosphorylated and the phosphorylation of the head of NF-L is thought to be important in regulating the assembly of the three neurofilament proteins to form the neurofilament (Nixon and Sihag, 1991; Hisanaga *et al.*1994). The tail domain, linked to the rod by a glutamate-rich region, is believed to extend as a 'sidearm' from the polymerized core of the neurofilament into the cytoplasm (Hisanaga and Hirokawa, 1988). The differences in degree of phosphorylation of the neurofilament proteins and the differences in the immunohistochemical specificity of the phosphorylation-dependent antibodies are both associated with the tail domain. The tail is the longest in NF-H and contains the most phosphorylation sites. The serines of a lysine-serine-proline [KSP] amino acid triplet, embedded within longer repeated sequences, were found to be the sites of phosphorylation (Geisler *et al.*1987). In the rat NF-H, there are 52 such sequences each with an embedded KSP triplet. The sequences, similar in length and composition, follow one after another to form a tandem repeat (Breen *et al.*1988; Lieberburg *et al.*1989; Dautigny *et al.*1988). The tail is shorter in NF-M in the rat, with only six phosphorylatable KSP groups (or their KSD and ESP variants). Only two of the six are embedded in tandem sequence repeats (Napolitano *et al.*1987; Xu *et al.*1992). The tail is short in rat NF-L and, since what is known of its sequence is similar to other sequences (Julien *et al.*1985; Palgi *et al.*1990), it can be inferred that the tail domain has no embedded KSP repeats.

The discrepancy between relative molecular weights of NF-H and NF-M before and after dephosphorylation has been linked to the state of phosphorylation of serine

residues on NF-H and NF-M (Jones and Williams, 1982; Julien and Mushynski, 1982; Hisanaga *et al.* 1991). But the relationship between degree of phosphorylation and increase in electrophoretic mobility after dephosphorylation is not a simple one. Like NF-H and NF-M, NF-L is phosphorylated. However, unlike NF-H and NF-M, NF-L has no KSP groups within its tail domain. If the post-dephosphorylation increase in electrophoretic mobility was due to dephosphorylation of serines in tail-domain KSP triplets, no shift in mobility would be expected for NF-L. None is observed. There are almost nine times as many phosphorylatable sites on the tail domain of rat NF-H as on rat NF-M. If a linear relationship existed between number of phosphorylated KSP serines and electrophoretic mobility of the neurofilament protein, dephosphorylation would cause a much larger change in the M_r of NF-H than NF-M. This is not the case. Dephosphorylation of pNF-M causes a shift in M_r almost equal to that found after dephosphorylation of pNF-H (see this paper). This observation suggests that the shift in M_r is not a function of the total number of serines phosphorylated. Rather, the shift may be due to dephosphorylation of specific tail domain KSP triplets embedded within specific sequences. Dephosphorylation of this select group of sequences would cause changes in the higher-order structure of the two larger neurofilament proteins that would be sufficient to change their electrophoretic mobility . Hisanaga and colleagues found that many protein kinases phosphorylate NF-H and M (Hisanaga *et al.* 1993; Hisanaga *et al.* 1991). However, they found that only cdc2 protein kinase and tau protein kinase II, restored the M_r of dephosphorylated rat NF-H (Hisanaga *et al.* 1993). Both cdc2 protein kinase and tau protein kinase II are specific for the sequence KSPXK. This motif is

found in only eight of the 52 possible KSP-containing sequences in the NF-H tail domain. The ability of cdc2 protein kinase and tau protein kinase II to alter electrophoretic mobility is limited to NF-H. Although the rat NF-M tail domain includes the KSPXK motif, and although it is a substrate for cdc2-like kinases, its M_r is not restored upon phosphorylation (Hisanaga *et al.* 1993). The specificity of cdc2 protein kinase and tau protein kinase II must depend on more than just the KSPXK motif. Other cdc2-like kinases have been purified. Although they also exhibit specificity for the KSPXK motif, they do not restore the M_r of NF-H (Shetty *et al.* 1993; Guan *et al.* 1992; Lew and Wang, 1995). Expression of cdc2-like kinases has been linked to development (Lew and Wang, 1995). Since the Hisanaga studies suggest that the kinase responsible for producing mature, high M_r NF-H is highly specific, and that it shares specificity with other developmentally regulated enzymes, the appearance of high M_r pNF-H could be a visible manifestation of this as of yet elusive, highly specific, potentially developmentally regulated protein kinase.

c. Neurofilament structure and function

If the phosphorylation of one or a limited number of KSP triplets is responsible for the large shift in electrophoretic mobility of NF-H, the phosphorylation of that particular group must cause a change in the structure of NF-H. Even without phosphorylation, the tandem repeated sequences with their embedded KSP triplets are thought to impose intra-molecular associations to form specific secondary structures

(Lang *et al.* 1994). Phosphorylation forces a change in the structure of NF-H which is thought to lead to a change in immunospecificity (Carden *et al.* 1985). However, the change in neurofilament structure upon phosphorylation has proven difficult to document. In the adult rat, the axons projecting from retinal ganglion cells into the optic nerve do not bind monoclonal antibodies specifi or phosphorylated heavy neurofilament protein [pNF-H] for a distance of 100 μm after the exit of the nerve from the orbit. The appearance of phosphorylated epitopes beyond this point is associated with an increase in axonal diameter (Nixon *et al.* 1994). Similarly, the increase in diameter of rat optic nerve axons after birth (Cuenca *et al.* 1987; Peters and Vaughn, 1967; Pachter and Liem, 1984) is associated with the appearance of pNF-H (Shaw and Weber, 1983; Yokoyama *et al.* 1981; Pachter and Liem, 1984) and specifically for antibodies binding the KSP repeated sequences on the neurofilament protein tail domains (Watson *et al.* 1989). The onset of immunoreactivity of pNF-H during development is also associated with a decrease in the rate of transport of the neurofilament proteins to levels found in the adult (Glicksman *et al.* 1987; Willard and Simon, 1983). Some have hypothesized that phosphorylation of NF-H causes the sidearms of the neurofilament to extend (de Waegh *et al.* 1992). This increases the interaction of the neurofilament with its environment and allows links to be formed with other structures. The subsequent build-up leads to an increase in axonal diameter. Hagestedt and colleagues (Hagestedt *et al.* 1989) looking for structural changes at the electron microscopic level, found that another cytoskeletal protein, tau, when phosphorylated on serines of its KSP triplets, (Shaw, 1991) becomes long and stiff. Hirokawa, using low-angle rotary shadowing to highlight structures, found

that the extension of sidearms from the neurofilament was independent of its level of phosphorylation (Hisanaga and Hirokawa, 1989). However, Hirokawa *et al.* did note that the binding of NF-H to microtubules (Hirokawa, 1982) was dependent on the state of NF-H phosphorylation (Hisanaga and Hirokawa, 1990). Furthermore, they found that the decreased binding of phosphorylated NF-H to microtubules was caused by a change in steric factors rather than a change in binding affinity (Miyasaka *et al.* 1993). Phosphorylation of NF-H therefore leads to changes in its higher-order structure. However, the change is probably not sufficient to extend the sidearms of the neurofilament. Whatever the mechanism of increase in axonal diameter and slowing of neurofilament transport, these two phenomena become apparent as axons mature. The onset of phosphorylation of NF-H is linked to these two developmentally regulated phenomena, slowing of neurofilament transport and increase in axonal diameter, and therefore appears to be an index of axonal maturation.

d. Regional appearance of pNF-H during development

The amino acid sequences of the neurofilament proteins are similar in the rat and mouse (Shaw, 1991; Soifer and Mack, 1990). Fischer and Shea analyzed the appearance of pNF-H in six regions of the developing mouse brain biochemically (Fischer and Shea, 1991). They determined levels of pNF-H in immunoblots of cytoskeletal preparations on the day of birth, and seven, fourteen and twenty-one days thereafter. Phosphorylated NF-H was found in the brainstem, cerebellum, cortex and hippocampus at birth. All of these

areas presented a sigmoidal increase in immunostaining as pNF-H levels rose from baseline levels at birth to adult plateaus. In the brainstem, adult levels of pNF-H were quickly reached during the first postnatal week. A slower rate of increase, extending over two weeks, was found in the cerebellum. The results presented by Fischer and Shea suggest that increases in the levels of pNF-H in the hippocampus and (although they state otherwise) cortex were delayed until postnatal day 14. Phosphorylated NF-H was undetectable in the olfactory bulb and hypothalamus at birth but also rapidly increased by postnatal day 14. Fischer and Shea's results suggested that for most brain regions, the most rapid increases in pNF-H immunoreactivity occurred between the first and second postnatal week. Preliminary studies suggest that the major effects of aluminum in the developing rat brain, as identified by a change levels of pNF-H detected immunohistochemically, occur around postnatal day 11 (Poulos *et al.* 1995). The rat also experiences novel sensory stimuli within this period. Eye and ear canal opening occur during P10-14 (Weihe, 1987; Karlsson, 1967), reflex behaviors appear (Altman and Sudarshan, 1975) and exploratory behavior begins (Tilney, 1933). The second week of development is therefore particularly rich in CNS structures that are receiving their first direct sensory stimulation and in structures in which higher levels of pNF-H are beginning to appear. If onset of immunoreactivity of pNF-H were a true index of axonal maturation, and is linked to specific CNS structures which become active during this time, the levels of pNF-H within those structures would be expected to rise as those structures become active. A detailed examination of CNS structures within the period of time extending from postnatal day 9 through 15, a period of time when the search for an

association between functional maturation of the CNS and onset of appearance of pNF-H would have the greatest chance of being fruitful, was therefore chosen to assess this potential link. An examination of the daily changes in immunoreactivity of pNF-H in serial sections through the midbrain, diencephalon and telencephalon, has pointed out the anatomic structures within these regions responsible for the increases observed by Fischer and Shea.

Modification of the pattern of NF-H immunoreactivity during development after maternal exposure to aluminum lactate

Maternal exposure to high oral doses of aluminum lactate during gestation leads to behavioral deficits in rat pups which can be demonstrated even during the early postnatal period (Bernuzzi *et al.* 1989; Muller *et al.* 1990). When aluminum lactate is injected subcutaneously or directly into the brain of another animal, the young rabbit, aluminum lactate not only leads to behavioral changes (Yokel, 1989; Yokel *et al.* 1988) but also to neurohistopathology. The rapidly developing histological lesions include accumulation of neurofilaments in the neuronal soma (Forrester and Yokel, 1985; Farnell *et al.* 1982; DeBoni *et al.* 1976) as well as increases in the amount of perikaryal pNF-H (Troncoso *et al.* 1986). Unlike the case of the rabbit, intracerebral injection of aluminum compounds does not produce neurofilament accumulations in the rat (King *et al.* 1975; Wisniewski *et al.* 1977). However as in the case of the rabbit, exposing the rat to aluminum lactate leads to increases in the amount of pNF-H (Johnson and Jope, 1988;

Johnson *et al.* 1992). The lesions associated with aluminum-induced neurofilament accumulations in the rabbit brain are quite extensive and the rabbit rapidly progresses from spontaneous nystagmus and ataxia to prostration, seizures with opisthotonos, and death (Farnell *et al.* 1982; Klatzo *et al.* 1965; Terry and Peña, 1965; Siem, 1886; Döllken, 1898; Scherp and Church, 1937). Since aluminum does not cause such extensive neuropathologic lesions in the rat, using the rat rather than the rabbit as an experimental model minimizes the possibility that changes in NF-H phosphorylation levels that are secondary to neural degeneration are misinterpreted as primary effects of aluminum toxicity. Any direct affects that aluminum toxicity may have in changing levels of pNF-H immunoreactivity are consequently easier to follow in the rat. In addition, serial sectioning is accomplished more quickly in the smaller rat brain; a wider range of developmental atlases are available for the rat than the rabbit brain; and more correlative behavioral data is available for the rat. The rat model was therefore chosen to assess how aluminum, a neurotoxin known to affect behavioral development and levels of pNF-H immunoreactivity, would alter the normal topographical and temporal sequence of pNF-H immunoreactivity in the developing pup brain.

a. Pharmacokinetics of aluminum

In the behavioral studies of Muller *et al.* (Muller *et al.* 1990) and Bernuzzi *et al.* (Bernuzzi *et al.* 1989), aluminum lactate was delivered to the rat dams by an oral route. To affect the brains of the pups during gestation, the aluminum must breach the barrier

of the maternal gastrointestinal wall, travel through her bloodstream, breach the placental barrier, travel in the fetal bloodstream then enter the target area in the fetal brain. The uptake of orally ingested aluminum is a function of the aluminum salt used (Greger *et al.*1985; Yokel and McNamara, 1988) and the maternal stomach contents (Danielsson and Spar'n, 1995). Aluminum citrate is better a: ›rbed from the digestive tract than aluminum lactate (Froment *et al.*1989). However once these aluminum compounds cross the gastrointestinal barrier, the situation reverses. Higher tissue levels have been obtained after direct exposure of intestine (Froment *et al.*1989) or brain (Yokel *et al.*1991) to aluminum lactate. Silicon and citrate are both found in normal rat chow. Silicon decreases the amount of aluminum absorbed (Edwardson *et al.*1993) and citric acid increases absorption (Domingo *et al.*1993; van der Voet *et al.*1989). The sensitivity of aluminum uptake to other constituents in the diet may lead one to question whether aluminum could possibly be absorbed. Yet blood and brain aluminum levels do increase after oral treatment of rats with aluminum lactate (Cherroret *et al.*1992; Muller *et al.*1990; Greger *et al.*1985). Aluminum has been shown to be absorbed in the proximal intestine (Froment *et al.*1989). However, the pharmacokinetics of aluminum is complicated by other factors. Aluminum can precipitate and adhere to the intestinal wall blocking further uptake of aluminum (Powell *et al.*1994). The highest tissue levels of aluminum in aluminum-exposed rats are found in bone (Walker *et al.*1994; Wilhelm *et al.*1992; Greger *et al.*1985). Sequestered aluminum may be leached from the bone and intestine and slowly redistribute to other tissues. Although these complications in aluminum pharmacokinetics do exist, the fact remains that aluminum administered orally

as aluminum lactate is absorbed by the dam (Muller *et al.* 1993). Beside being found in the brain (Muller *et al.* 1990), aluminum has also been shown to accumulate in the dam's liver, spleen and kidneys (Muller *et al.* 1993). Metals, especially iron, zinc and calcium, are redistributed from the dam to the fetus during the second half of pregnancy (Romeu *et al.* 1986). However, even when absorption of orally administered aluminum is enhanced by use of aluminum citrate or citric acid supplements (Gomez *et al.* 1991), aluminum, although found in the placenta (Gomez *et al.* 1991), is not found in the fetus (Gomez *et al.* 1991; Muller *et al.* 1993). The placenta may therefore be an effective barrier to the transfer of aluminum from the rat dam to the fetus during gestation.

Maternal ingestion of high levels of aluminum does affect her fetuses. Fetuses of aluminum-exposed dams weigh less than control fetuses and have delayed ossification (Gomez *et al.* 1991). Although transfer of aluminum to the fetus cannot be detected during gestation, even at the high resolution of graphite furnace atomic absorption spectrometry (Gomez *et al.* 1991; Muller *et al.* 1993), perhaps transfer of aluminum may still occur during lactation. To affect the brains of the pups during lactation, orally administered aluminum must travel through the maternal gastrointestinal wall, be transported in the maternal bloodstream to the mammary gland, breach the mammary gland and be transported in the dam's milk to the pup. The aluminum then must cross the pup's gastrointestinal wall and travel in the pup's bloodstream to its brain. Depending on the stage of development, the aluminum may then have to penetrate the pup's blood-brain-barrier and enter the target site. As was discussed above, aluminum, orally

administered as aluminum lactate, is absorbed by the dam. Data is not available for aluminum lactate treatment, but aluminum was found in the milk of rat dams injected intraperitoneally for the first twelve postnatal days with aluminum chloride (Muller *et al.* 1992). Similarly, elevated levels of aluminum were found in the milk of rabbit does receiving subcutaneous injections of aluminum lactate during the postnatal period (Yokel, 1984). However, in both the case of the rat (Muller *et al.* 1992) and in the case of the rabbit (Yokel, 1984), no increase in aluminum levels was detected in either blood or tissues of the offspring. Despite, or perhaps because of the immaturity of the rat pup and rabbit kit digestive system, the gastrointestinal wall seems to be an effective barrier to aluminum absorption.

Aluminum could be sequestered in a location within the fetus or neonate that makes its detection difficult. Unless this is the case, transfer of aluminum from the rat dam to her litter is unlikely.

b. Possible sites of aluminum toxicity

High levels of aluminum in the human bloodstream are found in dialysis dementia. This syndrome occurs when the blood of patients with kidney failure is dialyzed against water containing high levels of aluminum (Alfrey *et al.* 1976). The human is a good model for assessment of toxicities because, as humans are the most highly studied organism on earth, anomalies quickly become evident. Beside impairment

of cognitive abilities, including loss of visual memory, attention and concentration, and impairment of volitional control, including altered speech, apraxia and asterixis (Bolla *et al.* 1992; Alfrey *et al.* 1972), the high serum aluminum also compromises non-CNS systems. Two systems in which secondary anomalies are most evident are the skeletal system and the hematopoietic system. The patient with dialysis dementia often suffers vitamin D-resistant osteomalacia. This pathology is characterized by inadequate mineralization of the bone matrix (D'Haese *et al.* 1989; Ward *et al.* 1978). The patient also suffers anemia, the form with small, pale erythrocytes. This anemia is otherwise known as microcytic hypochromic anemia (Touam *et al.* 1983; Elliot *et al.* 1978). Experimental animal models have been developed which mimic both these aluminum-induced states (Chmielnicka *et al.* 1994; Cannata *et al.* 1991; Rodriguez *et al.* 1989).

Except for one clinical report in which a diagnosis of dialysis dementia was complicated by the concomitant rejection of a transplanted kidney (Scholtz *et al.* 1990), patients suffering dialysis dementia do not accumulate neurofilaments within the neural perikaryon to form tangles. As with the rat, the primary site of the aluminum-associated encephalopathy is therefore difficult to localize. However, the same biochemical pathways and the same biophysiological mechanisms are reutilized in different organ systems. A toxin which disrupts a pathway or mechanism in one organ system may alter that same biochemical pathway or biophysiological mechanism in another organ system. Since aluminum-induced dialysis dementia leads to more than one lesion, the CNS and non-CNS lesions may have a common etiology. The mechanism of non-CNS

pathophysiology can therefore be examined for biochemical or biophysical characteristics which are shared by the nervous system. These common characteristics can then be used to suggest hypothetical causes for the dementia which can then be evaluated in animal models.

The pathophysiology of osteomalacia is unknown. At the moment, osteomalacia therefore lends little to the understanding of the mechanism of aluminum pathology. This may not be the case with the aluminum-induced anemia. Anemia, a decrease in blood hemoglobin, is not one entity. The etiology of a particular anemia can be diagnosed by comparing standard erythrocyte parameters to those found in the anemic patient. The microcytic, hypochromic anemia found in dialysis dementia has usually been associated with iron deficiency. Iron deficiency itself may be caused by 1) excessive iron loss, 2) inadequate diet, 3) increased iron demands, or 4) decreased uptake of iron. The first cause cannot be ruled out as an explanation of the anemia of dialysis dementia. Experimental rat models of aluminum toxicity suggest that aluminum may induce increased bile flow; the bile may then capture iron and lead to its loss in the feces (Allain *et al.*1988; Klein *et al.*1988). However, the anemia in dialysis dementia can only be partially attributed to increased biliary iron loss (Allain *et al.*1988).

The second cause of iron deficiency, inadequate diet, can be discounted. Iron deficiency through inadequate diet is unusual in chronic renal failure because patients with chronic renal failure receiving dialysis usually obtain adequate nutrition.

The third cause of iron deficiency, increased demand, can also be discounted. Patients with chronic renal failure, but without dialysis dementia, are also anemic. However, the anemia is the normochromic, normocytic type (Kokko, 1988). This type of anemia has been attributed to deficiency of erythropoietin, a glycoprotein normally produced in the kidney in response to anoxia. Since the apparatus for production of erythropoietin is destroyed in chronic renal failure, aluminum cannot stimulate erythropoiesis and an increase in iron demand. Alumium must be present in the blood before the normochromic, normocytic anemia in the patient with chronic renal failure becomes the hypochromic, microcytic type of anemia associated with the complication of dialysis dementia.

The only realistic etiology for iron deficiency in aluminum-induced dialysis dementia is decreased uptake of iron. Aluminum may effectively compete with iron for the same carrier protein, transferrin [Tf]. Aluminum is oxidized to an insoluble form in water at physiologic pH and must be bound to a carrier if it is to be transported in the blood. Two carrier molecules, citrate and transferrin, have been implicated in transport of the biologically active aluminum. Although their stability constants and aluminum binding capacities per liter of serum are similar, transferrin, the metal transport protein, is thought to be the major carrier (González *et al.* 1989; Wilhelm *et al.* 1990). Although the exact nature of the competition of aluminum and iron for binding of transferrin is not known, an inverse correlation exists in hemodialysis patients between aluminum level in the blood and saturation of transferrin with iron (Huang *et al.* 1992; Cannata *et al.* 1993).

The higher aluminum levels are in the blood, the lower the iron levels. This inverse correlation is also reflected in normal subjects with accidental aluminum overdose. In accidental overdose, not only are blood levels of iron low when aluminum levels are high, erythrocyte levels of iron are low and erythrocyte aluminum levels high (Caramelo *et al.* 1995). Blood levels of these metals reflect cellular levels. Although the mechanism of action of the blockage is also unknown, transferrin saturated with aluminum has been shown to inhibit hemoglobin synthesis, and therefore iron utilization, in erythroleukemia cells (Abreo *et al.* 1990). Aluminum therefore seems to effectively block iron from being used by the erythrocyte and leads to microcytic hypochromic anemia.

Uptake of aluminum into the brain is also inversely correlated with blood iron levels (Cannata *et al.* 1991). Transferrin mediates iron, and presumably aluminum, transport into the CNS (Fishman *et al.* 1987). Many theories have suggested the site of action of aluminum in the CNS. However, if transferrin is handled in the CNS the same way it is handled on the other side of the blood-brain-barrier (Roskams and Connor, 1990), the number of possible targets of aluminum action decreases.

To utilize the iron bound to transferrin, cells have developed a endocytic mechanism for rapidly capturing transferrin, releasing its iron into the cell and then recycling the spent transferrin. At a target cell, one with transferrin receptors [TfR] on its cell surface, a Tf-TfR complex is formed. A specific sequence on the transferrin receptor then promotes clustering of the receptor into clathrin-coated pits (Collawn *et*

*al.*1990; Miller *et al.*1991). The pit then undergoes endocytosis and, after dissociation of the clathrin, the resulting endocytic vesicle fuses with a tubulo-vesicular structure: the sorting endosome (Gruenberg and Maxfield, 1995). A H^+-ATPase then mediates the acidification of these early endosomes - with Cl^- inflow and Na^+ outflow maintaining electric neutrality. By adjusting the Na^+ gradient, a Na^+,K^+-ATPase limits the acidification of the sorting endosome to pH 6 (Fuchs *et al.*1994; Cain *et al.*1989). At this pH, the iron dissociates as Fe^{3+} from one of two possible iron-binding sites on transferrin (Núñez *et al.*1990). The Fe^{3+} is then enzymatically reduced to Fe^{2+}. This form of iron can translocate, via a membrane binder/carrier specific for Fe^{2+}, across the vesicle membrane into the cytoplasm (Núñez *et al.*1990). The iron is then bound to a cytoplasmic carrier (possibly citrate, a nucleotide or other small carrier molecule) and the Tf-TfR complex, now found in the recycling endosome, returns to the surface of the cell (Núñez *et al.*1990). At neutral pH, non-saturated transferrin [apotransferrin] binds less tightly to the transferrin receptor than does saturated transferrin. After the recycling endosome fuses with the surface of the cell, apotransferrin is released to the interstitial fluid (Bali *et al.*1991).

It is unlikely aluminum can be released from transferrin into the cell if it is handled by this same endocytic process. At pH 6.0, the pH of the sorting endosome, aluminum exists as an almost equimolar mixture of two ionic species $Al(OH)_4^-$ and $Al(OH)_2^+$ (Martin, 1986). If the Al^{3+} state must be reached before aluminum is dissociated from the transferrin, rather than being recycled, the early endosome must first

"mature" into or be transported into a multivesicular body [also known as the endosomal carrier vesicle] and then into the late endosome (Gruenberg and Maxfield, 1995). In becoming a late endosome, the early endosome loses its Na^+,K^+-ATPase and the pH of the endosome can lower to 5.5 (Cain *et al.* 1989). At pH 5.5 aluminum exists as an almost equimolar mixture of three ionic species Al^{3+}, $Al(OH)^{2+}$ and $Al(OH)_2^+$ (Martin, 1986). Further acidification increases Al^{3+} to the detriment of the other two species. At this pH, Al^{3+} would resemble the Fe^{3+} and could dissociate from the transferrin.

However, another potential problem arises. Without the so called "binder/carrier specific for Fe^{2+}" (Núñez *et al.* 1990), the charged ferrous ion, like all charged ions, would have difficulty crossing the lipid membrane barrier of the early endosome and entering the cytoplasm. Whereas iron has two common oxidation states, Fe^{2+} and Fe^{3+}, aluminum only has one, Al^{3+}. The Fe^{2+} transporter requires iron to be in the ferrous form. Aluminum, in any of its ionic forms, may not be able to bind to this transporter and would therefore be locked up, unable to leave the late endosome. Aluminum would not be able to enter the cytoplasm and would be effectively shielded from interacting with other components of the cytosol by the endosomal lipid bilayer. If this is indeed the case, schemes that require aluminum to interact directly with components of the cytosol to alter the physical properties of the neurofilament (Shea and Beermann, 1994; Cherroret *et al.* 1992; Shea *et al.* 1992; Shea *et al.* 1992; Shetty *et al.* 1992; Diaz-Nido and Avila, 1990; Nixon *et al.* 1990; Troncoso *et al.* 1990; Pierson and Evenson, 1988), would not be realistic.

On the other hand, lysosomes, which fuse with late endosomes to form secondary lysosomes, might be a target of aluminum toxicity. Stekhoven *et al.* cultured rat brain slices in a medium which included aluminum chloride. Electron probe analysis of the lysosomes of cortical neurons revealed an accumulation of aluminum and a decrease in the amount of iron (Steckhoven *et al.*1990). Gruca and Wisniewski (Gruca and Wisniewski, 1984) found that injection of aluminum chloride into the rabbit cisterna magnum leads to an increase in numbers of lysosomes and secondary lysosomes in hippocampal and spinal cord neurons. Most transferrin in the brain is found in the cells responsible for the formation of the axonal myelin sheath, the oligodendrocytes (Connor *et al.*1987). Immunohistochemical localization of transferrin is temporally and spatially associated with the onset of myelination (Connor and Fine, 1987). If aluminum is toxic during development and, as the dialysis dementia model suggests, it operates by altering the processing of transferrin, damage might be expected to be most extensive in oligodendrocytes. Phosphorylated NF-H is especially rich in large myelinated axons. The levels of pNF-H within these axons might therefore be altered if the oligodendroglia surrounding these axons are damaged. Since myelination, and the onset of pNF-H appearance both occur during the early postnatal period, if aluminum is toxic to oligodendrocytes and if myelination is linked to appearance of pNF-H, the toxicity should be especially evident during development. However the information linking myelination to the appearance of pNF-H during development is incomplete.

The purpose of this study was therefore to document the spatial and temporal onset of phosphorylation of NF-H in the developing rat brain during a critical period in development. The resulting observations were then to be compared to the regional biochemical analysis of onset of pNF-H immunoreactivity presented by Fischer and Shea (Fischer and Shea, 1991). The onset of appearance of pNF-H from the present study was then to be correlated with other indices of CNS development, including onset of myelination. With these correlations and the pattern of development of staining established, the sensitivity of this method in exposing any changes in the rate of maturation of specific neurons as a consequence of aluminum exposure during development could then be assessed.

Materials and Methods:

Isolation and dephosphorylation of Triton-insoluble cytoskeletons

The detergent insoluble cytoskeleton was extracted from frozen, stripped adult rat spinal cords (Pelfreeze) in a two step procedure (Chiu and Norton, 1982) which employs several modifications of a fundamental MME solution (100mM MES, 0.5 mM $MgCl_2$, and 1 mM EGTA in water with leupeptin (1mg/l) and PMSF (0.5 mM) added to inhibit proteolysis) (Czosnek *et al.*1981). The tissue was first homogenized in a 50ml Potter-Elvehjem tissue grinder (Kontes) kept cool in a beaker of ice. Seven strokes of a Teflon pestle rotating at 1455 rpm (Rockwell/Delta drill press) were used to homogenize the tissue in twenty times its weight of ice-cold MME-T (0.5% (vol/vol) Triton X-100 in MME). The homogenate was centrifuged for 15 minutes at 11000 rpm (14,600 x g) at 4°C in a Sorvall RC-5B centrifuge and the supernatant, containing triton-soluble material, was discarded. The pellet was resuspended with three strokes of the pestle of an ice-cold Potter-Elvehjem tissue grinder, rotating at 1455 rpm. This second resuspension, in 0.9M sucrose in MME-T, was carried out in a volume equal to that in which the original tissue sample was homogenized. The suspension was then centrifuged as described above. The supernatant, including a superficial a fatty layer containing membrane and myelin-bound proteins was aspirated and discarded. The remaining pellet was washed with cold MME and resuspended in a minimal amount of MME (usually 1

ml) using a dounce homogenizer with an 'A' pestle (Kontes). The final wash of the pellet is important because bubbles from a solution containing Triton X-100 can interfere with subsequent determination of protein quantities using the Bradford protein assay (Davis, 1988) and unpublished observations of D.Soifer).

The detergent-insoluble cytoskeleton was dephosphorylated using a modification of the procedure of Georges and colleagues (Georges *et al.* 1986). Briefly, 1 mg of protein from the cytoskeleton solution prepared as described above was diluted in MME (with 0.5 mg/l leupeptin added) to bring the total volume up to 90 µl. To this, 10 µl of *E. coli* alkaline phosphatase (approximately 1.2 IU) was added and allowed to incubate overnight in a 25°C water bath. Aliquots were then frozen at -80°C.

Gel electrophoresis and immunoblot analysis

The concentration of protein in the native and dephosphorylated detergent insoluble cytoskeleton prepared above was determined by a modification of the Bradford assay (Bradford, 1976). Briefly, 20 µl aliquots of a range of known concentrations of bovine serum albumin (Sigma) dissolved in MME were placed in wells of a 96 well tissue culture plate (Falcon). The same volume of several dilutions of the samples were placed in other wells. The proteins were dissolved by incubation in 40 µl of 1 N NaOH at 37°C for 60 minutes; then neutralized by the addition of an equal volume of 1 N HCl. The solutions in the wells were then incubated with 200 µl of a 0.0125% solution of

Coomassie Brilliant Blue G-250 dissolved in 23.5% (vol/vol) ethanol, 42.5% (vol/vol) phosphoric acid (in water) for 30 minutes at room temperature. The absorbance of 600 nm light by the samples (Beckman Biomek 1000 spectrophotometer) was compared to that of the standard BSA solutions. Concentration of the unknown sample were then extrapolated from those of the known standards. Samples and standards were run in triplicate.

The proteins were separated by gel electrophoresis using a 7.5% acrylamide gel in a discontinuous, dissociating (0.1%SDS) buffer system (Laemmli, 1970; Studier, 1973). The proteins in the cytoskeletal samples were denatured and dissociated by boiling them for three minutes in a "sample buffer [SB]" solution (final concentrations: 1mM DTT, 1%(w/v)SDS, 10mM Tris HCl (pH 6.8) and 8%(w/v) glycerol; in water). A few grains of Bromophenol Blue (Sigma) and pyronin Y (Sigma) had also been added to the SB solution as a tracking dye. Ten of fifteen wells molded into the stacking gel each received 100 ng of denatured cytoskeleton. The remaining wells received 1 μg of denatured cytoskeleton (native or dephosphorylated), high molecular weight standard (BioRad), or buffer. Two gel setups were used - one was loaded with native cytoskeleton, one with dephosphorylated cytoskeleton. The 60 mA current was maintained at maximal voltage (Hoefer Scientific Instruments PS500X) until the dye front flattened against the gel-gel interface. When this occurred, the current was increased to 100 mA.

Just before the pyronin Y dye front eluted into the minigel buffer reservoir, the current was turned off and the gel removed. Lanes loaded with 100 ng of either the native or dephosphorylated cytoskeleton were separated from the rest of the gel and transferred to nitrocellulose (see below). The remaining lanes were stained with Coomassie Blue R-250. The staining procedure began with a 15 min immersion in a solution (50% methanol, 11% glacial acetic acid (w/w) in water) of 0.25% Coomassie Blue R-250 stain (Sigma). The gels were then briefly rinsed in "fast" destainer (8% glacial acetic acid, 50% ethanol (v/v) in water); then dehydrated in fresh fast destainer for 15 minutes. The gels were subsequently rehydrated in "slow" destainer (7.5% acetic acid 5%methanol (v/v) in water) and kept in the slow destainer until a photographic record of their staining pattern was made. All incubations were carried out at room temperature in covered containers continually mixed on an orbital rocking table.

In the ideal Western transfer of neurofilament proteins from gel to nitrocellulose, as the proteins solubilized by the gel's SDS migrate to the nitrocellulose, the SDS is eluted, thereby allowing the proteins to come out of solution and precipitate onto the nitrocellulose. To increase the efficiency of this system, two transfer buffers were used: a Tris base, glycine, ethanol mixture (37mM Tris Base, 242mM glycine, 20% ethanol, in water) [TB] and 0.1% SDS in the same Tris base, glycine, ethanol buffer [TB-S]. By soaking all cassette pads and filter paper on the gel side of the cassette in TB-S, a high concentration of SDS was sustained within the gel for a longer period of time . This was done to increase the amount of protein eluted from the gel. All other materials, including

the nitrocellulose membrane (Schleichter & Schuell, BA85), were soaked in TB. The gel and nitrocellulose were sandwiched in a cassette between filter paper and cassette pads and placed in the reservoir, filled with TB, of the BioRad transfer unit. With voltage at maximum, the current was raised to 60 mA for 20 minutes then to 120 mA for 1 hour. The gels were then separated from the nitrocell ɔse membrane and stained with Coomassie Blue (as above). A mark was made on the nitrocellulose to indicate the limits of the gel using a soft (number 1) pencil. The nitrocellulose was washed twice in PBS for 5 minutes and twice in 0.05% Tween 20 in PBS [PBS-T] for 5 minutes. The blots were then left in block (2% goat whole serum, 2%BSA, 0.001%NaN_3 in PBS-T) overnight at 4°C.

The blots were washed for 5 minutes on a shaking platform at room temperature in PBS. The 5 minute wash was repeated in 0.05% Tween 20 in PBS [PBS-T], and repeated for 5 minutes in PBS. The blots were cut into 5 mm wide strips in a direction parallel to the electric field of the original gel and placed in Accutron disposable incubation trays (Schleicher & Schuell). The strips were incubated with primary antibody for 2 hours at 37°C on a rocking platform. Primary antibodies, all in ascites fluid, included SMI31 (1:2000 Sternberger Monoclonals Incorporated (also known as clone S6 and as clone 06-17) (Sternberger and Sternberger, 1983)), and three monoclonal antibodies from the laboratory of V. M. -Y. Lee: RMO102 (1:4000 (Lee *et al.*1988)), RMO217 (1:4000 (Lee *et al.*1987)) and RMO24.9(1:3000 (Lee *et al.*1987; Goldstein *et al.*1987)). Aliquots of ascites from RMO24.9 were also immunoabsorbed

by incubation with pNF-H or pNF-M (see "immunoprecipitation of antibodies," below) and diluted to the same final concentration as the original RMO24.9 (1:3000). The antibodies were then aspirated and the strips washed for 5 minutes each with PBS, PBS-T and then PBS. The strips were then incubated at 37°C for 1 hour on a rocking platform in secondary antibody. The secondary antibody, alkaline phosphatase conjugated goat anti-mouse IgG heavy and light chain proteins (HyClone) had been diluted 1:4000 with block. The secondary antibody was then aspirated and the strips washed on a rocking platform for 5 minutes each with PBS, PBS-T and then PBS. The strips were then washed twice for 5 minutes in sterile deionized water and stained using BCIP/NBT [5-bromo-4chloro-3-indoxyl phophate/nitro blue tetrazolium chloride] (Sigma) as the substrate for the alkaline phosphatase (Leary *et al.*1983). The freshly prepared substrate/chromogen reaction mixture consisted of 6μM NBT and 6.7μM BCIP in 100mM Tris base, 100mM NaCl and 50 mM $MgCl_2$ at pH 9.5. The strips were incubated on a shaking platform in the reaction mixture. When the complete banding pattern was apparent, the reaction was stopped by washing the strips twice in sterile distilled water. The strips were dried between two pieces of 3MM Watman filter paper and photographed.

Immunoprecipitation of antibodies

Purified rat NF-H and NF-M were donated by F.-C. Chiu and were prepared by reverse-phase high-performance liquid chromatography (Hui *et al.*1986). The

neurofilament protein samples were dissolved in 8M urea in 10% BSA. The urea was then removed by overnight dialysis against PBS at 4°C using Spectrapor® (Fisher) membrane tubing (molecular weight cutoff 12-14kDa). Fifteen microliters of the monoclonal antibody RMO24.9 was incubated at 4°C overnight with 15µg of the dialyzed neurofilament protein on a shaking table. The mixture was then centrifuged for 10 minutes at the maximum setting of a Beckman microfuge. The superficial layer was carefully removed, diluted and applied to selected strips blotted with transferred neurofilament proteins (see above).

Rat breeding and oral administration of aluminum

In a preliminary experiment, the pregnant dams drank 120 mM aluminum lactate solution *ad lib.*. After the birth of their pups, they drank tap water *ad lib.*. Control dams drank tap water *ad. lib.* throughout pregnancy and lactation. Their pups were removed from unculled litters on P0, P5, P11 and P14 for tissue processing and microscopic examination.

For a second set of experiments, thirty sexually mature female (age: ≥P70) and seven sexually mature male (age: ≥P56) virgin Long-Evans rats (Blue Spruce) were quarantined in sexually segregated communal cages for one week. Thereafter they were housed in separate plastic cages and given free access to food (Purina rat chow) and

water (tap water) until they were bred. At the beginning of the study each male was habituated to his own metal wire breeding cage by being placed alone in it for three successive nights. Coincidentally, three of six female rats were given free access to 70mM aluminum lactate (Fluka) in their drinking water (Great Bear® purified water). The pH of the solution was adjusted to 6.5 with 6M NaOH and was made fresh at least every other day to avoid visible precipitation of the aluminum (Corain *et al.* 1992). The remaining three control females, paired by weight, received the same amount of drinking water (without aluminum lactate) as the treated females had consumed the day before.

After the six females had followed this pair-watering regimen for at least a week, they were each placed overnight in a separate breeding cage with a male. The breeding couples were not given food or water. If vaginal plugs were found on the rat board under the cage on the following morning, the mating was considered successful. On this day, the first embryonic day [E0], the drinking water of pregnant dams was increased to 120mM aluminum lactate. All successfully bred, treated females were given free access to the chow and to the 120mM aluminum lactate solution. Pregnant control dams were paired with treated dams by weight and day of conception ($\leq$ 2d apart). They received food *ad lib.* and the same amount of water the pregnant treated animals had consumed the day before. The following week, another set of six females, half of which drank 70mM aluminum lactate for at least 7 days and their paired controls were bred. This breeding schedule was maintained until all the females were successfully bred. Litters were culled to 10 pups within 12 hours after the last pup was born [P0]. Dams and litters

were weighed twice a week. One pup was processed from each litter on P9 through P15. The average water consumption during gestation and lactation was comparable to rats given free access to water (Rabe *et al.* 1985).

Tissue processing and immunohistochemistry

Pups were anesthetized with Nembutal (50 mg/kg (ip)) and perfused via an intracardiac catheter with normal saline. When their livers became pale, a solution of 4% paraformaldehyde in phosphate buffered saline [PBS] was perfused using the same catheter. Although Bouin's solution is said to give the best results for immunohistochemistry, (Smitt *et al.* 1993). I found comparable results with paraformaldehyde with the antibodies used in these studies. However, with its higher signal to noise ratio, paraformaldehyde is the better choice of fixative if the tissue is subsequently used for *in situ* hybridization (Singer *et al.* 1987). To allow for this eventuality, 4% paraformaldehyde was therefore chosen as the fixative for this study. The brains were removed and placed in 4% paraformaldehyde for a total of four hours. The organs were washed 4 times in PBS and then stored in PBS at 4° C until the whole brains were embedded in paraffin for serial sectioning.

The brains of adult rats were used for studies of monoclonal antibody specificity. Adult rats, and pups used in preliminary experiments, were perfused, via intracardiac catheter, with normal saline followed by Bouin's solution. Their brains were removed

and remained in Bouin's solution for 24 hours. They were then washed in five to six changes of 70% ethanol over a two week period to extract the picric acid. The adult brains were then cut coronally into four to six pieces, embedded in paraffin and subsequently cut on a microtome into six-micron thick coronal sections.

For the present study, brains from pups of average weight for their age and from three different litters were prepared for analysis. The brains were cut on a microtome into six-micron thick horizontal serial sections. Horizontal sectioning was chosen because fewer sections would be necessary to describe the whole brain than would be necessary for coronal sections and more structures could be identified in horizontal sections than in sagittal sections (Yokoyama *et al.* 1981). Every fifteenth section was immunohistologically stained using the monoclonal RMO24.9, a mouse anti rat neurofilament protein antibody that specifically binds phosphorylated NF-H (Lee *et al.* 1987). The Zymed streptavidin-biotin Histostain-SP kit was used to visualize the bound antibody. Briefly, after the sections were deparaffinized and rehydrated, endogenous peroxidases were blocked by placing the sections in 3% H_2O_2 for 5 minutes. The sections were made isosmotic with the antibodies by placing them in PBS for 5 minutes and in block (2% BSA, 2% rabbit serum in PBS) for 5 minutes. The sections were exposed to RMO24.9 (diluted 1:3000) for 60 minutes followed by two 5 minute washes in PBS. The biotinylated second antibody (rabbit anti-mouse IgM, IgA and IgG) was applied to the sections for 10 minutes. After two washes in PBS, streptavidin-peroxidase conjugate was applied to the sections. After two washes in PBS, the

substrate, aminoethyl carbazole was applied to the sections. The precipitation of substrate was stopped by washing the slides in distilled deionized water.

Adult brain sections were immunohistochemically stained in an identical manner and also with supernatant from primary antibody that had been immunoprecipitated with purified pNF-H or pNF-M (see above).

Analysis of stained sections

Immunostained sections were viewed through a Nikon light microscope equipped with a didymium filter to enhance detection of the precipitated red stain. Structures were identified using standard rat brain atlases (Paxinos, 1990; Paxinos and Watson, 1986; Sherwood and Timeras, 1970). Their relative intensities were graded on a five level scale as shown in table 1. Horizontal sections are bilaterally symmetric. If the intensity of staining of any given structure was different on the left and right sides of the brain section, the higher relative intensity was chosen.

relative intensity	observation
0	no staining
1	staining detected with 10x objective
2	staining detected with 5x objective
3	staining of complete structure
4	structure overstained (bright red)

Table 1 Relative intensity of staining

The assessed intensity of an identified structure was entered into a Paradox for Windows relational database (Borland, version 5.0) Structures were placed into regional divisions of the brain following suggestions by Bloom (Bloom, 1990). The immunoreactivity of pNF-H in a given structure was considered to be positive, and entered in table 2, when the relative intensity of staining of any slide including that structure was ≥ 1 in the brains of all three pups. This method of assessment avoids confounding variations in brain density present during development (OOrschot, 1994). The onset of appearance of pNF-H in a given structure was defined as the day after birth that positive immunoreactivity (as defined above) was seen for the first time.

Jacobson's light microscopic study on the appearance of myelination in the developing rat brain (Jacobson, 1963) included the period of time covered in the present study. Whereas the present study reports appearance of pNF-H staining on every day

from P9 to P15, Jacobson's study only included P7, P10, P12 and P14. To compare the present single-day results to the less precise results of Jacobson, the day that pNF-H appears in each structure was found and the maximal and minimal possible differences of first day of appearance of myelination for that structure determined. These calculations were repeated for each structure included in both studies and two sets of distributions were obtained. One set assumed maximal differences between the two sets of data, the other assumed minimal differences. To determine the temporal relationship between onset of myelination and the onset of pNF-H immunoreactivity, the two calculated distributions were each compared to the pNF-H data using the Wilcoxon matched pairs-test (Statistica for Windows version 4.5, Statsoft Inc). With this non-parametric statistic, it could be determined if the onset of myelination systematically occurred before or after onset of pNF-H immunoreactivity in the majority of the structures or if onset of myelination occurred randomly both before and after onset of pNF-H immunoreactivity in the majority of the structures. The weights of aluminum exposed dams were compared to those of control dams using a Student's *t-test* (Quattro Pro for Windows version 6.0, Novell, Inc.).

Results:

The documentation of the initiation of phosphorylation of the heavy neurofilament protein in tracts of the central nervous system serves as the foundation upon which this report is based. Since all other analyses follow from this immunohistochemical description of the developing rat brain, it was necessary to confirm that the monoclonal antibody chosen to document first appearance of pNF-H had a high affinity for pNF-H and that it could distinguish pNF-H from all other proteins. In particular, the monoclonal antibody had to differentiate pNF-H from the structurally similar neurofilament proteins NF-M and NF-L and distinguish pNF-H from its dephosphorylated form, dpNF-H. Two distinct methods were use to prepare neurofilaments for biochemical and histological analysis of monoclonal antibody specificity. Because these procedures each exposed the neurofilament proteins to different physicochemical environments, the three-dimensional structure of pNF-H, and therefore the epitopes presented to the monoclonal antibody may have differed. Once a monoclonal antibody was chosen for its immunobiochemical specificity, it was therefore necessary to confirm its immunohistochemical specificity.

The litters from dams that were not exposed to supplemental aluminum in their drinking water during gestation and lactation were used to document normal CNS development. Because these dams were pair-watered, that is, given the same amount of water the aluminum-treated dams had drunken the preceding day, it was necessary to

ascertain whether or not the control rats used in the present study were water deprived. Since the experimental protocol used in the present study did not include a group of dams given water *ad libitum*, the water consumption of the control dams was compared to the consumption by the dams in a developmental study carried out by another investigator.

Once specificity of the monoclonal antibody and identity of the experimental litters was established, the structures were identified which present immunohistochemical staining on each day of the seven day developmental window extending from P9 through and including P15. Although this information could have been presented many different ways, this study was conceived to be a higher resolution analysis of the results of Fischer and Shea (Fischer and Shea, 1991). The observations of the present study were therefore grouped to reflect the same anatomic divisions made in their biochemical analysis of the appearance of pNF-H immunoreactivity.

These results were then to be used as a baseline to detect perturbations in the developmental appearance of pNF-H in aluminum-exposed pups. Unfortunately, aluminum was found to produce pathological changes in the rat dams that made assessment of changes in the brains of pups in their litters impossible.

Specificity of the monoclonal antibody

The relative molecular weights [M_r] of proteins prepared from adult rat spinal cords as well as the immunobiochemical specificity of several antibodies for the neurofilament proteins are shown in Figure 2. The electrophoretic mobility of the neurofilament proteins prepared from adult rat spinal cords and separated on a 7.5% SDS polyacrylamide gel (figure 2, lane 2), increased when the prepared proteins were first dephosphorylated with *E. coli* alkaline phosphatase (figure 2, lane 3). The shift was most noticeable with NF-H and NF-M. Relative to molecular weight standards (Figure 2, lane 1), the molecular weight of NF-H changed from 200,000 Daltons (pNF-H) to 165,000 Daltons (dpNF-H). The relative molecular weight of NF-M changed from 160,000 Daltons (pNF-M) to 130,000 Daltons (dpNF-M). This change in M_r upon dephosphorylation corresponds to a 35,000 Dalton shift in the M_r for the heavy neurofilament protein and a similar 30,000 Dalton shift for the mid-sized neurofilament protein (see introduction for a discussion of the significance of this similarity). To determine the specificity of different monoclonal antibodies, Western blots of cytoskeletal proteins transferred from native cytoskeleton (similar to lane 2 of the 7.5% SDS polyacrylamide gel) were incubated with various primary antibodies. A single band, corresponding to pNF-H, appeared when RMO24.9 was chosen as the primary antibody (figure 2, lane 4). The specificity of this monoclonal binding to pNF-H was tested by attempting to immunoprecipitate out the antibody with its specific antigen, pNF-H, and also with the structurally similar protein pNF-M. Staining was not present

Figure 2: Biochemical analysis of monoclonal antibody binding specificity for pNF-H. 7.5% SDS-PAGE (lanes 1, 2, 3) of detergent-insoluble rat spinal cord cytoskeleton (lane 2) shows the shift, relative to high molecular weight standards (lane 1), of pNF-H and pNF-M to a lower relative molecular weight when dephosphorylated with *E. coli* alkaline phosphatase (lane 3) . Positions of pNF-H and dpNF-H are marked to the right of lane 10, positions of pNF-M (marked by a six-sided star (✶)), dpNF-M (marked by a eight-sided star(✷)), and NF-L (marked by and asterisk (✻)) are shown to the right of lane 3. Western blots of the native cytoskeleton (lanes 4-6, 8-10) confirm the specificity of binding of RMO 24.9 (diluted 1:3000 with block) to pNF-H (lane 4). Antibody binding activity can be absorbed out with purified pNF-H (lane 5), but not with purified pNF-M (lane 6). The same dilution of RMO 24.9 also does not bind to a Western blot of dephosphorylated cytoskeleton (lane 7). RMO 24.9 only binds to pNF-H in a blot of native cytoskeleton (lane 4). Other antibodies, SMI31(diluted 1:2000), TA51 (diluted 1:4000), RMO 217 (diluted 1:4000), incubated with similar blots, bind to other proteins as well as pNF-H, as shown in lanes 8-10, respectively. RMO 24.9 therefore binds the heavy neurofilament protein in its phosphorylated form and, of the available antibodies is the most specific in its affinity for pNF-H.

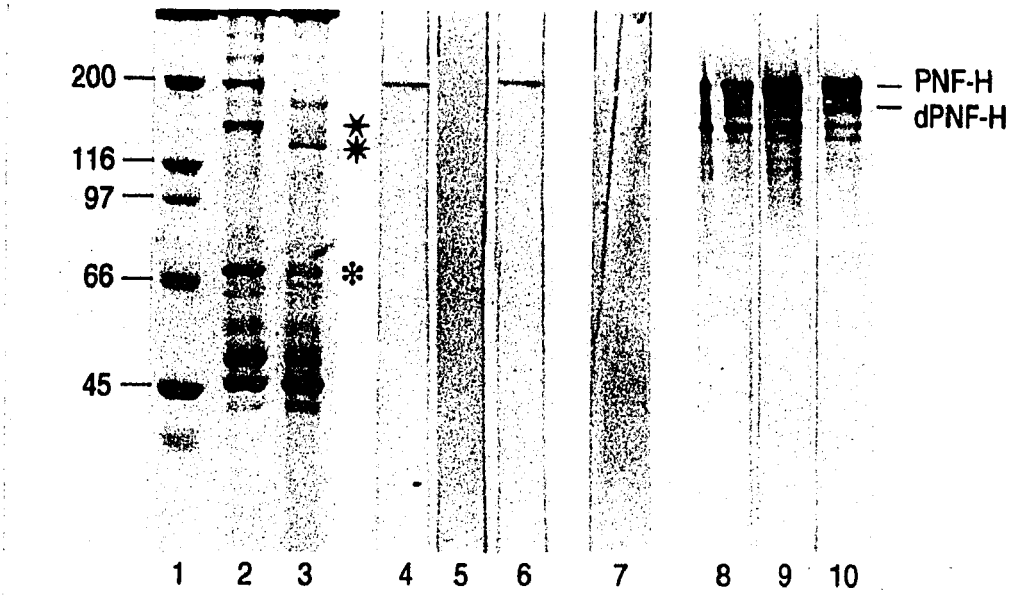
200
116
97
66
45
PNF-H
dPNF-H
1
2
3
4
5
6
7
8
9
10

when RMO24.9 had been immunoprecipitated with pNF-H (figure 2, lane 5). However, immunostaining of the blot remained after immunoprecipitation was attempted with pNF-M (figure 2, lane 6). The specificity of RMO24.9 for pNF-H rather than dpNF-H was also ascertained. Staining was not present if RMO24.9 was used as the primary antibody on a Western blot of dephosphorylated spinal cord cytoskeletal proteins similar to those found in lane 3 (figure 2, lane 7). Unlike other monoclonal antibodies which bind pNF-H, including SMI31 (figure 2, lane 8), TA51 (figure 2, lane 9) and RMO217 (figure 2, lane 10), RMO24.9 did not cross-react with pNF-M and other proteins - and showed a single banding pattern even when dilutions lower than 1:3000 were used (results not shown).

RMO24.9 proved to be a useful antibody for biochemical analysis of a neurofilament-enriched homogenate. However, RMO24.9 was prepared from ascites and therefore could be composed of up to 15% non-specific antibodies (Campbell, 1984). When used as the primary antibody in immunohistochemistry, and therefore exposed to a wider array of potential binding sites, RMO24.9 might exhibit non-specific binding. The neurofilament proteins are only found in neurons. If significant non-specific binding did exist, extra-neuronal binding sites of the non-specific immunoglobulins would become evident after immunoprecipitation of the pNF-H-specific immunoglobulins with pNF-H protein. To test this, RMO24.9 was absorbed to purified pNF-H, the complex precipitated by centrifugation, and the resulting supernatant used as the primary antibody in immunohistochemical staining of adult rat brain sections . Relative to normal

immunohistochemical staining of an adjacent section using RMO24.9 as the primary antibody (figure 3a), supernatant from RMO24.9 immunoabsorbed with the pNF-H, did not elicit any immunohistochemical staining (figure 3b). To rule out staining of proteins antigenically similar to pNF-H, supernatant from RMO24.9 ascites, that had been absorbed to and immunopreciptated with purified pNF-M, was used as a primary antibody. Brain sections stained immunohistochemically using this absorbed RMO24.9 showed a distribution and intensity of staining of nerve tracts similar to that by RMO24.9 alone (compare figure 3a and figure 3c). Therefore, even when exposed to a wider array of antigenic sites, RMO24.9 remained specific to sites rich in pNF-H.

For the most part, RMO24.9, whose paratope specifically binds phosphoserines found in the tandem repeats of the tail domain of NF-H, immunohistochemically stained axons in the rat CNS. However, in agreement with other studies, the soma of some neurons, especially those related to sympathetic and sensory systems, were found to stain. These included neurons within the dorsal root ganglion (Klosen and van den Bosch de Aguilar, 1994; Itoh *et al.*1992; Perry *et al.*1991; Vickers and Costa, 1991), the mesencephalic trigeminal nucleus (Poltorak and Freed, 1987; Klosen and van den Bosch de Aguilar, 1994), Gasser's trigeminal ganglion (Klosen and van den Bosch de Aguilar, 1994), and also transiently in the reticulated thalamic nucleus and lateral lemniscal fields. Although others have documented binding to cell bodies within the triangular septal nucleus (Klosen and van den Bosch de Aguilar, 1992), RMO24.9 did not bind to this nucleus during the developmental period included in the present study.

Figure 3: Immunohistochemical evidence for tract-specific binding of RMO24.9. These three coronal serial sections taken from the same adult rat brain and reproduced at the same magnification, include fiber tracts of the internal capsule [ic] running through the striatum [CPu and GP] as well as tracts intrinsic to the striatum. Also shown are tracts of the stria medullaris termini [sm], the fornix [f], the ventral hippocampal commissure [vhc], the cingulum [cg] and the corpus callosum [cc]. The asterisk (*) identifies a landmark on the vhc which is common to all three sections. All sections are immunohistochemically stained using RMO24.9 (diluted 1:3000) as the primary antibody however the antibody used for the section shown in 3b had been absorbed to purified pNF-H and precipitated by centrifugation. RMO24.9 used as the primary antibody in figure 3c had been absorbed to purified pNF-M and centrifuged. The normal pattern of nerve tracts staining seen in figure 3a is also found after absorption to purified pHF-M and centrifugation (figure 3c) but not after absorption to purified pNF-H followed by centrifugation (figure 3b). These results suggest that RMO24.9 only binds to tracts within the rat CNS.

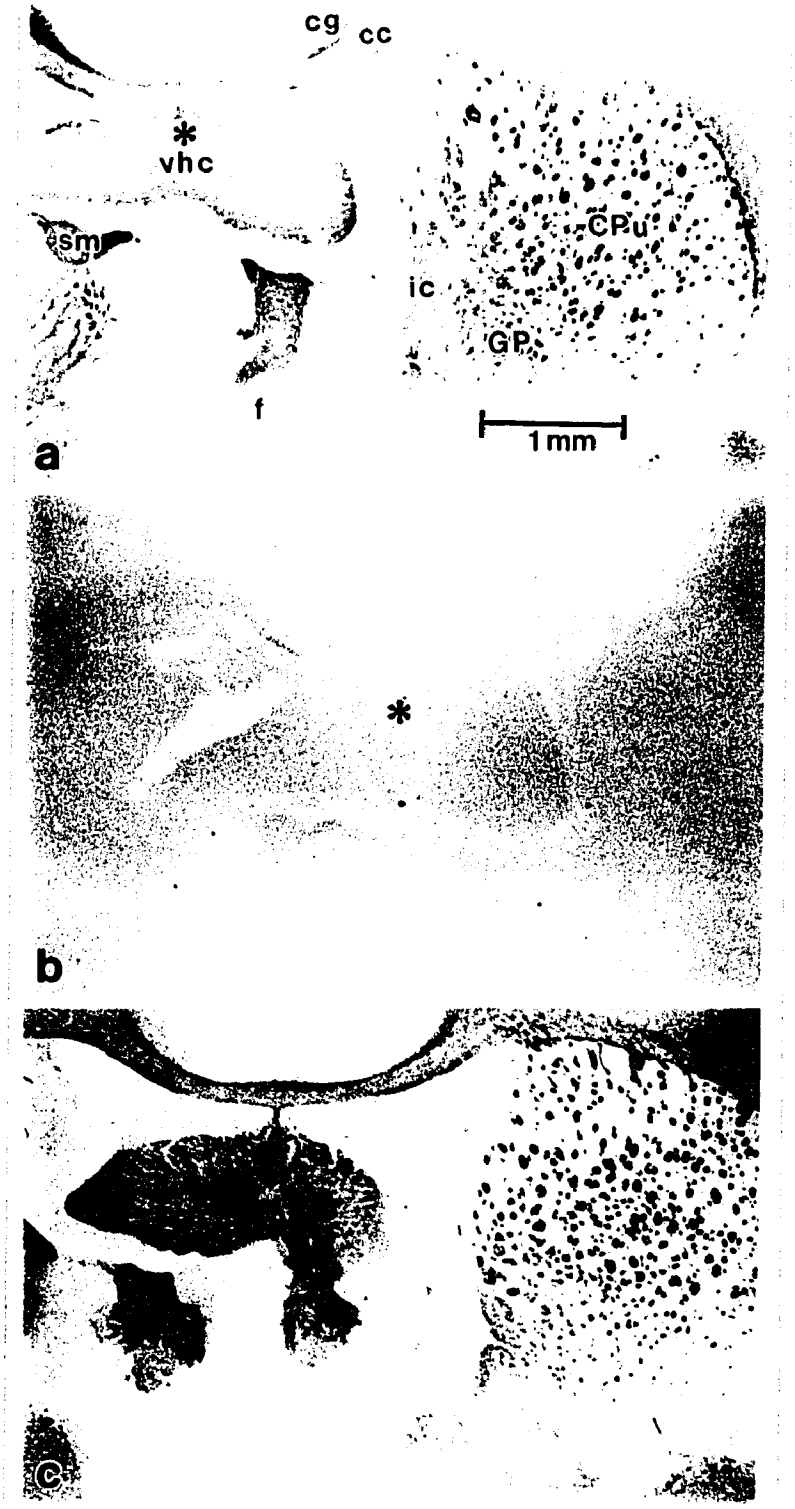
cg
cc
vhc
sm
CPu
ic
GP
f
1mm
a
b
c

Fluid and aluminum lactate consumption during gestation and lactation

a. Preliminary studies

In the preliminary experiments aluminum-exposed dams consumed an average of 300 mg per day of aluminum (as aluminum lactate) per kilogram of body weight during gestation. These same dams drank tap water during lactation. Data for the normal development of pNF-H staining before P9 was derived from the results of brain sections of control pups stained during these preliminary experiments. These pups came from litters of dams that were given free access to tap water during gestation and lactation.

b. Pair-watered versus free-access watered dams

Normal neural tract development of pups on P9 through P15 was followed using litters from dams that served as pair-fed controls to aluminum-exposed dams. Brains of pups from these dams, dams that drank Great Bear® water during gestation and lactation and whose litters were not cross-fostered, were used to document normal onset of pNF-H specific staining. During the period before mating, these control rats consumed an average of 0.09 ml of Great Bear® water per gram body weight. Consumption of water increased during gestation to 0.10 ± 0.02 ml / g body weight. This consumption is comparable to that of another study in which rats, given free access to tap water during gestation, drank an average of 0.12 ± 0.01 ml of water per gram body weight per day

(Rabe *et al.* 1985). During the first 21 days after birth, the dams that drank Great Bear® Water drank an average of 0.15 ± 0.04 ml of water per gram body weight. The increase in consumption of water during the postnatal period is also consistent with the study of Rabe *et al.* where the dams drank 0.20 ± 0.01 ml of tap water per gram body weight (Rabe *et al.* 1985).

The dams that kept their own litters and drank Great Bear® water weighed an average of 278.4 ± 26.7 grams before pregnancy, 307.3 ± 37.8 grams during gestation, and 303.2 ± 37.6 grams during the first 21 days after birth of their litters. These dams therefore drank an average of 30.7 grams of water per day during gestation and 45.5 grams of water, or 48% more, during lactation. The dams in A. Rabe's study weighed more than the Great Bear® dams, an average of 346 grams prenatally and 320 grams postnatally. They consumed 41.5 grams of tap water per day during gestation and 64 grams, or 54% more, during lactation. The water consumption of the pair-watered Great Bear® dams is therefore similar to that of the freely drinking tap water consuming dams.

c. Aluminum lactate consumption during gestation

Rat dams that were exposed to aluminum lactate, became pregnant and gave birth to litters that they nursed after birth consumed an average of 142 ± 21 mg/kg/d of aluminum as aluminum lactate before becoming pregnant (for 7.9 ± 5.1 days), 340 ± 52 mg/kg/d during gestation (for 22.8 ± 1.5 days) and 724 ± 261 mg/kg/d after giving birth

(for 24.0 ± 6.5 days). These eight dams were all examined for visceral histopathology. Four dams that were exposed to aluminum lactate, became pregnant but lost their litters perinatally through cannibalism (n=2) or resorption (n=2) consumed an average of 179 ± 16 mg/kg/d before becoming pregnant (for 18.3 ± 13.0 days) and 345 ± 87 mg/kg/d after becoming pregnant (for 57.5 ± 7.3 days). Two the dams with cannibalized litters and one of the dams with resorbed litters were examined for visceral histopathology.

Ontogeny of regional pNF-H immunohistochemical staining

Development of the rat CNS continues past weaning and into adulthood. The make-up and distribution of the proteins of the cytoskeleton, even in the young adult (1 month old), may not match that of older animals (4 months old) (Shetty and Turner, 1995). Some tracts, such as the lateral olfactory tract, high levels of pNF-H immunohistochemical staining are found throughout the P9-P15 developmental window (figure 4a). However, the steady state levels attained during this period might not be the same as the steady state levels that would be observed in the adult. The adult levels might be higher or lower. To avoid linking a definition of development to the day that maximal (or half-maximal) steady state levels of immunoreactivity were attained, the onset of immunopositivity of a particular tract was defined as the day pNF-H could first be immunohistochemically detected in that tract in all three animals. Ideally, all three animals would first stain for the presence of pNF-H on the same postnatal day. However, the temporal resolution of day of onset of pNF-H staining depended on the tract being

Figure 4: Onset of pNF-H immunoreactivity in structures associated with the hippocampus. Figures 4a through 4g depict typical temporal patterns of onset of pNF-H immunoreactivity as seen in structures within the developing rat brain from postnatal day 9 through 15. The x-axis is a time line beginning on P9 and divided into units of one day. The y-axis demonstrates the percentage of total sections which run through the selected structure that are stained. The z-axis shows the total number of pups with staining in the selected structure. Some structures, such as the lateral olfactory tract (figure 4a), are already completely stained by postnatal day 9. This particular structure maintains a high level of staining throughout the developmental window selected for the present study. Figures 4b and 4c demonstrate the latency between onset of staining in one animal and onset of staining in all three experimental animals for two different structures: the mammillothalamic tract (figure 4b) and axons within the dentate gyrus (figure 4c). An increasing percentage of axons within any structure may stain as development progresses. An increasing percentage of axons within the subiculum (figure 4d) and axons of the basket cells within the pyramidal cell layer of the CA3 region of the hippocampus (figure 4e) stain during the P9 through P15 developmental window. The increased staining may represent the initiation of staining in existent axons as well as death of axons (Cameron and Gould, 1994; Cowan *et al.*1984) which may not have produced pNF-H. Figures 4f and 4g demonstrate onset of pNF-H immunopositivity in the alveus and the radiata layer of the CA3 region of the hippocampus. The alveus includes axons originating in the pyramidal cells of the hippocampus and the radiata layer includes axons from gra[illegible]e cells in the dentate gyrus.

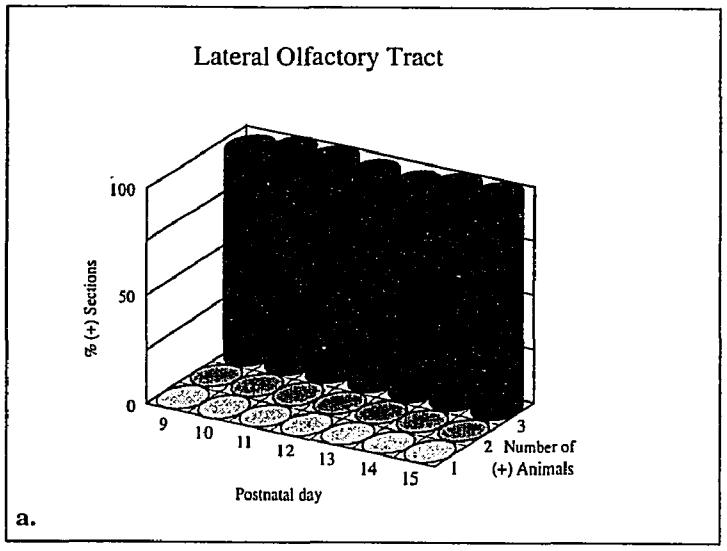
Lateral Olfactory Tract
100
50
0
% (+) Sections
9
10
11
12
13
14
15
Postnatal day
1
2
3
Number of
(+) Animals
a.

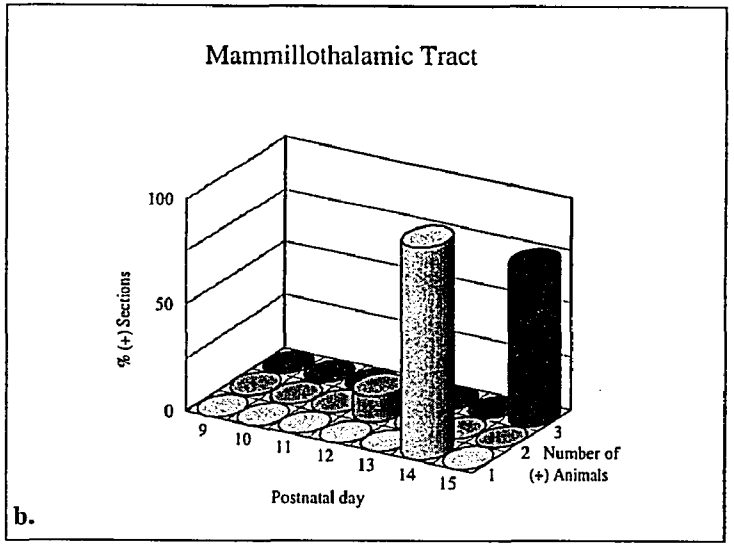
Mammillothalamic Tract
100
50
0
% (+) Sections
9
10
11
12
13
14
15
Postnatal day
1
2
3
Number of
(+) Animals
b.

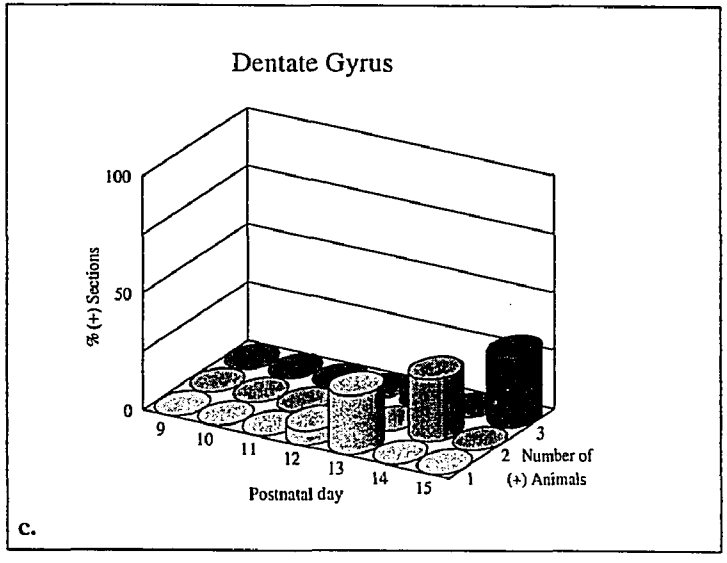
Dentate Gyrus
100
50
0
% (+) Sections
9
10
11
12
13
14
15
Postnatal day
1
2
3
Number of
(+) Animals
c.

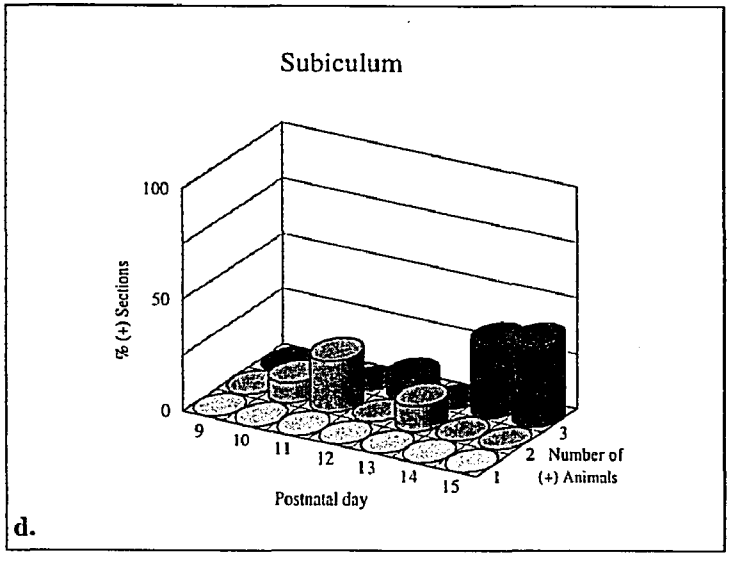
Subiculum
100
50
0
% (+) Sections
9
10
11
12
13
14
15
Postnatal day
1
2
3
Number of
(+) Animals
d.

Figure 4 (continued)

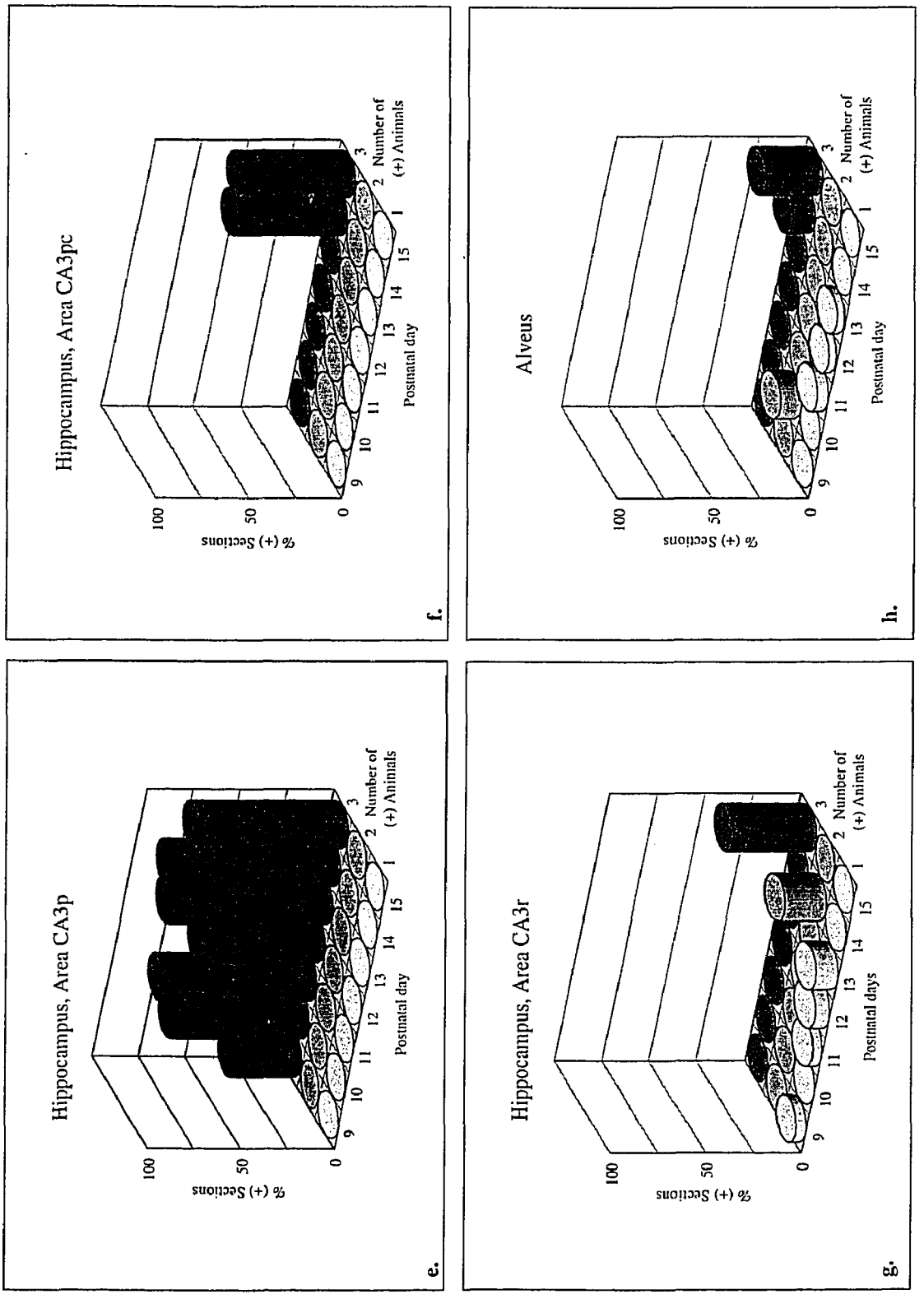

observed. In some tracts, such as the mammillothalamic tract (figure 4b), one day passed from the day one animal stained for the presence of pNF-H, to the day all three animals stained for the presence of pNF-H. In other areas, such as the dentate gyrus (figure 4c), it took up to two days before all three animals stained for the presence of pNF-H.

Although all three animals first stain for the presence of pNF-H in a particular structure on a given day, the axons within the entire structure may not have attained the same maturity simultaneously. This situation was seen in the subiculum and in the pyramidal cell layer of area CA3 of the hippocampus. In the subiculum (figure 4d), 8 percent of sections were stained for the presence of pNF-H in all three animals on P12. This rose to 32 percent and leveled off by P14. The axons of the basket cells in the pyramidal cell layer of area CA3 of the hippocampus, already positive for the presence of pNF-H in an average of 34 percent of sections on P9, become positive in an average of 80 percent of the sections by P12 (figure 4e).

Table 2 lists the structures in the rat CNS that stain for the presence of pNF-H (marked by an "x") and gives the days during the P9-P15 developmental window that positive staining was observed for each of these structures. Structures listed by Jacobson that stain for the presence of myelin (Jacobson, 1963) are marked by an "o". Both tracts and brain nuclei are listed. In the present study, no attempt was made to identify the origin of axons running through a tract (most carried both afferent and efferent fibers) or to identify whether axons found in a nucleus were from tracts running through the

nucleus (*en passage*) or from tracts terminating on the nucleus. Axons from neurons intrinsic to a structure (such as those originating from the basket cells in the hippocampal pyramidal cell layer) are noted when they occur.

The criteria for positive staining are list. in the Methods section. The first day a structure fulfilled these criteria was considered the day of onset of immunoreactivity for pNF-H in that structure. Once staining was positive for a structure, positive staining was not necessarily maintained during subsequent days (see table 2). Generally, the failure to reach the criteria for positivity was due to lack of staining in one of the three brains studied on a particular postnatal day. Since the same treatment schedule was fastidiously maintained and reagents freshly prepared for all sections stained, variations in staining due to technique were minimized. The cause or causes for inconstant staining are found elsewhere. In a few cases, as with the optic nerve (figure 5a) and optic chiasm (figure 5b), the failure to find staining was due to the fact that these small structures were not found in the sections selected for immunohistochemical staining. This was also the case for the vomeronasal nerve [vn] on P12 and P14 (see table 2). In all other instances, another cause for the inconstant staining must be found.

Perhaps the simplest explanation for inconstant staining is that individual pups mature at different rates (Jacobson, 1963; Watson, 1903). Since it is impossible to follow development of a single pup using immunohistochemistry, each postnatal day represents the data collected from the brain sections of three new pups. Development of

Figure 5: Immunoreactivity of pNF-H in structures associated with the visual system. Figures 5a through 5e depict typical temporal patterns of pNF-H immunoreactivity as seen in structures within the developing rat brain from postnatal day 9 through 15. The x-axis is a time line beginning on P9 and divided into units of one day. The y-axis demonstrates the percentage of total sections which run through the selected structure that are stained. The z-axis shows the total number of pups with staining in the selected structure. Once immunopositivity has been acheived, subsequent immunoreactivity may be discontinuous, as is seen in Table 2. Possible causes for this discontinuity are discussed in the text.

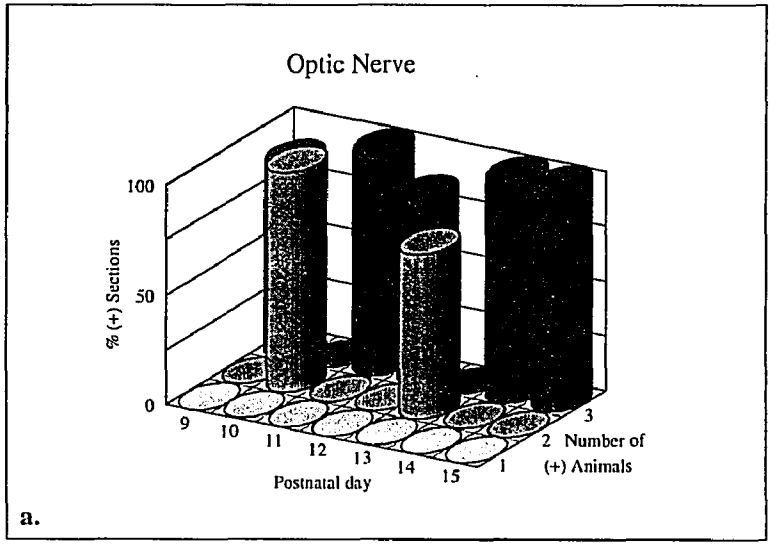
Optic Nerve
100
50
0
% (+) Sections
9
10
11
12
13
14
15
Postnatal day
1
2
3
Number of
(+) Animals
a.

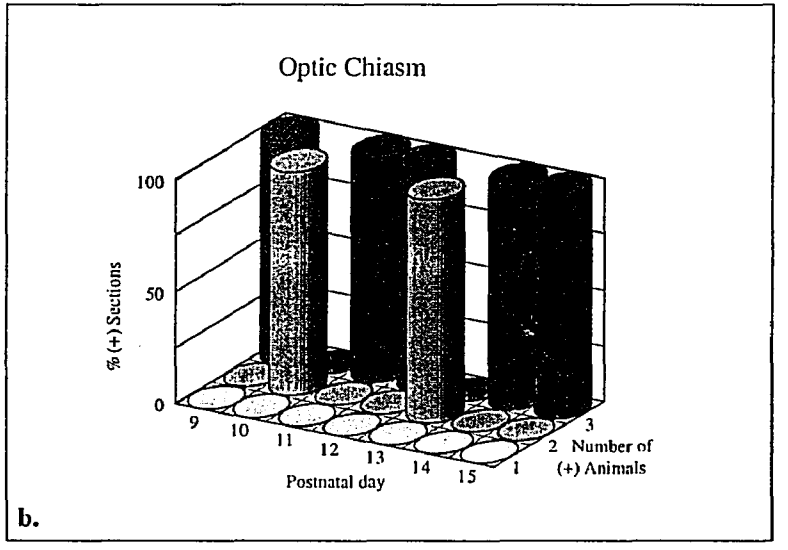
Optic Chiasm
100
50
0
% (+) Sections
9
10
11
12
13
14
15
Postnatal day
1
2
3
Number of
(+) Animals
b.

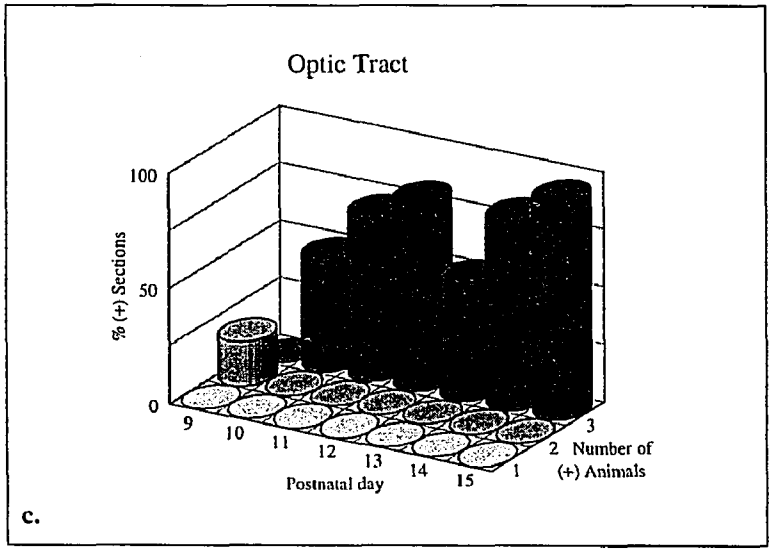
Optic Tract
100
50
0
% (+) Sections
9
10
11
12
13
14
15
Postnatal day
1
2
3
Number of
(+) Animals
c.

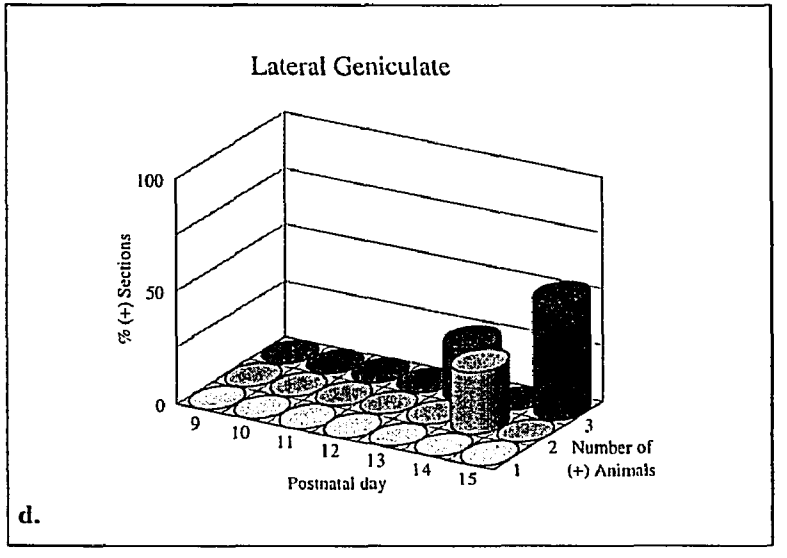
Lateral Geniculate
100
50
0
% (+) Sections
9
10
11
12
13
14
15
Postnatal day
1
2
3
Number of
(+) Animals
d.

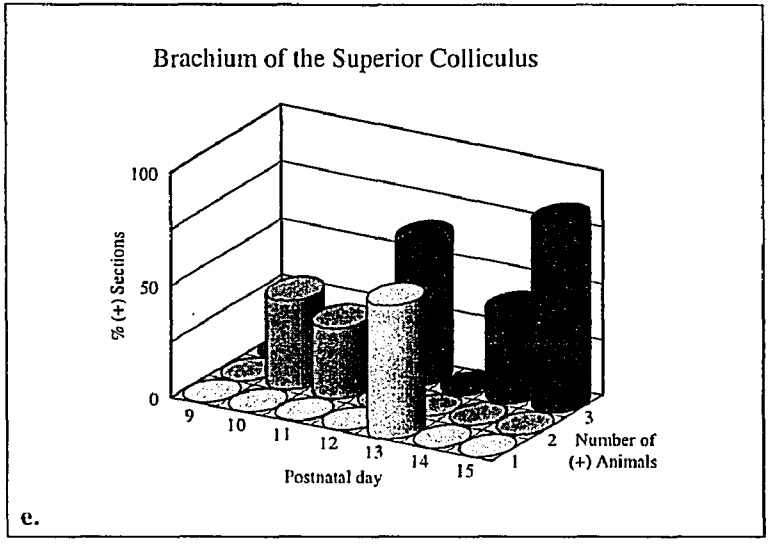

Figure 5 (continued)

one of these pups may be slow relative to the two others. For a particular structure, that single slowly-developing pup may not be producing pNF-H. As was stated in the Methods section, all three pups must immunohistochemically stain for the presence of pNF-H in the selected structure to be considered positive. If one of the pups is developing slowly, there is a failure to reach this criterion for positivity and staining is considered negative for that particular structure on that particular postnatal day. Because of that one slowly developing pup, the immunoreactivity of pNF-H after the onset of appearance of NF-H is therefore apparently, although not actually, discontinuous. If it was possible to follow the appearance of pNF-H in one animal, this explaination would suggest that once pNF-H appeared, it would be detected on all subsequent days.

Another explanation suggests that the discontinuity of positive immunoreactivity is real. In an effort to minimize differences in rates of development that are dependent on nutritional status, the pups chosen for this study were selected by weight. The weight of each of the three pups chosen to represent a given postnatal day was closest to the mean weight of all the pups that had been sacrificed on that day. It turned out that the chosen pups were all from the same three litters. Since, for each postnatal day, the pups were all of the same average weight and from the same three litters, differences in rates of development caused by nutritional factors should have been minimal. Since they were all housed in the same animal colony and maintained in the same manner, the differences in environmental stimulation should have been minimal. In short, the pups sacrificed on a given postnatal day should all be at the same stage of development.

Rather than describing a two level state, where the accumulation of a new biological product follows a smooth sigmoidal rise from steady baseline levels to a new plateau, onset of production during development seems to rapidly rise from baseline levels to a high level then to undergo a series of dampened oscillations until the new, high level is maintained (Harden *et al.* 1977; K.. :son, 1967). This situation is reflected in results that follow the development of pNF-H immunoreactivity in the optic tract (figure 5c). The onset of pNF-H immunoreactivity occurs on P10. The percentage of optic tract sections which stain for pNF-H increases until P13, whereupon the percentage drops. During the following days, the percentage of sections which stain for pNF-H again increases. Within the temporal resolution of this study, immunoreactivity of pNF-H seems to follow a oscillatory pattern. This situation may also have occurred in a more dramatic fashion in the lateral geniculate (figure 5d). In this case, immunoreactivity of pNF-H, initiated on P13, may have ceased altogether on P14 in one animal. A similar pattern is also illustrated in the subiculum (figure 4d) and is replicated in most of the other instances of interrupted immunoreactivity documented in table 2. Perhaps with higher temporal resolution, the situation found in the brachium of the superior colliculus (figure 5e), where only one animal is found to stain for the presence of pNF-H one day after onset of appearance of pNF-H, would be found in other structures.

Descriptions of pNF-H immunoreactivity which follow have been grouped to reflect the regions as they were dissected for analysis in the work of Fischer and Shea (Fischer and Shea, 1991).

a. Brainstem and cerebellum

Immunochemical evidence for the presence of pNF-H can be demonstrated in the brainstem and cerebellum before the developmental window chosen for this study (Carden *et al.* 1987). In a preliminary study carried out in our laboratory, it was observed that the spinal trigeminal tract and fibers within the trigeminal nucleus account for most of the pNF-H found in the brainstem at birth (see figure 6a-d). By postnatal day 5 [P5] immunohistochemical staining for the presence of pNF-H had rapidly spread and was found in the superior [scp] and middle cerebellar peduncles [mcp] and central [ctg] and dorsal [dtg] tegmental tracts (see figure 6e-h). Most structures in the adult brainstem, including the lateral lemniscus [ll], medial longitudinal fasciculus [mlf] and inferior cerebellar peduncles [cp], are positive for the presence of pNF-H by P10. However, new structures, including the tracts within the lateral vestibular nucleus [LVe], that first stained on P14, and tracts within the red nucleus [R], that first stained on P15, continued to be added to the list of brainstem structures immunopositive for the presence of pNF-H (see table 2).

Although preliminary evidence showed that the superior and middle cerebellar peduncles demonstrated the appearance of pNF-H early in postnatal development (see figure 6h), the white matter within the rostral cerebellar lobules did not stain for the presence of pNF-H until P10 (see CbIII and CbIV in Table 2). According to the criteria for positive staining, cerebellar basket cells, which stain for the presence of pNF-H in the

Figure 6: A preliminary immunohistochemical examination of the distribution of pNF-H during postnatal development of the rat brain. Coronal sections of rat brains taken from pups on postnatal days 0 (figure 6a-d), 5 (figure 6e-h) and 8 (figure 6i-l) immunohistochemically stained using RMO24.9 (diluted 1:3000) as the primary antibody. The limits of the cerebral parenchyma have been defined with a continuous fine line. The measurement bars represent a 1mm length on the photographs. Because different parts of the brain develop at different rates (Fujita, 1990), the forebrain sections were defined as the section which included the intersection of the forebrain with the rhinencephalon (figures 6a,e,i). This section corresponds to the incision Fischer and Shea used to define the rostral limit of the cortex (Fischer and Shea, 1991). The diencephalic sections (6b,f,j) were selected as the most rostral coronal section to include all three hippocampal subregions CA1-3. Midbrain sections (6c,g,k) were chosen to include the point where decussation of the superior cerebellar peduncle [xscp] crosses midline. Cerebellar sections (6d,h,l) were chosen to include the most caudal point of insertion of the sensory root of the trigeminal nerve [s5] into the pons. Other abbreviations include that for the nuclei of the trigeminal nerve [5N], the corpus callosum [cc], the cingulum [cg], the cerebellar peduncles [cp], the central tegmental tract [ctg], the dorsal tegmental bundle [dtg], the external capsule [ec], the internal capsule including fibers in the striatum [ic], the lateral lemniscus [ll], the lateral lemniscal fields [LLF], the lateral olfactory tract [lo], the caudal portion of the pontine reticular nucleus [PnC], the pyramidal tract [py], and the stria medullaris thalami [sm].

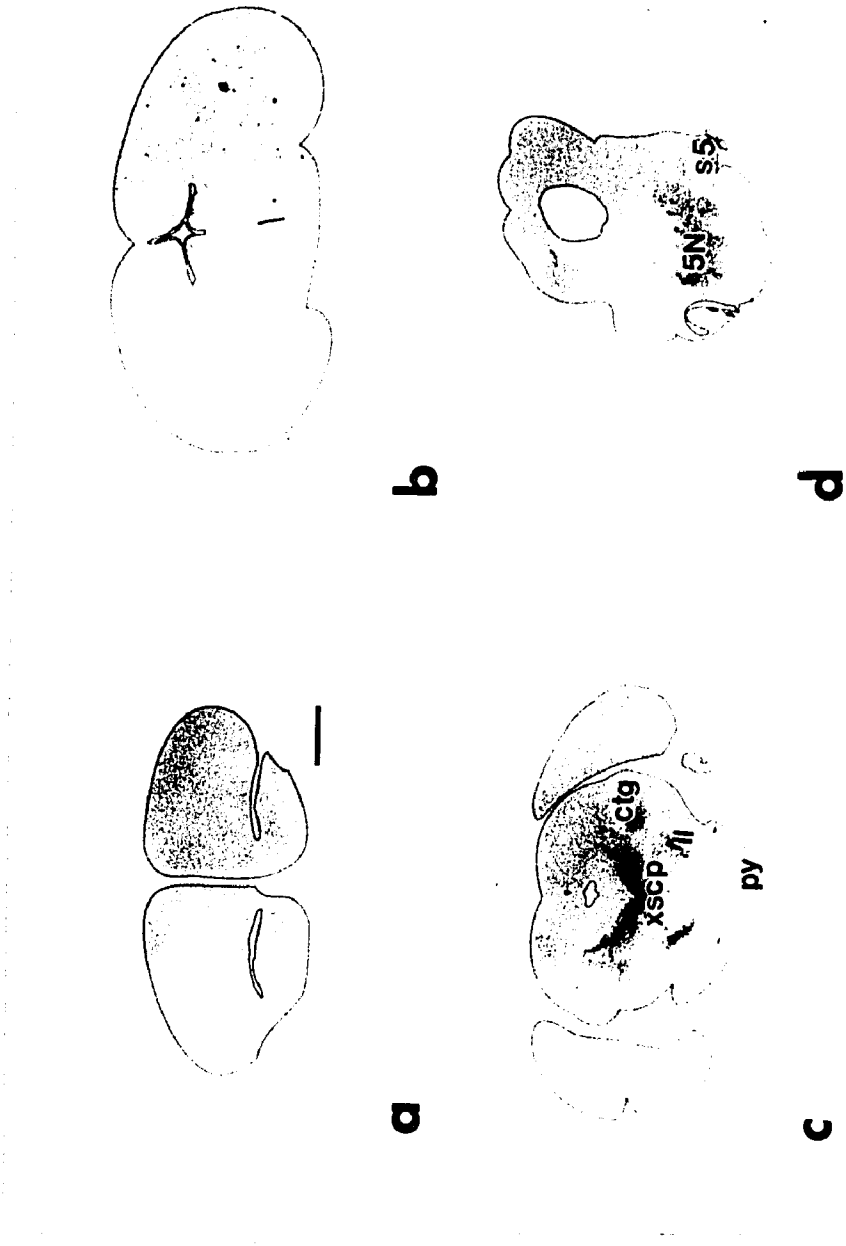
b
d
a
c
ctg
xscp
fil
py
5N
s5

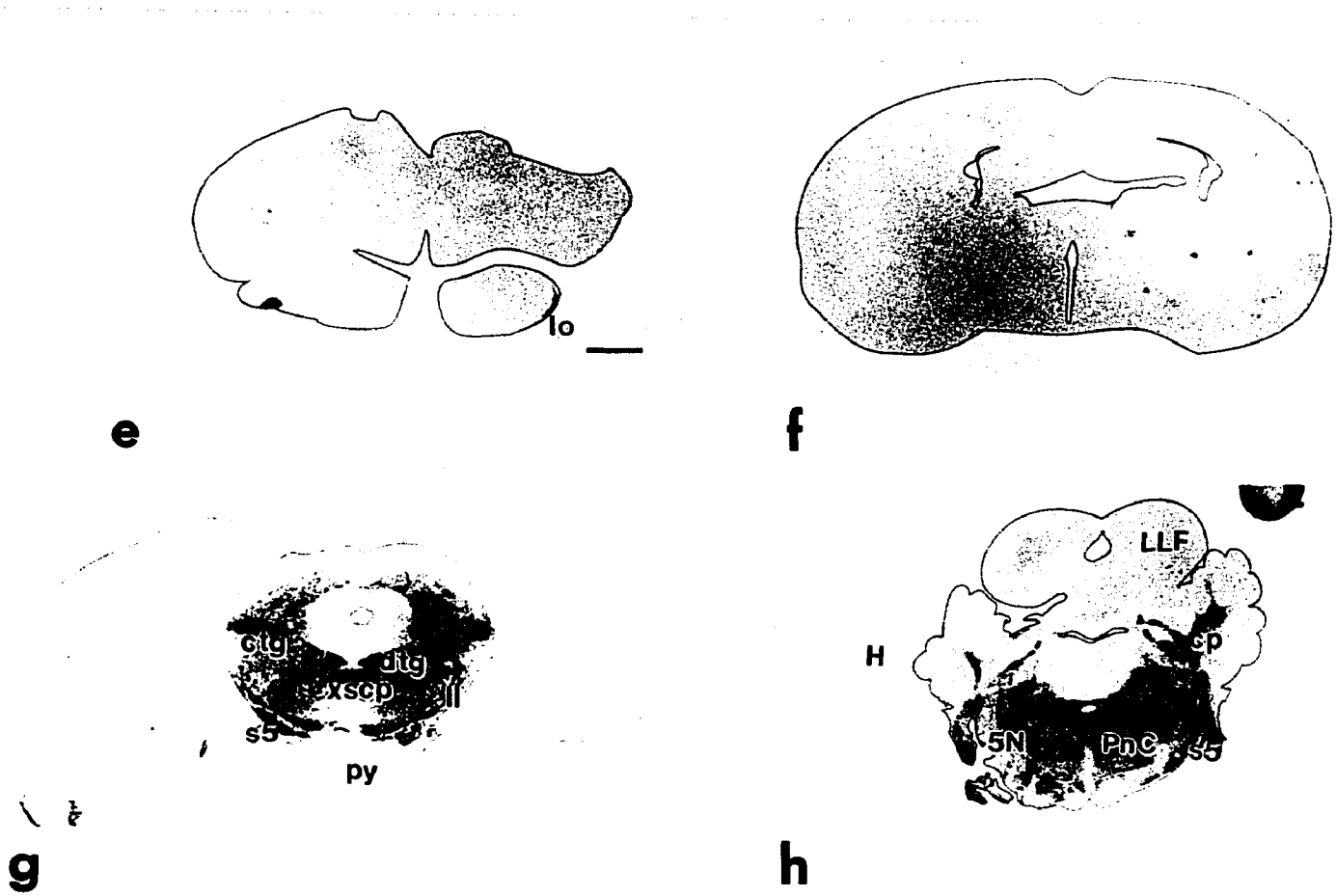

Figure 6 (continued)

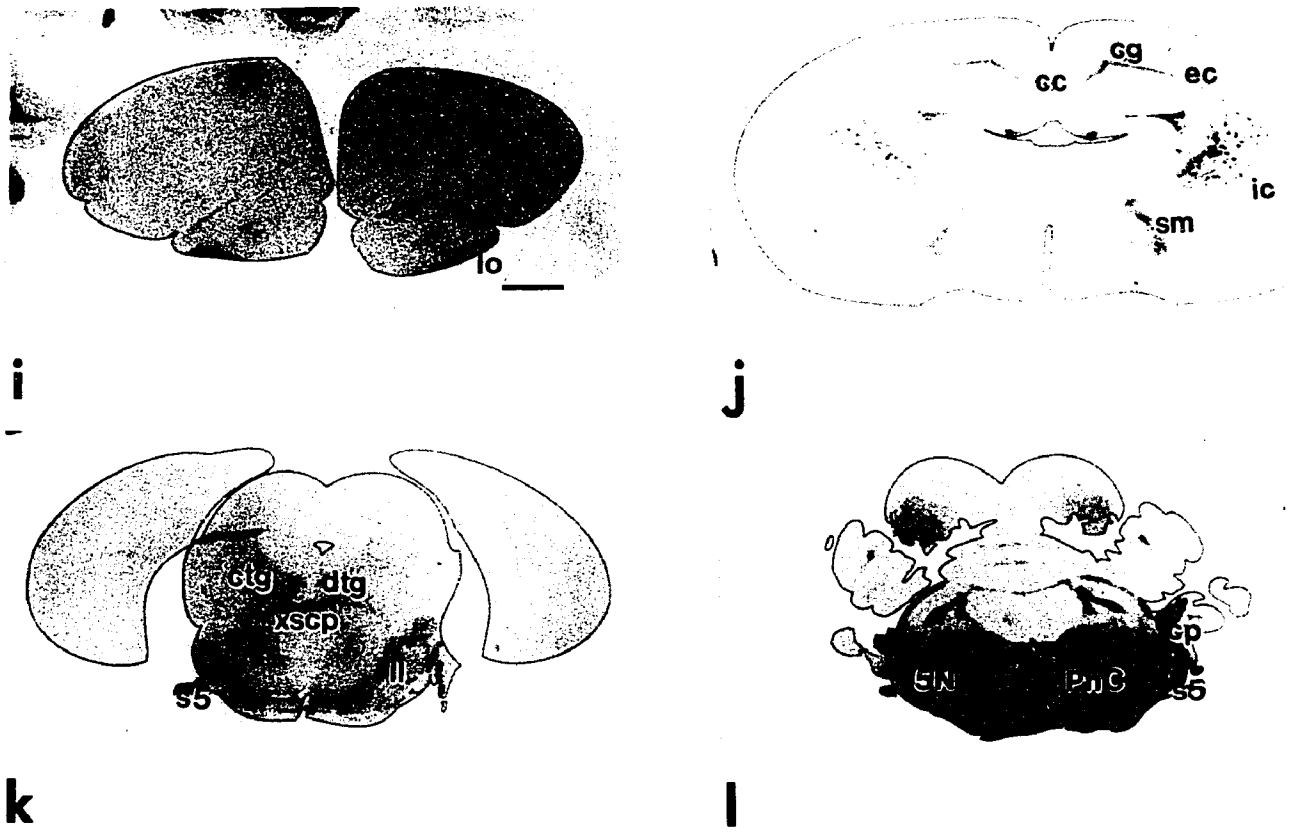

Figure 6 (continued)

adult (Troost *et al.* 1992), did not stain during the developmental window chosen in the present study.

b. cerebral cortex

The method of dissection Fischer and Shea used for removal of the cerebral cortex from the rest of the mouse brain excluded the hippocampus and assured that the lateral olfactory tract would be analyzed as if it were part of the cerebral cortex (Fischer and Shea, 1991). By postnatal day 8, the cerebral cortex proper was only showing background levels of pNF-H. On the other hand, the lateral olfactory tracts were staining for the presence of pNF-H at levels on or above intensity level 3 on that same day. Preliminary observations confirmed that, although not positive for pNF-H at birth, the lateral olfactory tracts reached adult levels of pNF-H staining by P5 (see figure 6e).

The cingulum [cg] reached significant levels of staining on P11, with most staining found in the more dorsal parts of this structure. None of the three subregions within the frontal, temporal or cir ·ılate cortex reached significant levels of staining. The Par 1 region of the parietal cortex stained transiently on P12. This was yet another case where staining was found in only one or two of the pups subsequent to the day of onset of pNF-H immunoreactivity. The occipital cortex was not included in the present study due to technical difficulties that arose during sectioning. The dorsal part of the brains which included the occipital regions would crumble apart under the microtome

blade and had a tendency to delaminate from the embedding block. The corpus callosum did not stain within the P9-P15 postnatal window.

c. hippocampus

By P9, axons of basket cells within the pyramidal cell layer in the CA3b region of the hippocampus [CA3p] stained at low relative intensities, but otherwise fulfilled all criteria for immunopositivity. Staining in this region remained at this low intensity, significant level throughout the study (see figure 4e). On P14, staining of basket cell axons in the CA3c region [CA3pc] became significant (see figure 4f). The following day, P15, staining of the radiata region of CA3 [CA3r] (see figure 4g), fibers within the dentate gyrus [DG] and the alveus [alv] became significant (figure 4c and 4h).

Although not included in the hippocampal dissection of Fischer and Shea (Fischer and Shea, 1991), hippocampal related structures including the fimbria [fi] and ventral hippocampal commissure [vhc] started staining for the presence of pNF-H on P12. The fornix , stria terminalis and nuclei of the amygdala did not stain during the period studied in the present study. However the habenular commissure [hbc] began to stain on P10, and the triangular septal nucleus [TS] on P11. Of the cortical regions related to the CA 1 through 4 regions of the hippocampus, entorhinal cortex [Ent] and its subregion, the amygdaloid fissure [AF], began to stain significantly on P10. The subiculum [S] did not stain until P12. Although an attempt was made to relate the temporal maturation of the

structures related to the hippocampus to classically described hippocampal circuits (Papez, 1937; Domesick, 1969; Domesick, 1970), no trans-synaptic sequence of maturation was apparent.

d. olfactory bulb

No significant staining of the olfactory bulb was present until P10. At that time, pNF-H staining became visible in fibers in the internal granular layer [IGr], internal plexiform layer [IPl] and intrabulbar anterior commissure [aci]. Fibers in the olfactory nerve [ON] stained for the presence of pNF-H by P12 and the vomeronasal tract [vn] by P13. The external plexiform layer [EPl] and mitral cell layers [Mi] of the olfactory bulb did not stain until P15. A discussion of lateral olfactory tract staining is included above in: "section b. cerebral cortex."

e. hypothalamus

None of the structures classically described as hypothalamic nuclei stained during the period of time included in this study. During this time period, the only structures to demonstrate the presence of pNF-H that were included in Fischer and Shea's (Fischer and Shea, 1991) "hypothalamic dissection," have their origin in the mammillary body. The mammillothalamic tract [mt] and the mammillary peduncle [mp] first showed evidence of staining on P15. Most of the axons in the mammillothalamic tract have their

Figure 7: The mammillothalamic tract. In this P15 rat brain, dark field (figure 7a and b) micrographs illustrate structures and bright field (figures 7c and d) micrographs illustrate areas immunohistochemically stained using RMO24.9 as the primary antibody. Figures 7a and 7c are the same horizontal serial section and are 480μm ventral to the horizontal section represented by figures 7b and 7d. Figures 7a and 7c represent an area of the hypothalamus close to the mamillary bodies, figures 7b and 7d represent an area closer to the main target of the mammillothalamic tract - the anterior ventral thalamic nucleus. The pale mammillothalamic tract is identified in figure 7a by an arrow; the pale optic tract by a flake symbol (✲). Although staining is apparent in the optic tract in figure 7c (also signified by the flake symbol (✲)), no staining for the presence of pNF-H is seen within the mammillothalamic tract (arrow in figure 7c). Staining of the mammillothalamic tract only becomes apparent as the tract approaches its main target (arrow in figures 7b and 7d). Other named structures include the anterior commissure [ac], anterior branch of the anterior commissure [aca], posterior branch of the anterior commissure [acp] and cerebral peduncle [cp]. The compact portion of the substantia nigra (identified in figure 7b by a star (✶) lying below the structure), is also stained (identified by the same star (✶)) in figure 7d.

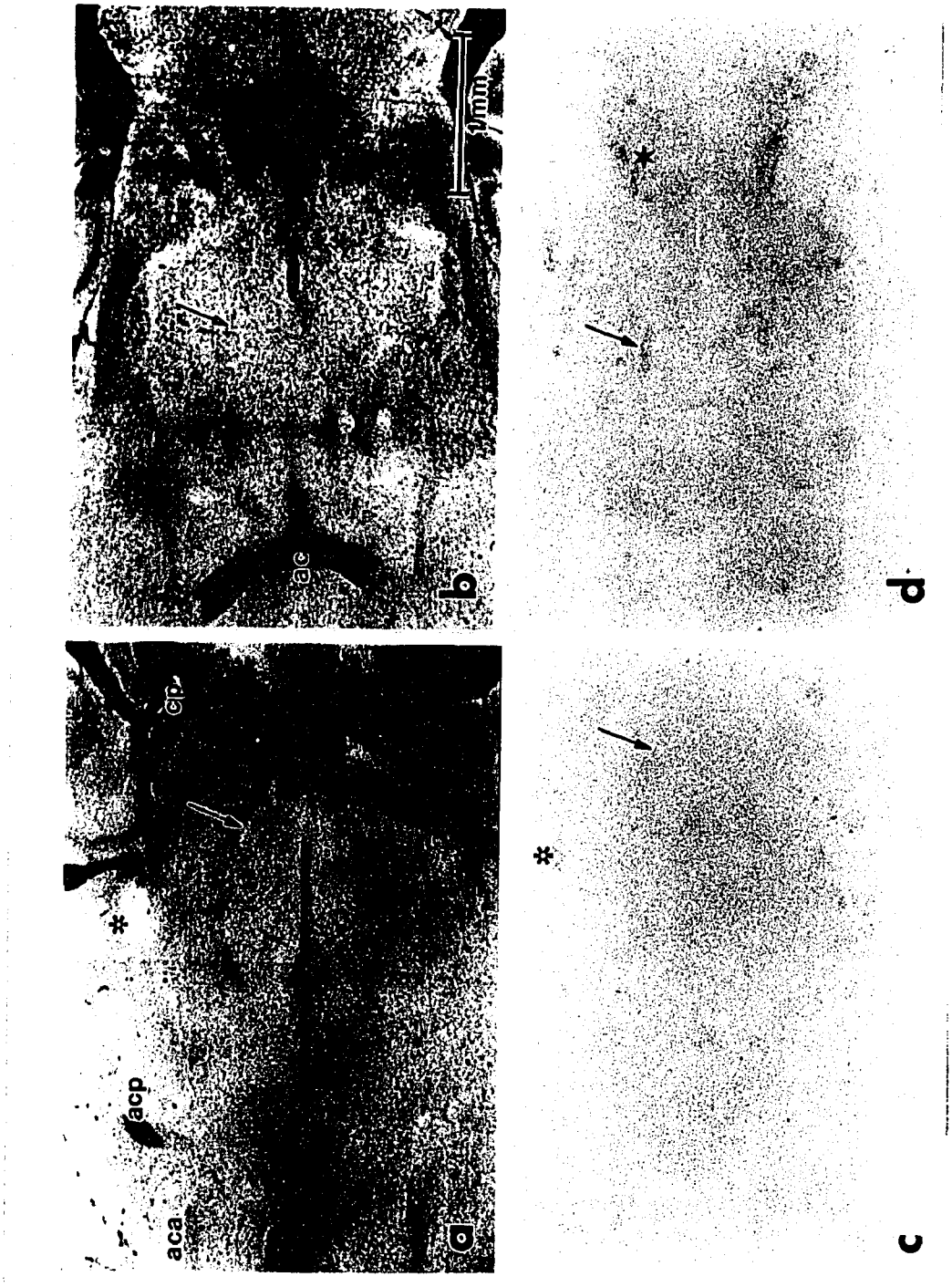
a
aca
acp
epa
*
b
ac
5mm
c
*
d
*

origin in the mammillary body (Cajal, 1955). Although the tract runs in a caudorostrad direction, staining for pNF-H follows a rostrocaudad gradient. No staining is seen near the nuclei of the mammillary body, immunostaining only becomes apparent as the tract approaches its main target - the anterior ventral thalamic nucleus (figure 7).

f. other telencephalic and diencephalic structures

In their dissection, Fisher and Shea (Fischer and Shea, 1991) discarded the striatum and diencephalon above the hypothalamus. Structures within these areas, which stain in at least one section for all three animals, are included in table 2.

Oral aluminum lactate toxicity

During the course of the study, and especially during lactation, the aluminum treated dams looked progressively more cachexic. Although maternal weight gain during gestation was comparable in aluminum-exposed and pair-fed controls (compare figure 8a and 8b), aluminum-treated dams lost weight while control dams maintained weight during lactation (compare figure 8c and 8d). The urine of the aluminum treated dams was darker than that of controls. Three of the experimental dams died perinatally (2 postnatally, 1 prenatally). One of the control dams developed a tumor. One of the aluminum exposed mothers and three of the control mothers were used to measure blood levels of aluminum and not prepared for histological examination (the results are not

Figure 8: Weight of rat dams during gestation and lactation. During gestation, the increase in weight of aluminum-exposed dams (figure 8c) was similar to that of Great Bear® pair-watered control dams (figure 8a). However, during lactation the weight of aluminum-exposed dams decreased (figure 8d) although the weight of control dams remained stable (figure 8b). The decrease in weight of the aluminum-exposed dams became significantly different from controls toward weaning (for P10-P12, $p \leq 0.02$ (marked by one asterisk (*)); for P13-P15, $p \leq 0.008$ (marked by two asterisks (**)); for P16-P18, $p \leq 0.0007$(marked by three asterisks(***))). Since dams were weighed twice a week (Monday and Friday) and matings were staggered, mean weights and error bars representing standard deviation of the samples were calculated from three day averages beginning on the first gestational or first postnatal day. The number of dams used in each calculation is found over each error bar. Significance of differences between experimental and control dam weights was calculated using a two-tailed Student's *t-test.*

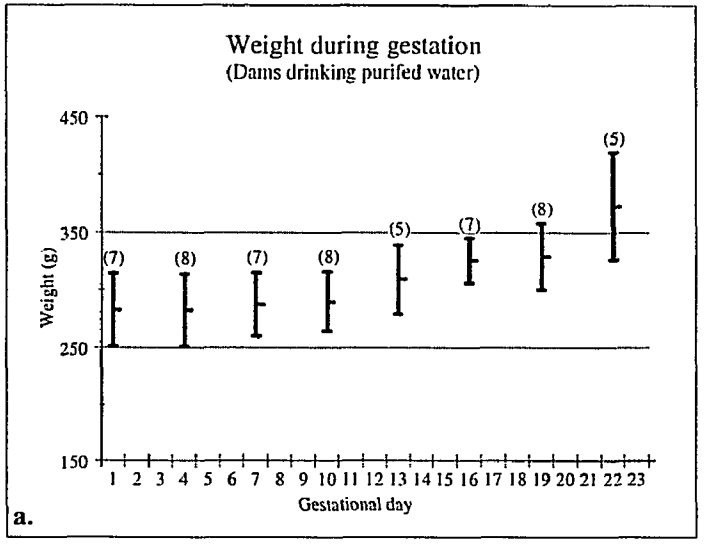
Weight during gestation
(Dams drinking purifed water)
Weight (g)
450
350
250
150
(7) (8) (7) (8) (5) (7) (8) (5)
1 2 3 4 5 6 7 8 9 10 11 12 13 14 15 16 17 18 19 20 21 22 23
Gestational day
a.

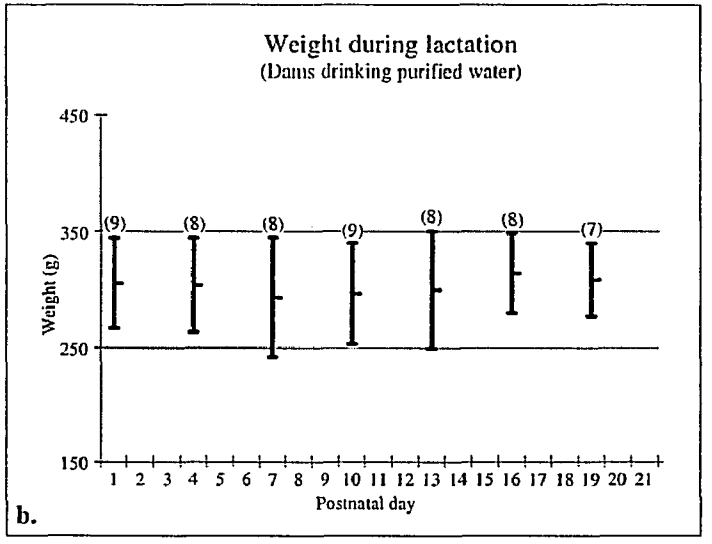
Weight during lactation
(Dams drinking purified water)
Weight (g)
450
350
250
150
(9) (8) (8) (9) (8) (8) (7)
1 2 3 4 5 6 7 8 9 10 11 12 13 14 15 16 17 18 19 20 21
Postnatal day
b.

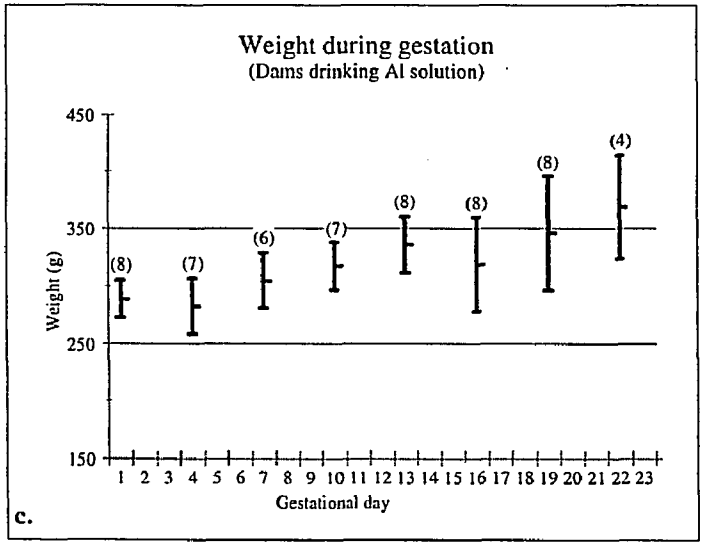
Weight during gestation
(Dams drinking Al solution)
Weight (g)
450
350
250
150
(8) (7) (6) (7) (8) (8) (8) (4)
1 2 3 4 5 6 7 8 9 10 11 12 13 14 15 16 17 18 19 20 21 22 23
Gestational day
c.

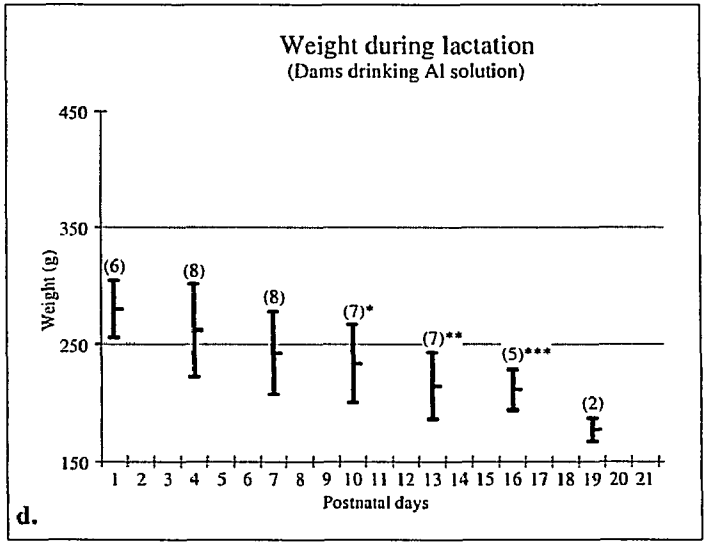
Weight during lactation
(Dams drinking Al solution)
Weight (g)
450
350
250
150
(6) (8) (8) (7)* (7)** (5)*** (2)
1 2 3 4 5 6 7 8 9 10 11 12 13 14 15 16 17 18 19 20 21
Postnatal days
d.

presented here).

a. Neuropathology of pup CNS:

Our initial results showed that, unlike the brain sections from control P11 pups, brain sections from a P11 pup born to and raised by an aluminum-treated mother showed little staining in tracts within the forebrain. Sections of brains from control pups stained strongly for the presence of pNF-H in the fimbria, stria medullaris thalami and internal capsule (figure 9A). The brain of the aluminum exposed pup stained weakly in these areas and not at all in the cingulum (figure 9a). By P14 staining patterns in both groups of pups were similar.

b. Histopathology of dam viscera:

The stomach and kidneys of the aluminum treated dams analyzed (11/11) all had lesions. All kidneys in treated dams contained calculi (figure 10a) which were not birefringent when examined in polarized light. The renal cortex was thinner than in untreated animals (figure 11a) and showed signs of tubular atrophy and loss (mostly proximal tubules). Clusters of cells with dark nuclei, eosinophilia and no lumen were indicative of tubular regeneration (figure 12a).

Gross examination of each stomach revealed multiple focal areas of ulceration and erosion (figure 10b). The glandular fundic stomach showed chronic active inflammation of lamina propria and submucosa (especially in eroded areas) with abundant eosinophils and plasma cells (figure 13a). Duodena and livers of treated mothers did not differ from controls. No lesions were found in the stomach and kidneys of any of the control mothers (figures 10A, 10B, 11A, 11B, 12A, 13A).

Figure 9: Delay of immunohistochemical staining for pNF-H in a pup's brain after maternal exposure to aluminum lactate. Postnatal day 12 pup brains (coronal section). (**A**)In the untreated control, RMO24.9 binds to tracts within the diencephalon. (**a**) When the pup's dam was given Al lactate in her drinking water a reduced number of tracts bind RMO24.9. (5x)

A a

Figure 10: Gross anatomy of the dams' kidneys (mid sagittal section) and stomachs (sectioned along the greater curvature). Kidneys of aluminum-exposed [Al-Rx] mothers have renal calculi (arrow in figure 9a) and (**b**) stomach ulcerations (arrows in figure 9b). These lesions were found in all the Al-Rx dams studied and none of the control dams studied. Pair-watered control dams show (**A**) normal kidneys and (**B**)normal stomachs. (2A, 1.7x; 2a, 1.7x; 2B, 1.7x; 2b, 1.7x)

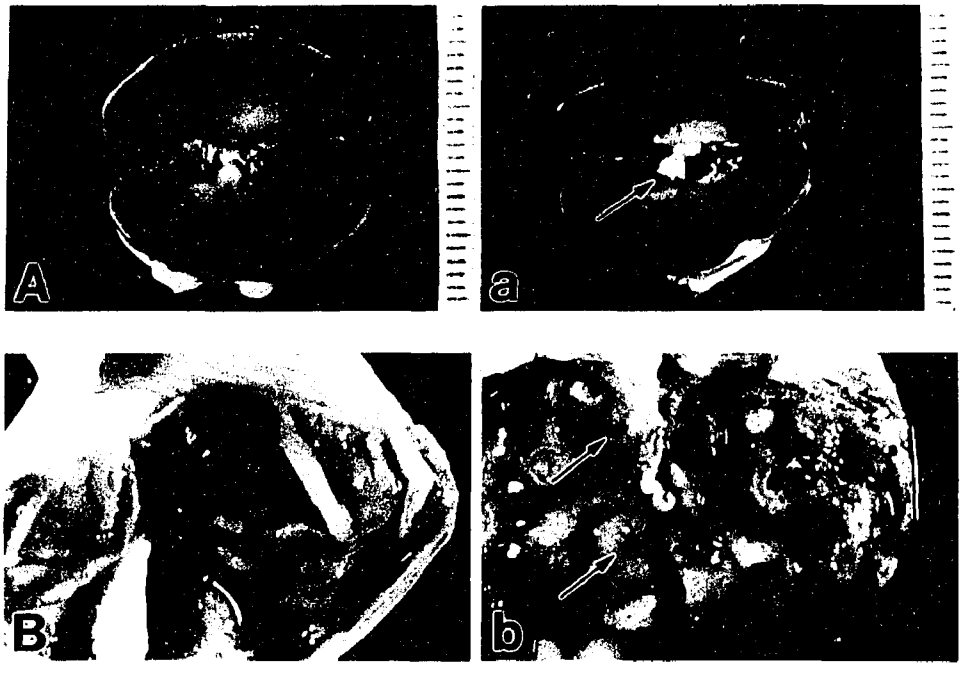
A
a
B
b

Figure 11: Low-magnification micrograph of the dams' kidneys (sectioned perpendicular to the long axis at the level of the pelvis) suggests thinning of the cortex in Al-Rx dam (**a**) versus that in control dam (**A**) (see bracketed areas). (12x)


A
a

Figure 12: High magnification of the dam's renal cortices. (**A**)Control dam's cortex. (**a**) Al-Rx dam's cortex shows tubulopathy (atrophic tubules or loss of tubules along with clusters of cells (arrowhead) suggesting tubular regeneration) and interstitial inflammatory cells (arrow). (2000x)

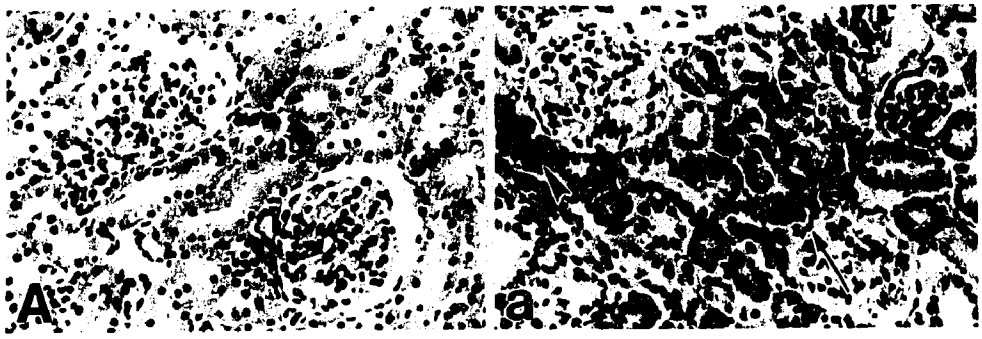
A
a

Figure 13: High magnification of the junction of the fundic stomach (glandular) and forestomach (nonglandular) shows its normal appearance in the (**A**) control dam and (**a**) erosion (arrow) and submucosal inflammation with both abundant eosinophils and plasma cells (arrowhead) in Al-Rx dam. (5A, 100x; 5a, 100x)


A
a

Discussion:

Many of the molecular and behavioral events that occur during the postnatal development of the nervous system are organized as a series of critical periods or critical milestones (Harden *et al.*1977; Walton *et al.*1992; Altman and Sudarshan, 1975; Nona *et al.*1985). Studies have approached both the molecular and the behavioral events of brain development by separating the events into their component parts and analyzing the factors influencing each step. However, because of the large amount of information to integrate, the relationship between molecular events and behavioral events remains unclear. Superficially, the development of behavior follows a linear course as simple behaviors become more and more elaborated and complex. But even the most simple behaviors rely on the integrated activity of several parts of the nervous system. If the biological development of the nervous system is a reflection of the behavioral development and also follows a linear pattern of maturation from the simple to the complex, it becomes imperative to identify and document the development of its functional biological units. Such documentation involves the collection and integration of a large amount of data. This part of the task has been facilitated by the use of computers and database software. Documentation of the pattern of development also demands selection of a marker of maturation. Part of the goal of this research has been to explore use of pNF-H as such a marker.

The ideal marker, selected to document any hierarchical process involved in

biological development of the CNS, must fulfill certain criteria. First, and perhaps most importantly, the marker must be specific to the neurons. Not only do different tissues develop at different rates as the whole organism ages, each tissue reacts in a unique way to changes in its local environment. Relating changes in the expression of a non-neuronal marker to neuronal events could be di. :ult. This would especially be true for a marker expressed in cells within the parenchyma of the nervous system but ancillary to the neurons. Secondly, the marker must be unique. Different neuronal markers, even those making up the cytoskeleton, are expressed at different times during development. If the characteristics of a marker are shared by more than one component of the neuron, it becomes impossible to disentangle causal or sequential relationships. Thirdly, since the neuron is a specialized cell with several specialized functions (eg. transduction of electrical or neurohumoral changes, integration of stimuli and transmission of a neural impulse), the relationship of the chosen marker, having one neural function, to other developmental markers, with other neural functions, should be known. Fourthly, if global development is to be observed, the marker should not be specific to a particular subsystem. For example, a marker for neurohypophyseal peptides could not give a global view of CNS development. Similarly, the ideal marker should describe all periods in the life of a neuron - from initial differentiation to cell death. To allow corroboration of evidence, it would also be desirable for the marker to be detectible at several different levels of resolution and by several different techniques. Its detection should be non-invasive and not require the introduction of a foreign substance into the living tissue. It would also be beneficial if the marker, though giving a representative sample of all parts

of the nervous system, did not saturate the technique for its detection. The following discussion suggests how closely pNF-H comes to this ideal.

Specificity

Other studies following the phosphorylation during the course of development have used monoclonal antibodies, especially the monoclonal SMI31 (Nukina *et al.* 1987; Fischer and Romano-Clarke, 1990), which recognize epitopes on both pNF-H and pNF-M (Bush and Gordon-Weeks, 1994; Liu *et al.* 1994; Sawant *et al.* 1994; Dahl *et al.* 1992; Fischer and Shea, 1991; Hewitt *et al.* 1991; Durham, 1990; Fischer and Romano-Clarke, 1990; Shea *et al.* 1989; Schilling *et al.* 1988; Dahl, 1987). Since the purpose of this study was to document the onset of NF-H phosphorylation rather than the onset of global neurofilament phosphorylation, a highly specific monoclonal antibody, RMO24.9 was selected to be used as the primary antibody in immunohistochemistry. When RMO24.9 was used as the primary antibody in Western blots of cytoskeletal proteins, it not only bound just one neurofilament protein - pNF-H, but it also did not bind other cytoskeletal proteins recognized by SMI31 - such as the developmentally regulated proteins tau and MAP1B (Fischer and Romano-Clarke, 1990; Bush and Gordon-Weeks, 1994; Lichtenberg-Kraag *et al.* 1992; Larcher *et al.* 1992). This binding activity was so specific that, in Western blots of cytoskeletal preparations and immunocytochemical staining of brain tissue, binding activity could be blocked by absorption with pNF-H, but not with the antigenically similar protein pNF-M.

As the concentration of an antibody increases, the probability that it binds non-specifically also increases. Other studies have ignored this possibility and did not dilute the RMO24 ascites (Carden *et al.* 1987). By using a dilution of RMO24.9 optimized for detection of pNF-H in the adult brain, the present study lessens the possibility that RMO24.9 binds to epitopes on other proteins or on NF-H before it has undergone sufficient post-translational phosphorylation to assume its adult form.

Once the primary antibody and optimal dilution for the primary antibody were selected, the criteria used to designate positive staining of a particular structure [immunopositivity] had to be chosen. The three critera chosen: 1) staining of any section 2) that includes a structure named in the Paxinos atlas of the rat brain (Paxinos and Watson, 1986), in the brains of 3) all three pups, all had to be present for a structure to be designated immunopositive. Since these criteria imposed restrictions on the study, these restrictions must be defined before the data can be correctly interpreted. Not all the subregions of a neuroanatomic structure mature at the same rate (Bayer, 1990; Altman, 1972) and J. Lund (personal communication)). Since a goal of this research was to obtain a global description of onset of pNF-H immunoreactivity, regional differences in time of onset of staining within a structure named in the Paxinos atlas of the rat brain were generally not considered. This criterion therefore biased the present study to call the date of onset of appearance of pNF-H of the whole neuroanatomic structure equal to that of the most rapidly developing sub-region within that structure. Similarly, different pups, even pups within the same litter, develop at different rates (Jacobson, 1963;

Watson, 1903). The last criterion for immunopositivity was that all three animals had to show positive staining of the chosen structure. Assuming all other factors were equal, the selection of this third criterion would bias the study to equate the day of onset of pNF-H immunopositivity in a chosen structure to the day that structure became immunoreactive in the most slowly developing animal. Since all three criteria must be met for immunopositivity, the day of onset of appearance of pNF-H for a given structure is actually the postnatal day that pNF-H is first found in the most rapidly developing subregion of the given structure within the most slowly developing pup brain.

By selecting a single monoclonal antibody specific for a single epitope, the appearance of pNF-H within some areas of the developing CNS might have been missed. However, the present study on the developing rat agrees, for the most part, with the biochemical analysis of Fischer and Shea on the developing mouse brain (Fischer and Shea, 1991). Our histochemical analysis therefore compliments and, by increasing the resolution of the analysis, extends their biochemical analysis on the onset of NF-H phosphorylation.

In a preliminary study, we found widespread pNF-H immunoreactivity in the brainstem by P9. These results are consistent with the those of Fischer and Shea (Fischer and Shea, 1991). Because of the limited temporal resolution of their observations, Fischer and Shea also suggested that pNF-H levels in the cerebellum increased gradually during the first two postnatal weeks. Our preliminary results demonstrate a rapid

increase in staining for the presence of pNF-H in the cerebellar peduncles during the first week (compare figure 6d to 6h and 6l). The rapid rise during the first week is followed by a slower increase in cerebellar sub-cortical pNF-H (unpublished observation from this laboratory). Since Fischer and Shea did not include results from within the first postnatal week, they would have missed the rapid rise in cerebellar pNF-H levels. If the findings of Fischer and Shea are reinterpreted with this missing information, our results are consistent with the data they present . Similarly, Fischer and Shea show low levels of pNF-H on or before P7 and high levels on or after P14 in the hippocampus (which includes areas CA3c, CA3r, the dentate gyrus and the alveus), fiber tracts in the olfactory bulb and the hypothalamus (which, in their dissection, includes the mammillothalamic tract). These observations are in agreement with the present findings of onset of pNF-H immunoreactivity in these areas between postnatal days ten through fifteen (table 2).

The only major discrepancy between the data presented by Fischer and Shea and the data presented here is found in the cerebral cortex. Fischer and Shea documented a rise of cerebral pNF-H from basal levels which preceded the rise found in the present study by one week. However, their dissection of the cerebral cortex included portions of the lateral olfactory tracts. In preliminary observations, it was found that pNF-H was beginning to appear in the lateral olfactory tract by P5 (see figure 6i). Although the volume of the lateral olfactory tract is much smaller than the volume of the cerebral cortex, extremely high levels of pNF-H are found there. Fischer and Shea's results were expressed as relative rather than absolute levels of pNF-H. Expressed in this way, even if

the pNF-H from lateral olfactory tract was diluted by the rest of the cerebral cortex, levels of cortical pNF-H would be significant. It would therefore be expected that the increases in pNF-H immunoreactivity they found (P7) to be much earlier than the increases found for the cingulum (P11), the parietal cortex (P12) and that others have found for the rat visual cortex (P10) (Nona *et al.* '85). The present study is therefore in close agreement with the results of Fischer and Shea, and, by further increasing the temporal and spatial resolution of NF-H phosphorylation within the CNS, this study allows the phosphorylation of NF-H to be associated with other indices of CNS maturation.

Table 2 lists structures that are immunopositive during postnatal days nine through fifteen. The onset of appearance of the epitope recognized by RMO24.9 varies temporally and spatially. Different tracts within the forebrain and midbrain bind RMO24.9 at different times after birth. Since binding of RMO24.9 varies temporally and spatially, the onset of activity of the kinase responsible for phosphorylation of the specific site on NF-H recognized by RMO24.9 therefore varies temporally and spatially. The kinase is therefore developmentally regulated. The appearance of NF-L and NF-M has been associated with the embryonic differentiation of primordial cells and the 'birth' of neurons (Carden *et al.* 1987). But pNF-H does not appear until after birth of the pups. With what is the postnatal activation of the RMO24.9 epitope kinase associated? Behavioral studies of the rat during the early postnatal period suggest that certain behaviors found in the adult are first produced at specific times after birth of the pup

(Tilney, 1933; Altman and Sudarshan, 1975). However, the behaviors that have been described, including pivoting, righting and homing are complex locomotor activities. As such, they involve the coordinated function of many discrete neural pathways. Behavioral indices of development which involve global neural activity cannot be correlated with onset of production of a specific kinase within a specific tract. However, there are other indices of development which can.

Postnatal development of the central nervous system involves onset of myelination, increases in numbers of mature synapses, and changes in the electrophysiology of discrete areas of the brain. Myelination of the axon has recently been associated with the phosphorylation of NF-H and therefore holds the most promise of associated development.

Myelination

NF-H is not homogeneously phosphorylated along the axon. Fast conducting axons in the central and peripheral nervous systems are wrapped in a myelin sheath. These internodal wrapped regions are separated by nodal breaks in the continuity of the sheath. Mata and colleagues (Mata *et al.* 1992), studying cross-sections of the adult rat sciatic nerve found that NF-H phosphorylation was also not continuous along the axon. The density of immunoreactive staining for pNF-H in the axon at the node is reduced 60% relative to the internodal region. Since density of immunoreactive staining for pNF-

H was reported as density of stain per cross-section area rather than percentage of total neurofilaments that were stained, the reduction in staining Mata and colleagues found might have simply been due to a decrease in packing density of the neurofilaments at the node. Indeed, Reles and Friede found that there was a reduction in numbers of neurofilaments - with 30-50% as many neurofilaments in the nodal region compared to the internodal region (Reles and Friede, 1991). Similarly, Price and colleagues found 15-41% as many neurofilaments (Price *et al.*1990). However, the cross-sectional area of the axon is also reduced and the packing density of the neurofilaments was found to be either the same in both regions, (Reles and Friede, 1991) or even increased in the node (Price *et al.*1990; Hsieh *et al.*1994). Therefore, if the neurofilament triplet ratio is maintained at the node as in the internode, the reduction in staining for pNF-H that Mata found at the node (Mata *et al.*1992) may reflect a reduction in phosphorylation of NF-H. Although his decrease in phosphorylation in areas with a reduced myelin sheath that Mata found in the rat must be confirmed by immunohistochemistry at the electron micrographic level, it has also been demonstrated in other animal models. De Waegh and colleagues replaced a section of sciatic nerve from a normal mouse with a graft of myelin-deficient sciatic nerve from a Trembler mutant mouse (de Waegh *et al.*1992). The sciatic nerve axon of the recipient mouse was allowed to regrow through the grafted section. The myelin-deficient grafted region responded as if it was in a myelin-deficient nodal region. Phosphorylation of NF-H in axons recovered from the myelin-deficient graft section was found to be reduced, the density of neurofilaments was twice normal and the mean axonal diameter was found to be reduced. Phosphorylation of NF-H in axons proximal to

the graft region approached normal high levels. The diameters of the axons were also normal. Transgenic mouse models in which myelination is disrupted by various amounts, have also confirmed the finding that the degree of phosphorylation of axonal NF-H is related to the degree of myelination of the surrounding sheath (Cole *et al.* 1994). The association between myelination and phosphorylation of NF-H is also evident in the central nervous system. Axons from retinal ganglion cells leave the orbit of the eye to form the optic nerve. In the adult rat, most of these axons are myelinated (Cuenca *et al.* 1987). However, myelination is not evident for a distance of 150-200μm from the exit of the optic nerve from the orbit (Nixon *et al.* 1994). Similarly, binding to the optic nerve of monoclonal antibodies specific for KSP triplets on NF-H (and M), is not found for 200μm from the exit (Nixon *et al.* 1994). Again, activity of the NF-H kinase seems to be related to the presence of myelin.

The sequence of events leading to myelination of the rat central nervous system axon has best been described from ultrastructural studies of the optic nerve by Hildebrand and Waxman (Hildebrand and Waxman, 1984). At birth, virtually all the retinal ganglion cell axons collected to form the rat optic nerve have formed their central connections (Lund and Bunt, 1976). However, these axons do not become ensheathed in oligodendrocytes until six to eight days after birth (Hildebrand and Waxman, 1984). After a two day hiatus, during which the sheath may become up to four cytoplasmic layers thick, Hildebrand and Waxman found that myelin condensation begins. Unlike Schwann cells in the peripheral nervous system, oligodendroglia on contiguous segments

of the same axon rarely touch. Around this period of time, a distinct axolemmal undercoating first becomes evident. This marks the appearance of the specialized node of Ranvier. Also around this time, a second glial cell, the astrocyte, becomes associated with the node (Hildebrand and Waxman, 1984; Black and Waxman, 1988).

Onset of myelination and onset of pNF-H immunoreactivity coincide during development. To reiterate, oligodendrocytes are first apparent in the rat optic nerve on P6 (Vaughn, 1969). By P10 myelination of the optic nerve has begun (reports vary: (Vaughn, 1969): onset between P8 and P10; (Cuenca *et al.*1987): onset between P5 and P9; (Foster *et al.*1982): onset between P7 and P9)). Cuenca and colleagues (Cuenca *et al.*1987) counted neurofilaments in electron micrographs and found an increase in the number of optic nerve neurofilaments between P9 and P13. Pachter and Liem, using gel electrophoresis, (Pachter and Liem, 1984) found an increase in pNF-H in the rat optic nerve between P10 and P20. The present study, using an immunohistochemical technique, showed that pNF-H first appeared in the optic nerve by P10 (see table 2). Onset of myelination (by P10) therefore preceded or coincided with the onset of pNF-H immunoreactivity in the optic nerve. Onset of myelination in the superior colliculus (P15) (Lund and Lund, 1972) also preceded onset of pNF-H immunoreactivity (P16 for the intermediate [InWh] and deep [DpWh] white layer of the superior colliculus (see table 2)). Jacobson (Jacobson, 1963) followed the appearance of staining using the Weigert myelin sheath stain. His study included postnatal days 7, 10 12 and 14 and his results showing the appearance of myelination are shown beside results from the present

study in Table 2 (marked as 'o'). Except for the optic tract [opt], brachium of the inferior colliculus [bic], and intrabulbar anterior commissure [aci], myelination of tracts and axons within nuclei in the developing rat brain precedes onset of appearance of pNF-H by 1-4 days in fifteen of the eighteen structures in which correlations can be made (CPu, DLG, DpWh, InWh, Parl, SNC, VPM, alv, cg, [illegible], dhc, fi, ml, mp, mt). In some structures (cp, ec, ic, ll, lo, pc, s5, scp, sm), myelination of axons and immunopositive pNF-H staining was present throughout the window of time included in the present study. No correlation could be made between onset of immunoreactivity of pNF-H and myelination of these latter structures because the developmental window used in the present study did not include the earlier postnatal days when staining first appeared. However, the eighteen structures for which correlations could be done were analyzed to find the temporal relationship between their onset. Unlike the present study, Jacobson did not analyze daily changes in staining. A structure that he reported to first stain on P10 might have been found to first stain on P10, P9 or P8 if he followed daily changes. A structure that he reported to first stain on P12 or on P14 might have first stained on those days or on the preceding day. For this reason, a non-parametric statistic was calculated using two sets of data. The first assumed the minimal difference between day of onset of myelination and onset of pNF-H immunopositivity. Using this assumption, no significant difference is found between the day of initiation of pNF-H immunopositivity and the day of onset of myelination ($p \leq 0.13$). The second data set assumed the maximal possible difference between day of onset of myelination and day of onset of pNF-H immunopositivity. Using this assumption, it was determined that onset of pNF-H

immunopositivity follows onset of myelination ($p \leq 0.001$). Therefore, although the onset of appearance of pNF-H and the onset of myelination each occur in different tracts at different times during the early postnatal period, a temporal relationship exists between the two parameters that is independent of the area of the brain these two occur. In statistical terms, there is no evidence that the onset of appearance of pNF-H is systematically found before the onset of myelination. In practical terms, myelination and the onset of pNF-H immunoreactivity are linked and the initiation of myelination may precede (by a mean of 2 days) or occur simultaneously with the initiation pNF-H immunoreactivity.

Electrophysiologic maturation and synaptogenesis

The interaction between onset of appearance of NF-H, synaptogenesis, and onset of electrophysiological maturation has been best documented in the visual system. The manner in which these parameters interrelate becomes most clear if the development of the visual cortex, and lateral geniculate, superior colliculus and retina are considered separately. The first postnatal day is defined as P0 in all the following papers.

Nona and colleagues, using the monoclonal antibody RT97 as the primary antibody for Western blots of the rat visual cortex, found no pNF-H prior to postnatal day 10 but high levels by P15 (Nona *et al.* 1985). An analysis of the immunohistochemical

distribution of pNF-H appearance over time has not been followed in the rat. However, Liu and coworkers, like Nona and coworkers, using a monoclonal antibody which recognized phosphorylated epitopes on both NF-M and NF-H (SMI31), found that immunocytochemical staining spread throughout the cat visual cortex in a ventricular (layers V and VI) to dural (layer IV then II and III) direction (Liu *et al.*1994). Axons from the lateral geniculate of the rat, entering the visual cortex through the subplate layer, also seemed to follow this pattern of development. Kageyama and colleagues, following anterograde movement of the fluorescent carbocyanine dye, DiI with light microscopy, noted that rat geniculocortical axons invaded layers V and VI of the visual cortex on the first postnatal day and the anlagen of layer IV by P2. They also noted that synapse formation followed axonal invasion of the visual cortex and proceeded in the same ventricular to dural direction. By P3 presynaptic profiles were found in electron micrographs of layers VI and IV and, on the following postnatal day, in all cortical layers (Kageyama and Robertson, 1993). Once synaptogenesis had begun, it also proceeded in a ventricular to dural direction. M. W. Miller, counting the number of synapses on Golgi-stained pyramidal cells of the rat visual cortex, found that the number of axosomatic synapses began to increase over baseline values in layer V between three and six days after birth (P3-P6) and in layer II/III between six and nine days after birth (P6-P9). The number of synapses in both areas rose slowly until they reached a plateau at around P21 (Miller, 1986). Bähr and Wolff confirmed this slow increase in number of synapses with electron microscopy and documented that the synapses were the mature Gray type 2 (symmetrical) synapses (Bähr and Wolff, 1985; Gray, 1959).

Electrophysiological maturation of the synapses coincided with their histological maturation. Excitatory post synaptic potentials could be recorded from layer V pyramidal neurons in *in vitro* slices of the rat visual cortex after P5 and inhibitory post synaptic potentials after P9 (Kasper *et al.*1994). In summary, synaptogenesis began soon after birth in the rat visual cortex. Late in the first or early in the second week, the number of mature synapses on pyramidal cells began to increase and continued to increase in a nearly linear fashion until the third week after birth. This slow, two week increase in the number of synapses, superimposed over a ventricular to dural developmental gradient, seemed to proceed independently of the rapid increase in pNF-H levels Nona and colleagues found between P10 and P14 (Nona *et al.*1985). Synaptogenesis and the appearance of pNF-H seem to proceed along independent time frames. Electrophysiologic maturation of the rat cortex also coincided more closely with synaptic maturation than onset of pNF-H immunoreactivity. Crain found that the activity recorded from electrocorticograms of the rat cerebral cortex during the first postnatal week was irregular, intermittent and of low amplitude. Between the seventh and tenth postnatal days, during the time synapses were beginning to mature, periods of electrical inactivity, frequent during the first week, disappeared. The amplitude of the electrical activity increased during this same period and the frequency increased from a few hertz to about 20 hertz. Although the amplitude of the electrical activity increased on the fourteenth postnatal day, the electrocorticogram was "basically similar" to that of the adult by postnatal day ten (Crain, 1952). Nona (Nona *et al.*1985), studying immunoblots found the onset of pNF-H immunoreactivity in the visual cortex between P10 and P14

and that it increases steadily; Jacobson found the onset of myelination of layer VI of area 17 between P12 and P14, layer V and layer IV between P15 and P17 and fibers parallel to the cortical surface in layer IV between P18 and P21 (Jacobson, 1963). Again, onset and development of pNF-H immunoreactivity in the visual cortex most closely paralleled the onset and development of myelination.

This same lack of association between onset of NF-H phosphorylation and electro/synaptogenesis and association between synaptogenesis and maturation of evoked potentials is found in other parts of the visual system. Electrophysiological maturation closely follows synaptic maturation of the rat retina. Between the twelfth the fourteenth days after birth the tracing of the rat electroretinogram assumes a form similar to that found in the adult (Weidman and Kuwabara, 1968). The electroretinogram does not begin to mature until synapses form in the inner plexiform layer of the retina on P12 (Weidman and Kuwabara, 1968). The ontogeny of pNF-H immunoreactivity occurs independently. The optic nerve [2n] becomes immunopositive for pNF-H before both of these events occur (before P9). The lateral geniculate and superior colliculus receive input from the retinal ganglion cell axons via the optic tract and brachium of the superior colliculus respectively. Although synapses were present at birth in both the lateral geniculate (Karlsson, 1967) and superior colliculus (Lund and Lund, 1972), the morphology of synapses in these structures remains stable until a rapid increase of spherical-vesicle containing synapses begins. In the lateral geniculate [DLG], this rapid increase begins the seventh day and reached a plateau by P13 (Karlsson, 1967). By the

time the onset of pNF-H immunoreactivity has become significant in the lateral geniculate (P13), the maximal number of mature synapses has therefore already been attained. Even pNF-H immunoreactivity in the optic tract [opt], beginning on P10, seems to proceed independently of synaptogenesis in its target structure. In the zonal and superficial gray regions of the superior colliculi the rapid increase in mature spherical-vesicle containing synapses begins as early as ten days old and continued until a plateau was reached at twenty-four days old. Axons within the deep and intermediate layers of the superior colliculus did not become immunopositive for the presence of pNF-H until P15; axons leading to the superior colliculus in the brachium of the superior colliculus [bsc] did not become immunopositive for pNF-H until P10. For the superior colliculus, as for the visual cortex, maturation of the synapses seems to proceed independently of the state of NF-H immunoreactivity.

Synaptogenesis of the primary projection areas of the retinal ganglion cells therefore seems to progress independently of onset of NF-H phosphorylation. However, in these area of the CNS, onset of myelination again corresponds more closely to onset of pNF-H immunoreactivity than onset of synaptogenesis or onset of electrical maturity. Myelination of the more superficial layers of the superior colliculus began between P14 and P17 (reports vary for the onset of myelination: (Lund and Lund, 1972) (P14), (Jacobson, 1963) (P14-P17)). The present study documents the onset of pNF-H immunopositivity began within this period, on P16. Myelination of the lateral geniculate nucleus began between P11 and P12 ((Karlsson, 1967) (P12), (Jacobson, 1963) (P11-

P12)). The present study documents that onset of pNF-H immunopositivity began just after this period, on P13.

Neurofilament transport and the node of Ranvier

A correlation between the rapid increase in appearance of pNF-H and the gradual increase in the formation of synapses is therefore unlikely. On the other hand, if the rapid initiation of myelination and the rapid initiation of phosphorylation of NF-H are linked, what is the nature of this link? After all, myelination has an active functional role in the electrophysiology of the neuron - it leads to efficient saltatory conduction of the action potential along the axon. The neurofilament has been given a purely passive anatomical role. It has been said to serve as the stuffing of the axon - providing a crosslinked axoplasmic matrix as well as increasing then stabilizing the axonal diameter. In light of the available evidence, the present study suggests that the onset of immunoreactivity of pNF-H is associated with the appearance of the nodes of Ranvier and, through this association, that neurofilaments may have a functional role as well as a structural one.

The passive role for the neurofilament was first suggested in early biochemical characterizations. The neurofilament was found to be composed of three proteins: NF-L, NF-M and NF-H (Hoffman and Lasek, 1975). Each of the proteins is encoded by its unique gene (Czosnek *et al.* 1980) and, following the dictates of axoplasmic transport,

(Weiss and Hiscoe, 1948) each is transported away from its site of synthesis in the axonal soma toward the peripheral synapse. Willard and coworkers, studying the rabbit optic nerve during the early postnatal period, found that two of the neurofilament proteins, NF-L and NF-M appear before NF-H. They also observed that the appearance of NF-H is associated with a eight-fold decrease in the rate of transport of all the neurofilament proteins along the optic nerve axons from high juvenile rates to the lower rates of the adult (Willard and Simon, 1983). The same group found that the phosphorylated form of heavy neurofilament protein is first appears during the period of time that the rate of neurofilament transport suddenly decreases (Glicksman *et al.* 1987). Hoffman and coworkers found a similar age-related retardation of transport of the neurofilament proteins in the rat peripheral nervous system (Hoffman *et al.* 1983). Again, the slowing of transport of the neurofilament proteins in the sciatic nerve coincided with phosphorylation of NF-H and particularly phosphorylation of the KSP triplets on NF-H (Watson *et al.* 1989).

Hirokawa studied electron micrographs of quick frozen, deep etched unfixed frog axons and found that neurofilament fibers are cross-linked (Hirokawa, 1982). Similar micrographs, but this time using the rabbit spinal cord, suggested and that the links that exist involve the sidearms of the heavy neurofilaments (Hirokawa *et al.* 1984). Both Hoffman and his associates (Hoffman *et al.* 1985) and the Willard group (Willard and Simon, 1983) suggested that these links, some of which are between neurofilaments, others of which are between neurofilaments and microtubules, are responsible for the

slowing of neurofilament protein transport. Massive crosslinking of the neurofilaments either causes an increased burden on the neurofilament transport mechanism through introduction of "additional drag" or creates a structure which obstructs the transport of components of the neurofilament (Willard and Simon, 1983). Glicksman (Glicksman *et al.* 1987) speculated that phosphorylation of the neurofilament, occurring coincidentally with the decreased rate of neurofilament transport, facilitates this cross-linking.

The slowing of neurofilament transport during development also coincides with an increase in diameter of the peripheral axons (Hoffman *et al.* 1985). This too was attributed to increased phosphorylation. It was speculated that as the sidearms of NF-M and NF-H become phosphorylated, the charge density of the sidearms becomes sufficient to repel them from the surface of the core of the neurofilament into the cytosol. The increased charge density also causes mutual repulsion between adjacent neurofilaments with concomitant increase in axon diameter (de Waegh *et al.* 1992).

The two theories of decreased neurofilament transport during development and of increased axonal caliber during development are both based on the assumption that phosphorylation of the neurofilament leads to an elaboration of the three-dimensional neurofilament matrix. Since decreased transport and increased axonal caliber occur at the same time phosphorylation of NF-H appears, it is not unreasonable to assume that they both require phosphorylation of NF-H sidearms. Unfortunately, the theories as stated are mutually exclusive. If, as the theory of increased axonal caliber suggests,

phosphorylation of the neurofilament sidearms leads to mutual repulsion between adjacent neurofilaments, the sidearms would not be able interact and form bridges, as the theory of decreased axonal transport requires. Unless a intermediate that neutralizes charge and links neurofilaments can be found, one of the theories must be incorrect. Hisanaga and Hirokawa found no visible difference in the extension of the neurofilament sidearms before and after isolated neurofilaments were dephosphorylated (Hisanaga and Hirokawa, 1989). Unlike other cytoskeletal proteins (Hagestedt *et al.* 1989), phosphorylation of the neurofilament protein sidearms does not cause them to extend in a pattern suggesting mutual repulsion. This finding does not support the assumptions of the theory of increased axon caliber. Gotow and Tanaka (Gotow and Tanaka, 1994) observed a decrease in labeling of phosphorylated epitopes in micrographs of neurofilaments in close proximity to microtubules but an increase in labeling of phosphorylated epitopes of neurofilaments in close proximity to other neurofilaments. They suggested that phosphorylation favors inter-neurofilament bridges, and disfavors interaction of neurofilaments with other cytoskeletal elements. Gotow and Tanaka's observations support the theory of decreased axoplasmic transport, which requires the formation of phosphorylated crossbridges, better than the theory of increased axon caliber, which ignores the possibility of crossbridges. Phosphorylation therefore does appear to be important in the elaboration of the neurofilament network. However, it is not a requisite for assembly of individual neurofilaments. Georges and colleagues found that dephosphorylation of dissociated neurofilament proteins did not compromise their ability to reassemble into filaments (Georges *et al.* 1986). Also, NF-H, expressed in non-

neuronal cells, spontaneously assembles with other intermediate filament proteins to form filaments. Immunohistochemical analysis of the cells using primary antibodies sensitive to the state of phosphorylation suggested that the NF-H had associated in a non-phosphorylated form (Chin and Liem, 1990; Soifer *et al.* 1991).

Therefore, although it is not required for the formation of neurofilaments, phosphorylation of NF-H favors construction of the complex scaffolding of the neurofilament network. However, rather than being a consequence of phosphorylation, the increase in cytoskeletal complexity as well as the increase in cytoskeletal phosphorylation may both be the consequence of a third factor, myelination. The results of the present study, when compared to the results of Jacobson (Jacobson, 1963), suggest a temporal association between the onset of myelination and the onset of phosphorylation of NF-H. Although onset of myelination and onset pNF-H immunoreactivity occur in different tracts in the CNS at different times after birth, onset of myelination always occurs on the same day or before the initial appearance of pNF-H. Myelination, or rather onset of oligodendrocyte compaction, has a similar temporal relationship with first appearance of the axolemmal nodal specialization typical of nodes of Ranvier. The nodes appear after onset of myelination. In a electron microscopic analysis of development of the rat optic nerve, Hildebrand and Waxman found that, although the first few nodes of Ranvier appear at the same time the compaction stage of myelination begins, appearance of large numbers of nodes of Ranvier appear four to eight days after onset of compaction (Hildebrand and Waxman, 1984).

Not only is there a temporal relationship between onset of myelination and onset of pNF-H immunoreactivity, and onset of myelination and appearance of the nodes of Ranvier, there is also an anatomic one that links elaboration of the neurofilament matrix to the appearance of the nodes. Price and colleagues noted that the radial distribution of neurofilaments is most highly organized in the nodal and paranodal regions (Price *et al.*1993). They systematically sampled packing densities of neurofilaments in cross-sections of axons in these regions and found that the distribution of neurofilaments is not random. They found that whereas the packing densities of neurofilaments in the internodal region assume a completely random distribution, the packing densities of neurofilaments in the nodal and paranodal regions are all clustered near midrange values. The high and the low packing densities expected from a normal distribution are not found. Price and colleagues attributed the increase in organization of the neurofilaments in the paranodal region to increased compressive forces by the thicker myelin sheath found surrounding this region. Constrained into a smaller space, the "side-by-side NF interactions appear to constrain significantly the stochastic movement of the NFs in the radial dimension." However other explanations of the increase in neurofilament organization around the node are possible.

Some membrane-associated proteins are only found in the nodal region of the axon. If the spacing between these proteins is maintained by a regular two-dimensional cytoskeletal matrix, any protein attached to the matrix would assume the same ordered arrangement. Hoffman, *et al.* (Hoffman *et al.*1985) and Ichimura and Ellisman

(Ichimura and Ellisman, 1991), studying electron micrographs of the paranodal regions of myelinated axons, found links between neurofilaments and the paranodal axolemma. Landon and Williams (Landon and Williams, 1963) also found filaments entering an area of increased electron density in electron micrographs of the nodal axolemma. Although the nature of the interaction between the neurofilament and the axolemma is unknown, these links have only been observed in the region of the node. But is there a regular array of proteins to which the neurofilaments can attach themselves? Among the proteins sequestered at the nodal region are channel proteins and cytoskeletal proteins. The voltage-sensitive sodium channel is found in the node and paranode (Wilson and Chiu, 1990; Black *et al.*1989; Ritchie *et al.*1990). Isolated from the brain, this channel has been shown to be associated with brain-derived ankyrin, a cytoskeletal protein (Srinivasan *et al.*1988). A isoform of ankyrin, ankyrin$_G$, is itself found associated with the node of Ranvier (Kordeli *et al.*1990; Kordeli *et al.*1995). Ankyrin binds to spectrin to form a regular polygonal structure just below the erythrocyte cell membrane (Byers and Branton, 1985; Liu *et al.*1987). Spectrin, another cytoskeletal protein, is also enriched at the node (Koenig and Repasky, 1985). The rod domain of NF-L binds to brain spectrin (Frappier *et al.*1991). If ankyrin and spectrin form a regular latticework, perhaps attached to the paracrystalline structure found embossed on the E-face (outer leaflet) of the freeze-fractured paranodal axolemma (Livingston *et al.*1973), neurofilament, attached to spectrin, would assume the same ordered structure (see figure 14 which illustrates this model of neurofilaments constrained at the node of Ranvier). One end of a neurofilament would therefore bind to spectrin in the nodal region. The

Figure 14: Schematic model depicting a possible association of neurofilaments with node of Ranvier. An axon is shown stripped of its myelin sheath. The narrow collar represents the node. The external surface of the node and paranode above the nodal collar are shown; the paranode below the nodal collar is seen in transparency. A paracrystalline structure found embossed on the E-face (outer leaflet) of the freeze-fractured paranodal axolemma (Livingston *et al.* 1973) is suggested by the jagged lines drawn on the external surface of the axon. This paracrystalline structure may align an internal latticework of spectrin and ankyrin (suggested by equally spaced dots on the internal surface of the transparent paranode) to which neurofilament binds. The bound or anchored neurofilaments are symbolized by long unbroken lines. Nixon has proposed that neurofilaments exist in one of two pools: a stationary pool and a mobile pool (Nixon *et al.* 1994; Lewis and Nixon, 1988). The anchored neurofilaments would be included in the stationary pool. The mobile pool of neurofilaments, symbolized by broken lines, would be free to move within the axon along with axoplasmic flow. Because neurofilaments interact by means of phosphorylated NF-H crossbridges, the mobile pool would interact with and be organized by the stable pool. This organization would be most evident in the nodal area - where the stable pool is itself most highly organized. A relatively high concentration of ATP due to an apparent accumulation of mitochondria (mitochondria are symbolized by the fusiform shape in the transparent paranode) would disfavor phosphorylation of NF-H in the nodal region.

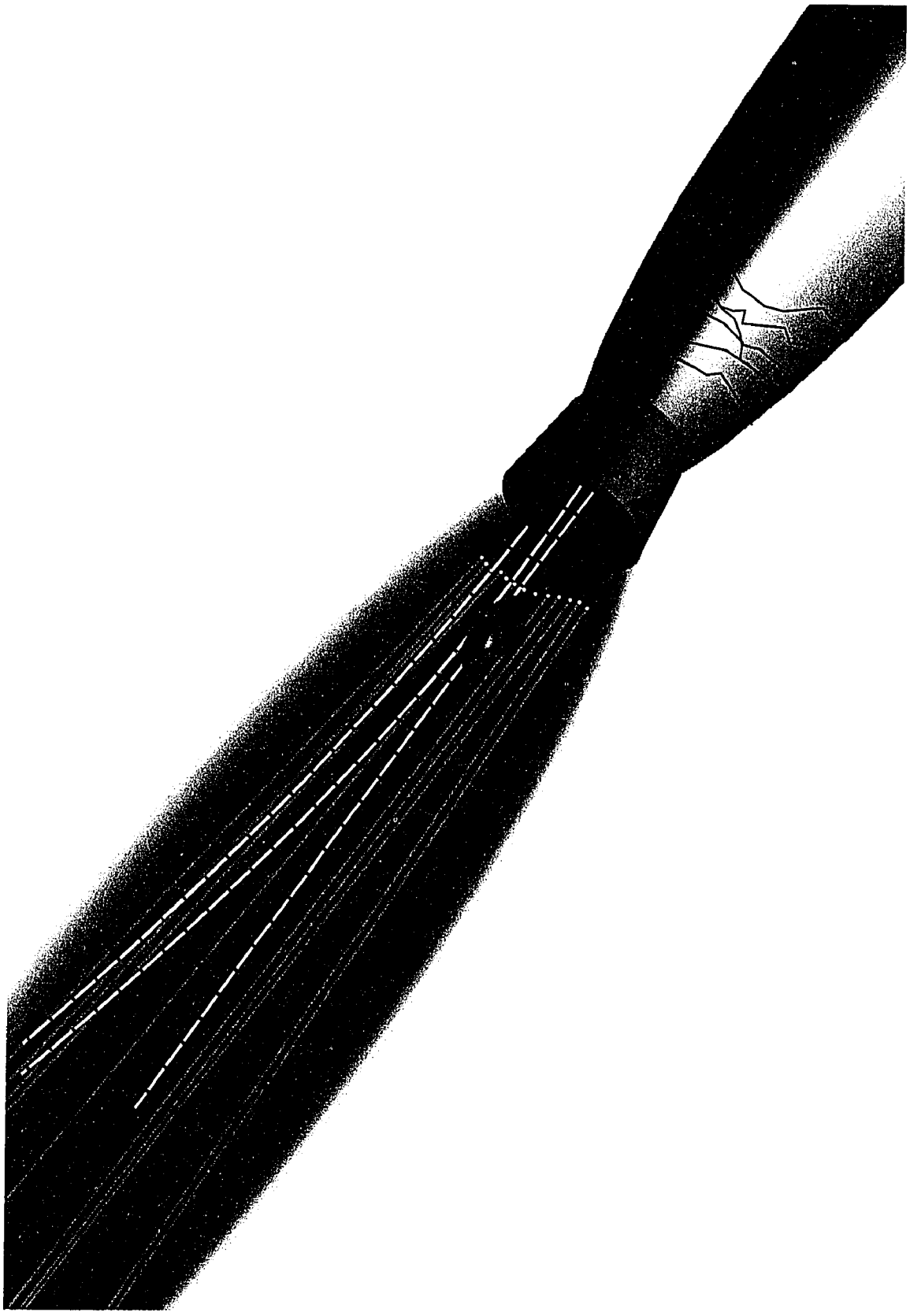

neurofilament would then extend down the axon and terminate either as a free ending or would attach to a spectrin binding site in another nodal region. Following the course of neurofilaments and microtubules reconstructed from serial sections of a myelinated axon, Tsukita and Ishikawa (Tsukita and Ishikawa, 1981) suggested that most neurofilaments become discontinuous in the paranodal region. Most of the neurofilaments in the tethered neurofilament model would therefore extend from spectrin to spectrin binding site, from nodal region to nodal region. Since neurofilaments form long spirallar structures rather than taut, straight ones (Tsukita and Ishikawa, 1981), the movement of the tethered ends of the neurofilaments would be more restricted than that of the center. In agreement with the observations of Price *et al.* (Price *et al.* 1993) the ends of the neurofilament, tethered to the regular two-dimensional paranodal/nodal cytoskeletal array would be more highly organized than the center, internodal part of the neurofilament.

Nixon has proposed that neurofilaments exist in one of two pools: a stationary pool and a mobile pool (Nixon *et al.* 1994; Lewis and Nixon, 1988). Tethered to the paranodal and nodal axolemma, the restrained neurofilaments could be included in the stable pool, the untethered neurofilaments could be included in the mobile pool. Since neurofilaments form cross-bridges between themselves, neighboring neurofilaments would tend to align. Tethered, stable, neurofilaments which are structured by an underlying cytoskeletal matrix would impose organization on the free, mobile neurofilaments. Again, in agreement with the observations of Price *et al.* (Price *et*

*al.*1993) and others (Hsieh *et al.*1994), this organization would be greatest at the area of highest restraint, the node and paranode, and would be lowest within the internode, where the neurofilaments would be more readily buffeted by other cytoskeletal elements.

A link also exists between formation of the nodes and phosphorylation. Bush and colleagues recently found that lowering the levels of ATP in the PC 12 neuronal model caused "striking" activation of a neurofilament kinase (Bush *et al.*1995). Roder and Ingram (Roder and Ingram, 1991) have isolated two kinases which phosphorylate NF-H at the KSP sequences and lead to an increase the Mr of dephosphorylated NF-H. These kinases are also inhibited by an excess of free ATP. Although phosphate groups can be transported along the axon, probably as ATP (Nixon *et al.*1994), the machinery for making ATP is not distributed equally along the myelinated axon. Mitochondria tend to accumulate in areas where the ATP they produce is rapidly consumed (Morris and Hollenbeck, 1993; Williams and Landon, 1963; Lund and Bunt, 1976). In the myelinated axon this area of high energy consumption is at the node. High densities of voltage-sensitive sodium channels are found at the node and at lower densities in the paranode (Dugandzija-Novakovic *et al.*1995; Ritchie *et al.*1990; Wilson and Chiu, 1990). The sodium which they allow into the axon must be pumped out in order to restore the resting potential of the neural cell membrane. Vorbrodt and colleagues (Vorbrodt *et al.*1982) and others (Waxman and Ritchie, 1993; Mata *et al.*1991) found that the enzyme necessary to expel sodium from the neuron, the ouabain-sensitive Na+,K+-ATPase, is

especially concentrated at the node and paranode. Light and electron micrographic evidence as well as biochemical evidence suggests an accumulation of mitochondria in the node and paranode (Williams and Landon, 1963; Berthold and Skoglund, 1967; Berthold *et al.* 1993; Fabricius *et al.* 1993) and an associated increase in concentration of ATP. A relatively low level of ATP at the internode could therefore favor phosphorylation of NF-H (by Bush, Roder and colleagues' neurofilament kinase) within the internode. During postnatal development, once myelination has started and the node of Ranvier is in place, neurofilaments anchored onto the paranode could lengthen into the internodal region and become phosphorylated. The phosphorylated neurofilaments would be less susceptible to degradation than nonphosphorylated neurofilament (Greenwood *et al.* 1993; Pant, 1988; Malik *et al.* 1986) and therefore would become part of the stable pool of neurofilaments.

Aluminum toxicity, a direct or an indirect affect?

Pregnant rats that drink high levels of aluminum in their water during gestation and lactation develop lesions in their kidneys and stomachs. Since chronic kidney pathology is associated with gastric ulcers, the erosions may be secondary to the renal pathology (Kokko, 1988). The lesions we observed are consistent with those reported by other investigators. In a study on learning behavior of aging rabbits, R.A.Yokel noted a deterioration of kidney function following chronic subcutaneous injections of aluminum lactate (Yokel, 1989). These injections were associated with abnormal aggregates of

phosphorylated cytoskeletal proteins - including pNF-H - in rabbit neurons (Forrester and Yokel, 1985). Non-CNS lesions were also found in the rat. Following a single intravenous injection of trace quantities of ^{26}Al into rats, mass spectrometric analysis of tissues three weeks after injection suggests that most of the sequestered dose is found in the bone (0.9% of administered dose per gram dry weight of tissue). However the kidney is the second largest repository of aluminum (0.2% of administered dose per gram dry weight of tissue) (Walker *et al.*1994) followed by the liver (0.06%), heart (0.03%) and brain and muscle (0.02%). Chronic intraperitoneal injection of aluminum chloride into rats leads to increased levels of lysosomal enzymes in the kidney, spleen and liver (Stein *et al.*1987). This biochemical index of lysosomal damage was confirmed by images of lysosomal damage in electron micrographs of the kidney (Chagnac *et al.*1987). Using a dosing scheme similar to the one Stein *et al.* used (Stein *et al.*1987), Chagnac (Chagnac *et al.*1987) localized the lysosomal damage to the proximal tubules. More recently, Roy and colleagues gave chronic oral, rather than chronic intraperitoneal, doses of aluminum sulfate or aluminum potassium sulfate to young rats (P60) and found lesions in the kidneys, stomach, liver, testes, bones and brain (Roy *et al.*1991). We did not observe liver pathology in our study, however different aluminum salts are known to vary in their biological effects. Chronic doses of aluminum can therefore cause renal damage. This damage is localized to the proximal tubule most likely involves lysosomes.

The delay in diencephalic immunopositivity of pNF-H in the brain of one pup is difficult to interpret. If, as the present study suggests, the onset of pNF-H immunoreactivity is linked to the formation of the node of Ranvier, delay in formation of the node could translate as a delay in onset of appearance of pNF-H. Adult rats given a powdered lab diet mixed with aluminum citrate over a period of months developed wide-spread vacuolation of the astrocytes (Florence *et al.* 1994). The astrocyte enters the nodal space at the time the node of Ranvier is being formed (Hildebrand and Waxman, 1984; Black and Waxman, 1988). If the astrocyte is compromised by aluminum coming from the mother's milk, production of pNF-H may also be compromised. However, the literature suggests that no aluminum is found in the fetus during gestation (Gomez *et al.* 1991; Muller *et al.* 1993) or in the pup during the early postnatal period (Muller *et al.* 1992). Unless it is sequestered in areas beyond the limit of resolution of graphite furnace atomic absorption spectrometry which was used in analysis of whole fetuses (Gomez *et al.* 1991; Muller *et al.* 1993) and neonate brain regions (Muller *et al.* 1992), aluminum cannot cause the pathology. But even more significant complications exist in the interpretation of the apparent delay of pNF-H immunoreactivity.

Gastric and renal pathology caused by aluminum consumption could significantly alter maternal metabolism. Pathology of this type leads to inadequate nutrition, to the accumulation of toxins, as well as to the imbalance of electrolytes and metabolites. These systemic biophysiochemical changes secondary to aluminum toxicity, could themselves alter behavior and also alter the phosphorylation of proteins within the brain

of the pup. The alterations in the dams' viscera, together with the fact that their progressively deteriorating state of health caused progressive changes of an already altered homeostasis, forced abandonment of further assessment of neonatal brain damage. It would have been impossible to ascribe an etiology to any of the changes in topography or delays in immunoreactive staining for the presence of pNF-H. Similarly, the changes in the level of phosphorylation of NF-H and MAP2 and in the amounts of MAP2 and spectrin in the CNS of adult rats chronically treated with aluminum (Johnson *et al.*1992; Johnson and Jope, 1988) and the behavioral deficits in neonatal rats (Bernuzzi *et al.*1989; Muller *et al.*1990) may therefore be secondary to non-CNS actions of aluminum rather than to direct toxicity of this metal.

Summary:

Phosphorylated NF-H, and in particular the epitope recognized by the monoclonal RMO24.9, fulfills important requirements of an ideal marker for CNS development. It is only found in neurons; no other cell type was immunohistochemically stained using RMO24.9 as a primary antibody. It is unique. Only pNF-H, which is only found in neurons, binds RMO24.9. However, limitations on its use as a developmental marker must be recognized. For most CNS structures, it can only be used as a marker of postnatal development . Only spinal cord and some medullary structures are stained by birth. Not all neurons stain for the presence of pNF-H. The most notable of the non-staining cells are the cerebellar granule cells. The development of this large population of cells which lack NF-H (Vitadello and Denis-Donini, 1990) cannot be followed with a marker for pNF-H. However, if these limitations are recognized, pNF-H can serve as a marker for postnatal development of axons, and in particular the large, myelinated axons which are found throughout the most of the CNS.

The spatial and temporal pattern of CNS staining found in the present study confirmed that found in the biochemical analysis by Fischer and Shea (Fischer and Shea, 1991). Because the present study followed onset of appearance of NF-H in tracts within the regions Fischer and Shea chose for study, the specific pathways responsible for the regional increases in pNF-H could be analyzed. This analysis pointed out misinterpretations of their data that arose from the fact that tracts do not respect regional

boundaries. Although further research is needed to determine the precise function of pNF-H and its relationship to other neural processes, the present study strongly suggests that the phosphorylation of NF-H is associated with myelination of the axon and perhaps the appearance of the node of Ranvier.

This study points out the extra-neuronal pathology caused by maternal oral aluminum lactate exposure during gestation and lactation. These pathological changes had a profound effect on the health of the rat dam and, quite independently of the action of aluminum, may have altered the development of the dams' pups. The primary agent of changes in the development of behaviors in rat pups whose mothers have been exposed to oral aluminum lactate is therefore unknown. The temporal and spatial database of pNF-H immunoreactivity in the rat CNS assembled in this study could therefore not be used to assess neuroanatomical correlates of behavioral changes caused by aluminum toxicity. If neurobehavioral effects of aluminum are to be assessed using the assembled database of postnatal development, aluminum must be introduced directly to the target to be assessed - in this case the brain of the rat pup.

Table 2: **Structures with positive immunohistochemical staining for the presence of pNF-H** marked with an "x". To be immunopositive, the intensity of staining for at least one section in given structure must be ≥1 in all three pups. Staining for the presence of myelin as reported by Jacobson using the Weigert method (Jacobson, 1963) marked with an "o". Structures not marked with an "o" had not been described by Jacobson. Structures marked "x," staining on P9, may have first become immunopositive for the presence of pNF-H on or before P9; otherwise, onset of appearance of pNF-H is as marked. Due to a lower sampling frequency, structures marked "o" staining on P10 may have first produced myelin on P10 or up to two days before; otherwise they first produce myelin on the first day they are positive or up to one day before.

Table 2 **Postnatal day** (birth=P0)

Structure (nuclei and regions)	9	10	11	12	13	14	15
oculomotor nucleus [3]						X	
trochlear nucleus [4]						X	
amygdaloid fissure [AF]		X	X			X	X
Anterior pretectal nucleus [APT]							X
Anterior pretectal nucleus, ventral par [APTV]	X	X		X	X	X	X
Bed nucleus of the anterior commissure [BAC]							X
Nucleus of the brachium of the inferior colliculus [BIC]						X	X
Field CA3 of Ammon's horn, pyramidal layer [CA3p]	X	X	X	X	X	X	X
Field CA3 of Ammon's horn, pyramidal layer,area [CA3pc]						X	X
Field CA3 of Ammon's horn, radiatum laye [CA3r]							X
Central nucleus of the inferior colliculus [CIC]						X	X
Caudate putamen (striatum) [CPu]		XO	X	XO	X	XO	X
Cerebellum [Cb]		X	X	X	X	X	X
3rd cerebellar lobule [CbIII]		X		X		X	
4th cerebellar lobule [CbIV]		X	X	X		X	
5th cerebellar lobule [CbV]	X	X	X	X		X	

Table 2 (continued)

	9	10	11	12	13	14	15
6th cerebellar lobule [CbVI]	X	X	X	X		X	
Dentate gyrus [DG]							X
Dorsal lateral geniculate nucleus [DLG]				O	X	O	X
Deep white layer of the superior colliculus [DpWh]				O		O	X
External cortex of the inferior colliculus [ECIC]		X				X	
External plexiform layer of the olfactory bulb [EPl]							X
Entorhinal cortex [Ent]		X		X		X	
Trigeminal ganglion [Vieussens,Gasser,G5]							X
Granular insular cortex [GI]				X			X
Internal granular layer of the olfactory bulb [IGr]		X		X		X	X
Internal plexiform layer of the olfactory bulb [IPl]		X		X		X	X
Intermediate white layer of the superior colliculus [InWh]						O	X
Lateral lemniscal fields [LLF]	X	XO	X	XO		XO	X
Lateral vestibular nucleus [LVe]						X	X
Magnocellular nucleus of the posterior commissure [MCPC]	X			X			
Mitral cell layer of the olfactory bulb [Mi]							X
Olfactory nerve layer [ON]				X	X	X	X

Table 2 (continued)

	9	10	11	12	13	14	15
Perirhinal cortex [PRh]		X	X	X	X		X
Parietal cortex, area 1 [Par1]		O		XO		O	
Piriform cortex [Pir]	X	X	X	X	X	X	X
Red nucleus [R]	X						X
Red nucleus, magnocellular part [RMC]						X	X
Subiculum [S]				X		X	X
Nucleus of the stria medullaris [SM]						X	
Substantia nigra, compact part [SNC]						O	X
Triangular septal nucleus [TS]			X	X	X	X	X
Olfactory tubercle [Tu]			X	X	X	X	X
Ventral posteromedial thalamic nucleus [VPM]						XO	
Zona incerta, ventral part [ZIV]							X

(tracts)

optic nerve [2n]	X		X	X		X	X
oculomotor nerve [3n]				X		X	
trigeminal nerve [5n]					X	X	X
Anterior commissure, intrabulbar part [aci]		X	O	X	O		X
Alveus of the hippocampus [alv]						XO	X
Brachium of the inferior colliculus [bic]		X	XO	X	XO	X	X
Brachium of the superior colliculus [bsc]				X		X	X
Cingulum [cg]		O	X	XO		XO	X

Table 2 (continued)

	9	10	11	12	13	14	15
Commissure of the inferior colliculus [cic]		XO	X	XO		XO	X
Cerebral peduncle, basal part [cp]	X	XO	X	XO	X	XO	X
Dorsal hippocampal commissure [dhc]				O		XO	X
External capsule [ec]	X	XO		XO		XO	X
External medullary lamina [eml]		X	X	X	X	X	X
Fimbria of the hippocampus [fi]				XO		XO	X
Fasciculus retroflexus [fr]		X					X
Habenular commissure [hbc]		X	X			X	X
Internal capsule [ic]	X	XO	X	XO	X	XO	X
Inferior cerebellar peduncle (restiform body) [icp]		X	X	X	X		X
Lateral lemniscus [ll]	X	XO	X	XO	X	XO	X
Lateral olfactory tract [lo]	X	XO	X	XO	X	XO	X
Middle cerebellar peduncle (brachium pontis)[mcp]	X	X	X	X	X	X	X
Medial lemniscus [ml]		XO	X	XO	X	XO	X
Medial longitudinal fasciculus [mlf]	X	X	X	X	X	X	X
Mammillary peduncle [mp]						O	X
Mammillothalamic tract [mt]						O	X
Optic tract [opt]		X	X	XO	X	XO	X
Optic chiasm [ox]	X		X	X		X	X
Posterior commissure [pc]	X	XO	X	XO	X	XO	X

Table 2 (continued)

	9	10	11	12	13	14	15
Sensory root of the trigeminal nerve [s5]	x	xo	x	xo	x	o	
Superior cerebellar peduncle (brachium conjunctivum) [scp]	x	xo	x	xo	x	xo	x
Stria medullaris of the thalamus [sm]	x	xo	x	xo	x	xo	x
Superior thalamic radiation [str]				x	x	x	x
Ventral hippocampal commissure [vhc]				x		x	x
Vomeronasal nerve [vn]		x	x		x		x
Ventral spinocerebellar tract [vsc]							x
Decussation of the superior cerebellar peduncle [xscp]	x	x		x	x		

Bibliography:

Abreo, K., Glass, J. and Sella, M'L. Aluminum inhibits hemoglobin synthesis but enhances iron uptake in Friend erythroleukemia cells. *Kidney International* 37:677-681, 1990.

Alfrey, A.C., LeGendre, G.R. and Kachny, W.D. The dialysis encephalopathy syndrome: possible aluminum intoxication. *The New England Journal of Medicine* 294:184-188, 1976.

Alfrey, A.C., Mischell, J.M. and Burks, J. Syndrome of dyspraxia and multifocal seizures associated with chronic hemodialysis. *Transactions of the American Society for Artificial Internal Organs* 18:257-261, 1972.

Allain, P., Leblondel, G. and Mauras, Y. Effect of aluminum and deferoxamine on biliary iron elimination in the rat. *Proceedings of the Society for Experimental Biology and Medicine* 188(4):471-473, 1988.

Altman, J. Postnatal development of the cerebellar cortex in the rat. II. Phases in the maturation of Purkinje cells and of the molecular layer. *The Journal of Comparative Neurology* 145:399-464, 1972.

Altman, J. and Sudarshan, K. Postnatal development of locomotion in the laboratory rat. *Animal Behaviour* 23:896-920, 1975.

Bali, P.K., Zak, O. and Aisen, P. A new role for the transferrin receptor in the release of iron from transferrin. *Biochemistry* 30:324-328, 1991.

Bayer, S.A. Neurogenic patterns in the medial limbic cortex of the rat related to anatomical connections with the thalamus and striatum. *Experimental Neurology* 107:132-142, 1990.

Bähr, S. and Wolff, J.R. Postnatal development of axosomatic synapses in the rat visual cortex: morphogenesis and quantitative evaluation. *The Journal of Comparative Neurology* 233:405-420, 1985.

Bernuzzi, V., Desor, D. and Lehr, P.R. Developmental alterations in offspring of female rats orally intoxicated by aluminum chloride or lactate during gestation. *Teratology* 40:21-27, 1989.

Berthold, C.-H., Rydmark, M. and Anders' n, B. Axoplasmic organelles at nodes of Ranvier. I. Occurrence and distribution in large myelinated spinal root axons of the adult cat. *Journal of Neurocytology* 22(11):925-940, 1993.

Berthold, C.-H. and Skoglund, S. Hisochemical and ultrastructural demonstration of mitochondria in the paranodal region of developing feline spinal roots and nerves. *Acta Societatis Medicorum upsaliensis* 72:37-70, 1967.

Black, J.A., Friedman, B., Waxman, S.G., Elmer, L.W. and Angelides, K.J. Immuno-ultrastructural localization of sodium channels at nodes of Ranvier and perinodal astrocytes in rat optic nerve. *Proceedings of the Royal Society of London. Series B: Biological Sciences* 238(1290):39-51, 1989.

Black, J.A. and Waxman, S.G. The perinodal astrocyte. *Glia* 1(3):169-183, 1988.

Bloom, F.E. Databases of Brain Information. In: *Three dimensional neuroimaging*, edited by Toga, A.W. New York: Raven Press, 1990, p. 273-306.

Bolla, K.I., Briefel, G., Spector, D., et al. Neurocognitive effects of aluminum. *Archives of Neurology* 49:1021-1026, 1992.

Bradford, M.M. A rapid and sensitive method for the quentitation of microgram quantities of protein utilizing the principle of protein-dye binding. *Analytical Biochemistry* 72:248-254, 1976.

Breen, K.C., Robinson, P.A., Wion, D. and Anderton, B.H. Partial sequence of the rat heavy neurofilament polypeptide (NF-H). Identification of putative phosphorylation sites. *FEBS Letters* 241(1,2):213-218, 1988.

Bush, M.L., Miyashiro, J.S. and Ingram, V.M. Activation of a neurofilament kinase, a tau kinase, and a tau phosphatase by decreasing ATP levels in nerve growth factor-differentiated PC-12 cells. *Proceedings of the National Academy of Sciences* 92:1861-1865, 1995.

Bush, M.S. and Gordon-Weeks, P.R. Distribution and expression of developmentally regulated phosphorylation epitopes on MAP 1B and neurofilament proteins in the developing rat spinal cord. *Journal of Neurocytology* 23:682-698, 1994.

Byers, T.J. and Branton, D. Visualization of the protein associations in the erythrocyte membrane skeleton. *Proceedings of the National Academy of Sciences* 82:6153-6157, 1985.

Cain, C.C., Sipe, D.M. and Murphy, R.F. Regulation of endocytic pH by the Na^+,K^+-ATPase in living cells. *Proceedings of the National Academy of Sciences* 86:544-548, 1989.

Cajal, S.R. General plan of the structure of the cerebral cortex. In: *Histologie du système nerveux de l'homme et des vert'br's*, Paris: Maloine, 1911, p. 519-598.

Cajal, S.R. *Histologie du système nerveux de l''homme et des vert'br's t. II*, Madrid:Montaña, 1955. pp. 456-474.

Cameron, H.A. and Gould, E. Adult neurogenesis is regulated by adrenal steroids in the dentate gyrus. *Neuroscience* 61(2):203-209, 1994.

Campbell, A.M. *Laboratory Techniques in Biochemistry and Molecular Biology*, New York:Elsevier, 1984.

Cannata, J.B., Alonso, C.G., Men'ndez, M.J.F., et al. Iron uptake in aluminium overload: in vivo and in vitro studies. *Nephrology,Dialysis and Transplantation* 6(9):637-642, 1991.

Cannata, J.B., Fernández-Soto, I., Fernández-Menendez, M.J., et al. Role of iron metabolism in absorption and cellular uptake of aluminum. *Kidney International* 39:799-803, 1991.

Cannata, J.B., Olaizola, I.R., Gomez-Alonso, C., Men'ndez-Fraga, P., Alonso-Suarez, M. and Diaz-Lopez, J.B. Serum aluminum transport and aluminum uptake in chronic renal failure: role of iron and aluminum metabolism. *Nephron* 65(1):141-146, 1993.

Caramelo, C.A., Cannata, J.B., Rodeles, M.R., et al. Mechanisms of aluminum-induced microcytosis: lessons from accidental aluminum intoxication. *Kidney International* 47(1):164-168, 1995.

Carden, M.J., Schlaepfer, W.W. and Lee, V.M.-Y. The structure, biochemical properties, and immunogenicity of neurofilament peripheral regions are determined by phosphorylation state. *The Journal of Biological Chemistry* 260(17):9805-9817, 1985.

Carden, M.J., Trojanowski, J.Q., Schlaepfer, W.W. and Lee, V.M.-Y. Two-stage expression of neurofilament polypeptides during rat neurogenesis with early establishment of adult phosphorylation patterns. *The Journal of Neuroscience* 7(11):3489-3504, 1987.

Chagnac, A., Ben-Bassat, M., Weinstein, T. and Levi, J. Effect of long-term aluminum administration on the renal structure of the rat. *Nephron* 47(1):66-69, 1987.

Cherroret, G., Bernuzzi, V., Desor, D., Hutin, M.-F., Burnel, D. and Lehr, P.R. Effects of postnatal aluminum exposure on choline acetyltransferase activity and learning abilities in the rat. *Neurotoxicology and Teratology* 14:259-264, 1992.

Chin, S.S.M. and Liem, R.K.H. Transfected rat high-molecular-weight neurofilament (NF-H) coassembles with vimentin in a predominantly nonphosphorylated form. *The Journal of Neuroscience* 10(11):3714-3726, 1990.

Chiu, F.-C. and Norton, W.T. Bulk preparation of CNS cytoskeleton and the separation of individual neurofilament proteins by gel filtration: dye-binding characteristics and amino acid composition. *Journal of Neurochemistry* 39:1252-1260, 1982.

Chmielnicka, J., Nasiadek, M., Pinkowski, R. and Paradowski, M. Disturbances of morphological parameters in blood of rats orally exposed to aluminum chloride. *Biological Trace Element Research* 42:191-199, 1994.

Cole, J.S., Messing, A., Trojanowski, J.Q. and Lee, V.M.-Y. Modulation of axon diameter and neurofilaments by hypomyelinating Schwann cells in transgenic mice. *The Journal of Neuroscience* 14(11):6956-6966, 1994.

Collawn, J.F., Stangel, M., Kuhn, L.A., et al. Transferrin receptor internalization sequence YXRF implicates a tight turn as the structural recognition motif for endocytosis. *Cell* 63:1061-1072, 1990.

Connor, J.R. and Fine, R.E. Development of transferrin-positive oligodendrocytes in the rat central nervous system. *Journal of Neuroscience Research* 17:51-59, 1987.

Connor, J.R., Phillips, T.M., Lakshman, M.R., Barron, K.D., Fine, R.E. and Csiza, C.K. Regional variation in the levels of transferrin in the CNS of normal and myelin-deficient rats. *Journal of Neurochemistry* 49:1523-1529, 1987.

Corain, B., Longato, B., Sheikh-Osman, A.A., Bombi, G.G. and Maccà, C. Aluminum carboxylates in aqueous solutions. Part 2. Metal speciation in the Al^{III}-lactate-OH^--H_2O system. *Journal of the Chemical Society,Dalton Transactions* 169-172, 1992.

Cowan, W.M., Fawcett, J.W., O'Leary, D.D.M. and Stanfield, B.B. Regressive events in neurogenesis. *Science* 225:1258-1265, 1984.

Crain, S.M. Development of electrical activity in the cerebral cortex of the albino rat. *Proceedings of the Society for Experimental Biology and Medicine* 81:49, 1952.

Cuenca, N., Fernandez, E., de Juan, J., Carreres, J.J. and Iniguez, C. Postnatal development of microtubules and neurofilaments in the rat optic nerve: a quantitative study. *The Journal of Comparative Neurology* 263:613-617, 1987.

Czosnek, H. and Soifer, D. Comparison of the proteins of 10 nm filaments from rabbit sciatic nerve and spinal cord by electrophoresis in two dimensions. *FEBS Letters* 117(1):175-178, 1980.

Czosnek, H., Soifer, D., Mack, K. and Wisniewski, H.M. Similarity of neurofilament proteins from different parts of the rabbit nervous system. *Brain Research* 216:387-898, 1981.

Czosnek, H., Soifer, D. and Wisniewski, H.M. Studies on the biosynthesis of neurofilament proteins. *The Journal of Cell Biology* 85:726-734, 1980.

Czosnek, H., Soifer, D. and Wisniewski, H.M. Heterogeneity of intermediate filament proteins from rabbit spinal cord. *Neurochemical Research* 5(7):777-793, 1980.

D'Haese, P.C., Lamberts, L.V. and De Broe, M.E. Aluminum accumulation/toxicity in dialysis patients: monitoring, diagnosis and therapy. *Toxicological and Environmental Chemistry* 23:17-25, 1989.

Dahl, D. Maturation of a large neurofilament protein (NF 150K) in rat postnatal development. *Journal of Neuroscience Research* 17:367-374, 1987.

Dahl, D., Crosby, C.J. and Bignami, A. Filament proteins in rat optic nerves undergoing wallerian degeneration. *Experimental Neurology* 71:421-430, 1981.

Dahl, D., Gilad, V.H., Maggini, L. and Bignami, A. Effect of the substrate on neurofilament phosphorylation in mixed cultures of rat embryo spinal cord and dorsal root ganglia. *International Journal of Developmental Neuroscience* 10(2):111-119, 1992.

Danielsson, L.G. and Spar' n, A. Aluminium fractionation in a simulated rat stomach: an *in vitro* study. *Analyst* 120(3):713-720, 1995.

Dautigny, A., Pham-Dinh, D., Roussel, C., Felix, J.M., Nussbaum, J.L. and Jollès, P. The large neurofilament subunit (NF-H) of the rat: cDNA cloning and *in situ* detection. *Biochemical and Biophysical Research Communications* 154(3):1099-1106, 1988.

Davis, E.M. Protein assays: a review of common techniques. *American Biotechnology Laboratory* July:28-37, 1988.

de Waegh, S.M., Lee, V.M.-Y. and Brady, S.T. Local modulation of neurofilament phosphorylation, axonal caliber, and slow axonal transport by myelinating Schwann cells. *Cell* 68:451-463, 1992.

DeBoni, U., Otvos, A., Scott, J.W. and Crapper, D.R. Neurofibrillary degeneration induced by systemic aluminum. *Acta Neuropathologica* 35:285-294, 1976.

Diaz-Nido, J. and Avila, J. Aluminum induces the *in vitro* aggregation of bovine cytoskeletal proteins. *Neuroscience Letters* 110:221-226, 1990.

Domesick, V.B. Projections from the cingulate cortex in the rat. *Brain Research* 12:296-320, 1969.

Domesick, V.B. The fasciculus cinguli in the rat. *Brain Research* 20:19-32, 1970.

Domingo, J.L., Gomez, M., Sanchez, D.J., LLobet, J.M. and Corbella, J. Effect of various dietary constituents on gastrointestinal absorption of aluminum from drinking water and diet. *Research Communications in Chemical Pathology and Pharmacology* 79(3):377-380, 1993.

Döllken, Ueber die Wirkung des Aluminiums mit besonderer Berücksichtigung der durch das Aluminium verursachten Läsionen im Centralnervensystem. *Archiv für Experimentelle Pathologie und Pharmakologie* 40:98-120, 1898.

Dugandzija-Novakovic, S., Koszowski, A.G., Levinson, S.R. and Shrager, P. Clustering of Na^+ channels and node of Ranvier formation in remyelinating axons. *The Journal of Neuroscience* 15(1):492-503, 1995.

Durham, H.D. Demonstration of hyperphosphorylated neurofilaments in neuronal perikarya *in vivo* by microinjection of antibodies into cultured spinal neurons. *Journal of Neuropathology and Experimental Neurology* 49(6):582-590, 1990.

Edwardson, J.A., Moore, P.B., Ferrier, I.N., et al. Effect of silicon on gastrointestinal absorption of aluminium. *The Lancet* 342:211-212, 1993.

Elliot, H.L., MacDougall, A.L. and Fell, G.S. Aluminum toxicity syndrome. *The Lancet* 1:1203, 1978.

Fabricius, C., Berthold, C.-H. and Rydmark, M. Axoplasmic organelles at nodes of Ranvier. II. Occurrence and distribution in large myelinated spinal cord axons of the adult cat. *Journal of Neurocytology* 22(11):941-954, 1993.

Farnell, B.J., DeBoni, U. and Crapper McLachlan, D.R. Aluminum neurotoxicity in the absence of neurofibrillary degeneration in CA1 hippocampal pyramidal neurons *in vitro*. *Experimental Neurology* 78:241-258, 1982.

Fischer, I. and Romano-Clarke, G. Changes in microtubule-associated protein MAP1B phosphorylation during rat brain development. *Journal of Neurochemistry* 55:328-333, 1990.

Fischer, I. and Shea, T.B. Differential appearance of extensively phosphorylated forms of the high molecular weight neurofilament protein in regions of mouse brain during postnatal development. *Journal of Neuroimmunology* 31:73-81, 1991.

Fishman, J.B., Rubin, J.B., Handrahan, J.V., Connor, J.R. and Fine, R.E. Receptor-mediated transcytosis of transferrin across the blood-brain barrier. *Journal of Neuroscience Research* 18(2):299-304, 1987.

Fliegner, K.H. and Liem, R.K.H. Cellular and molecular biology of neuronal intermediate filaments. *International Review of Cytology* 131:109-167, 1991.

Florence, A.L., Gauthier, A., Ponsar, C., van den Bosch de Aguilar, P. and Crichton, R.R. An experimental animal model of aluminium overload. *Neurodegeneration* 3:315-323, 1994.

Forrester, T.M. and Yokel, R.A. Comparative toxicity of intracerebroventricular and subcutaneous aluminum in the rabbit. *NeuroToxicology* 6(3):71-80, 1985.

Foster, R.E., Connors, B.W. and Waxman, S.G. Rat optic nerve: electrophysiological, pharmacological and anatomical studies during development. *Developmental Brain Research* 3:371-386, 1982.

Frappier, T., Stetzkowski-Marden, F. and Pradel, L.-A. Interaction domains of neurofilament light chain and brain spectrin. *Biochemical Pharmacology* 275:521-527, 1991.

Froment, D.H., Buddington, B., Miller, N.L. and Alfrey, A.C. Effect of solubility on the gastrointestinal absorption of aluminum from various aluminum compounds in the rat. *Journal of Laboratory and Clinical Medicine* 114(3):237-242, 1989.

Froment, D.H., Molitoris, B.A., Buddington, B., Miller, N. and Alfrey, A.C. Site and mechanism of enhanced gastrointestinal absorption of aluminum by citrate. *Kidney International* 36:978-984, 1989.

Fuchs, R., Schmid, S. and Mellman, I. A possible role for Na^+,K^+-ATPase in regulating ATP-dependent endosome acidification. *Proceedings of the National Academy of Sciences* 86:539-543, 1994.

Fujita, S. Morphogenesis of the brain as studied by 3-D computer graphics simulation. *Journal of Microscopy* 157(3):259-269, 1990.

Geisler, N., Vandekerckhove, J. and Weber, K. Location and sequence characterization of the major phosphorylation sites of the high molecular mass neurofilament proteins M and H. *FEBS Letters* 221(2):403-407, 1987.

Georges, E., Lefebvre, S. and Mushynski, W.E. Dephosphorylation of neurofilaments by exogenous phosphatases has no effect on reassembly of subunits. *Journal of Neurochemistry* 47:477-483, 1986.

Glicksman, M.A., Soppet, D. and Willard, M. Postranslational modification of neurofilament polypeptides in rabbit retina. *Journal of Neurobiology* 18(2):167-196, 1987.

Glicksman, M.A. and Willard, M. Differential expression of the three neurofilament polypeptides. *Annals of the New York Academy of Sciences* 455:479-491, 1985.

Goldstein, M.E., Cooper, H.S., Bruce, J., Carden, M.J., Lee, V.M.-Y. and Schlaepfer, W.W. Phosphorylation of neurofilament proteins and chromatolysis following transection of rat sciatic nerve. *The Journal of Neuroscience* 7(5):1586-1594, 1987.

Gomez, M., Domingo, J.L. and LLobet, J.M. Developmental toxicity evaluation of oral aluminum in rats: influence of citrate. *Neurotoxicology and Teratology* 13:323-328, 1991.

González, E.B., Parajón, J.P., Alonso, J.I.G. and Sanz-Medel, A. Analytical approaches to the problem of protein binding of aluminium in blood serum. *Journal for Analysis of Atomic Spectra* 4:175-179, 1989.

Gotow, T. and Tanaka, J. Phosphorylation of neurofilament H subunit as related to arrangement of neurofilaments. *Journal of Neuroscience Research* 37:691-713, 1994.

Gray, E.G. Axo-somatic and axo-dendritic synapses of the cerebral cortex. An electron microscope study. *Journal of Anatomy (London)* 93:420-433, 1959.

Greenwood, J.A., Troncoso, J.C., Costello, A.C. and Johnson, G.V.W. Phosphorylation modulates calpain-mediated proteolysis and calmodulin binding of the 200-kDa and 160-kDa neurofilament proteins. *Journal of Neurochemistry* 61:191-199, 1993.

Greger, J.L., Bula, E.N. and Gum, E.T. Mineral metabolism of rats fed moderate levels of various aluminum compounds for short periods of time. *Journal of Nutrition* 115(12):1708-1716, 1985.

Gruca, S. and Wisniewski, H.M. Cytochemical study on the effect of aluminum on neuronal golgi apparatus and lysosomes. *Acta Neuropathologica* 63:287-295, 1984.

Gruenberg, J. and Maxfield, F.R. Membrane transport in the endocytic pathway. *Current Opinion in Cell Biology* 7:552-563, 1995.

Guan, R.J., Hall, F.L. and Cohlberb, J.A. Proline-directed protein kinase ($p34^{cdc2}/p58^{cyclin\ A}$) phosphorylates bovine neurofilaments. *Journal of Neurochemistry* 58:1365-1371, 1992.

Hagestedt, T., Lichtenberg, B., Wille, H., Mandelkow, E.-M. and Mandelkow, E. Tau protein becomes long and stiff upon phosphorylation: correlation between paracrystalline structure and degree of phosphorylation. *The Journal of Cell Biology* 109:1643-1651, 1989.

Harden, T.K., Wolfe, B.B., Sporn, J.R., Poulos, B.K. and Molinoff, P.B. Effect of 6-hydroxydopamine on the development of the *beta* adrenergic receptor/adenylate cyclase system in rat cerebral cortex. *The Journal of Pharmacology and Experimental Therapeutics* 203(1):132-143, 1977.

Hewitt, C.D., Herman, M.M., Lopes, M.B.S., Savory, J. and Wills, M.R. Aluminium maltol-induced neurocytoskeletal changes in fetal rabbit midbrain in matrix culture. *Neuropathology and Applied Neurobiology* 17:47-60, 1991.

Hildebrand, C. and Waxman, S.G. Postnatal differentiation of the rat optic nerve fibers: Electron microscopic observations on the development of the nodes of Ranvier and axoglial relations. *Journal of Comparative Neurology* 224:25-37, 1984.

Hirokawa, N. Cross-linker system between neurofilaments, microtubules, and membranous organelles in frog axons revealed by the quick-freeze, deep-etching method. *Journal of Cell Biology* 94:129-142, 1982.

Hirokawa, N., Glicksman, M.A. and Willard, M.B. Organization of mammalian neurofilament polypeptides within the neuronal cytoskeleton. *The Journal of Cell Biology* 98:1523-1536, 1984.

Hisanaga, S. and Hirokawa, N. The effects of dephosphorylation on the structure of the projections of neurofilament. *The Journal of Neuroscience* 9(3):959-966, 1989.

Hisanaga, S. and Hirokawa, N. Dephosphorylation-induced interactions of neurofilaments with microtubules. *The Journal of Biological Chemistry* 265(35):21852-21858, 1990.

Hisanaga, S.-I. and Hirokawa, N. Structure of the peripheral domains of neurofilaments revealed by low angle rotary shadowing. *Journal of Molecular Biology* 202:297-305, 1988.

Hisanaga, S.-I., Ishiguro, K., Uchida, T., Okumura, E., Okano, T. and Kishimoto, T. Tau protein kinase II has a similar characteristic to cdc2 kinase for phosphorylating neurofilament proteins. *The Journal of Biological Chemistry* 268(20):15056-15060, 1993.

Hisanaga, S.-I., Kusubata, M., Okumura, E. and Kishimoto, T. Phosphorylation of neurofilament H subunit at the tail domain by CDC2 kinase dissociates the association of microtubules. *The Journal of Biological Chemistry* 266(32):21798-21803, 1991.

Hisanaga, S.-I., Matsuoka, Y., Nishizawa, K., Saito, T., Inagaki, M. and Hirokawa, N. Phosphorylation of native and reassembled neurofilaments composed of NF-L, MF-M, and NF-H by the catalytic subunit of cAMP-dependent protein kinase. *Molecular Biology of the Cell* 5:161-172, 1994.

Hoffman, P.N., Griffin, J.W., Gold, B.G. and Price, D.L. Slowing of neurofilament transport and the radial growth of developing nerve fibers. *The Journal of Neuroscience* 5(11):2920-2929, 1985.

Hoffman, P.N. and Lasek, R.J. The slow component of axonal transport: Identification of major structural polypeptides of the axon and their generality among mammalian neurons. *The Journal of Cell Biology* 66:351-366, 1975.

Hoffman, P.N., Lasek, R.J., Griffin, J.W. and Price, D.L. Slowing of the axonal transport of neurofilament proteins during development. *The Journal of Neuroscience* 3(8):1694-1700, 1983.

Hsieh, S.-T., Crawford, T.O. and Griffin, J.W. Neurofilament distribution and organization in the myelinated axons of the peripheral nervous system. *Brain Research* 642:316-326, 1994.

Hsieh, S.-T., Kidd, G.J., Crawford, T.O., et al. Regional modulation of neurofilament organization by myelination in normal axons. *The Journal of Neuroscience* 14(11):6392-6401, 1994.

Huang, J.-Y., Huang, C.-C., Lim, P.S., Wu, M.-S. and Leu, M.-L. Effect of body iron stores on serum aluminum level in hemodialysis patients. *Nephron* 61:158-162, 1992.

Hui, K.-S., Hui, M., Chiu, F.-C., et al. Separation and purification of individual neurofilament proteins by reverse-phase high-performance liquid chromatography. *Analytical Biochemistry* 153:230-234, 1986.

Ichimura, T. and Ellisman, M.H. Three-dimensional fine structure of cytoskeletal-membrane interactions at nodes of Ranvier. *Journal of Neurocytology* 20:667-681, 1991.

Itoh, T., Sobue, G., Ken, E., Mitsuma, T., Takahashi, A. and Trojanowski, J.Q. Phosphorylated high molecular weight neurofilament protein in the peripheral motor, sensory and sympathetic neuronal perikarya: system-dependent normal variations and changes in amyotrophic lateral sclerosis and multiple system atrophy. *Acta Neuropathologica* 83:240-245, 1992.

Jacobson, S. Sequence of myelinization in the brain of the albino rat A. Cerebral cortex, thalamus and related structures. *Journal of Comparative Neurology* 121:5-29, 1963.

Johnson, G.V.W. and Jope, R.S. Phosphorylation of rat brain cytoskeletal proteins in increased after orally administered aluminum. *Brain Research* 456:95-103, 1988.

Johnson, G.V.W., Watson, A.L.Jr, Lartius, R., Uemura, E. and Jope, R.S. Dietary aluminum selectively decreases MAP-2 in brains of developing and adult rats. *NeuroToxicology* 13:463-474, 1992.

Jones, S.M. and Williams, R.C.,Jr. Phosphate content of mammalian neurofilaments. *The Journal of Biological Chemistry* 257(17):9902-9905, 1982.

Julien, J.-P. and Mushynski, W.E. Multiple phosphorylation sites in mammalian neurofilament polypeptides. *The Journal of Biological Chemistry* 257(17):10467-10470, 1982.

Julien, J.-P., Ramachandran, K. and Grosveld, F. Cloning of a cDNA encoding the smallest neurofilament protein. *Biochimica et Biophysica Acta* 825:398-404, 1985.

Kageyama, G.H. and Robertson, R.T. Development of geniculocortical projections to visual cortex in rat: evidence for early ingrowth and synaptogenesis. *The Journal of Comparative Neurology* 335:123-148, 1993.

Karlsson, U. Observations on the postnatal development of neuronal structures in the lateral geniculate nucleus of the rat by electron microscopy. *Journal of Ultrastructure Research* 17:158-175, 1967.

Kasper, K.M., Larkman, A.U., Lübke, J. and Blakemore, C. Pyramidal neurons in layer 5 of the rat visual cortex. II. Development of electrophysiological properties. *The Journal of Comparative Neurology* 339:475-494, 1994.

King, G.A., DeBoni, U. and Crapper, D.R. Effect of aluminum upon conditioned avoidance response acquisition in the absence of neurofibrillary degeneration. *Pharmacology and Biochemistry of Behavior* 3:1003-1009, 1975.

Klatzo, I., Wisniewski, H.M. and Streicher, E. Experimental production of neurofibrillary degeneration. 1. Light microscopic observation. *Journal of Neuropathology and Experimental Neurology* 24:187-199, 1965.

Klein, G.L., Heyman, M.B., Lee, T.C., et al. Aluminum-associated hepatobiliary dysfunction in rats: relationships to dosage and duration of exposure. *Pediatric Research* 23(3):275-278, 1988.

Klosen, P. and van den Bosch de Aguilar, P. Spontaneous perikaryal neurofilament phosphorylation in the septofimbrial nucleus of the rat. *Neuroscience Letters* 139:108-113, 1992.

Klosen, P. and van den Bosch de Aguilar, P. Phosphorylated neurofilament epitopes in neuronal perikarya in the septum, mesencephalon and dorsal root ganglia of mammals and birds. *Journal of Neurocytology* 23:297-311, 1994.

Koenig, E. and Repasky, E. A regional analysis of alpha-spectrin in the isolated Mauthner neuron and in isolated axons of the goldfish and rabbit. *The Journal of Neuroscience* 5:705-714, 1985.

Kokko, J. Chronic Renal Failure. In: *Cecil Textbook of Medicine*, edited by Wyngaarden, J.B. and Smith, L.H. Philadelphia: W.B.Saunders Company, 1988, p. 563-573.

Kordeli, E., Davis, J., Trapp, B. and Bennett, V. An isoform of ankyrin is localized at nodes of Ranvier in myelinated axons of central and peripheral nerves. *Journal of Cell Biology* 110(4):1341-1352, 1990.

Kordeli, E., Lambert, S. and Bennett, V. $Ankyrin_G$ A new ankyrin gene with neural-specific isoforms localized at the axonal initial segment and node of Ranvier. *The Journal of Biological Chemistry* 270(5):2352-2359, 1995.

Laemmli, U.K. Cleavage of structural proteins during the assembly of the head of bacteriophage T4. *Nature* 227:680-685, 1970.

Landon, D.N. and Williams, P.L. Ultrastructure of the node of Ranvier. *Nature* 199:575-577, 1963.

Lang, E., Szendrei, G.I., Lee, V.M.-Y. and Otvos, L.,Jr. Spectroscopic evidence that monoclonal antibodies recognize the dominant conformation of medium-sized synthetic peptides. *Journal of Immunological Methods* 170:103-115, 1994.

Larcher, J.C., Boucher, D., Ginzburg, I., Gros, F. and Denoulet, P. Heterogeneity of tau proteins during mouse brain development and differentiation of cultured neurons. *Developmental Biology* 154:195-204, 1992.

Leary, J.J., Brigati, D.J. and Ward, D.C. Rapid and sensitive colorimetric method for visualizing biotin-labled DNA probes hybridized to DNA or RNA immobilized on nitrocellulose: Bio-blots. *Proceedings of the National Academy of Sciences* 80:4045-4049, 1983.

Lee, V.M.-Y., Carden, M.J., Schlaepfer, W.W. and Trojanowski, J.Q. Monoclonal antibodies distinguish several differentially phosphorylated states of the two largest rat neurofilament subunits (NF-H and NF-M) and demonstrate their existence in the normal nervous system of adult rats. *The Journal of Neuroscience* 7(11):3474-3488, 1987.

Lee, V.M.-Y., Otvos, L.,Jr., Schmidt, M.L. and Trojanowski, J.Q. Alzheimer disease tangles share immunological similarities with multiphosphorylation repeats in the two large neurofilament proteins. *Proceedings of the National Academy of Sciences* 85:7384-7388, 1988.

Lees, J.F., Shneidman, P.S., Skuntz, S.F., Carden, M.J. and Lazzarini, R.J. The structure and organization of the human heavy neurofilament subunit (NF-H) and the gene encoding it. *The EMBO Journal* 7(7):1947-1955, 1988.

Lew, J. and Wang, J.H. Neuronal cdc2-like kinase. *Trends in Biochemical Sciences* 20:33-37, 1995.

Lewis, S.E. and Nixon, R.A. Multiple phosphorylated variants of the high molecular mass subunit of neurofilaments in axons of retinal cell neurons: characterization and evidence for their differential association with stationary and moving neurofilaments. *Journal of Cell Biology* 107:2689-2702, 1988.

Lichtenberg-Kraag, B., Mandelkow, E.-M., Biernat, J., et al. Phosphorylation-dependent epitopes of neurofilament antibodies on tau protein and relationship with Alzheimer tau. *Proceedings of the National Academy of Sciences* 89:5384-5388, 1992.

Lieberburg, I., Spinner, N., Snyder, S., et al. Cloning of a cDNA encoding the rat high molecular weight neurofilament peptide (NF-H): Developmental and tissue expression in the rat, and mapping of its human homologue to chromosomes 1 and 22. *Proceedings of the National Academy of Sciences* 86:2463-2467, 1989.

Liem, R.K., Yen, S.-H., Salomon, G.D. and Shelanski, M.L. Intermediate filaments in nervous tissues. *Journal of Cell Biology* 79:637-645, 1978.

Liu, S.C., Derick, L.H. and Palek, J. Visualization of the hexagonal lattice in the erythrocyte membrane skeleton. *Journal of Cell Biology* 104:527-536, 1987.

Liu, Y., Dyck, R. and Cynader, M. The correlation between cortical neuron maturation and neurofilament phosphorylation: a developmental study of phosphorylated 200 kDa neurofilament protein in cat visual cortex. *Developmental Brain Research* 81:151-161, 1994.

Livingston, R.B., Pfenninger, K., Moor, H. and Akert, K. Specialized paranodal and interparanodal glial-axonal junctions in the peripheral and central nervous system: A freeze-etching study. *Brain Research* 58:1-24, 1973.

Lund, R.D. and Bunt, A.H. Prenatal development of central optic pathways in albino rats. *Journal of Comparative Neurology* 165:247-264, 1976.

Lund, R.D. and Lund, J.S. Development of synaptic patterns in the superior colliculus of the rat. *Brain Research* 42:1-20, 1972.

Malik, M., Sheikh, A.M., Fenko, M.D. and Wisniewski, H.M. Purification and degradation of purified neurofilament proteins by the brain calcium-activated proteases. *Life Sciences* 39:1335-1343, 1986.

Martin, R.B. The chemistry of aluminum as related to biology and medicine. *Clinical Chemistry* 32(10):1797-1806, 1986.

Mata, M., Fink, D.J., Ernst, S.A. and Siegel, G.J. Immunocytochemical demonstration of Na^+,K^+-ATPase in internodal axolemma of myelinated fibers of rat sciatic and optic nerves. *Journal of Neurochemistry* 57:184-192, 1991.

Mata, M., Kupina, N. and Fink, D.J. Phosphorylation-dependent neurofilament epitopes are reduced at the node of Ranvier. *Journal of Neurocytology* 21:199-210, 1992.

Miller, K., Shipman, M., Trowbridge, I.S. and Hopkins, C.R. Transferrin receptors promote the formation of clathrin lattices. *Cell* 65:621-632, 1991.

Miller, M.W. Maturation of rat visual cortex. III. Postnatal morphogenesis and synaptogenesis of local circuit neurons. *Developmental Brain Research* 25:271-285, 1986.

Miyasaka, H., Okabe, S., Ishiguro, K., Uchida, T. and Hirokawa, N. Interaction of the tail domain of high molecular weight subunits of neurofilaments with the COOH-terminal region of tubulin and its regulation by tau protein kinase II. *The Journal of Biological Chemistry* 268(30):22695-22702, 1993.

Morris, R.L. and Hollenbeck, P.J. The regulation of bidirectional mitochondrial transport is coordinated with axonal outgrowth. *Journal of Cell Science* 104:917-927, 1993.

Muller, G., Bernuzzi, V., Desor, D., Hutin, M.-F., Burnel, D. and Lehr, P.R. Developmental alterations in offspring of female rats orally intoxicated by aluminum lactate at different gestation periods. *Teratology* 42:253-261, 1990.

Muller, G., Burnel, D., Gery, A. and Lehr, P.R. Element variations in pregnant and nonpregnant rats orally intoxicated by aluminum lactate. *Biological Trace Element Research* 39:211-219, 1993.

Muller, G., Hutin, M.-F., Burnel, D. and Lehr, P.R. Aluminum transfer through milk in female rats intoxicated by aluminum chloride. *Biological Trace Element Research* 34:79-87, 1992.

Napolitano, E.W., Chin, S.S.M., Colman, D.R. and Liem, R.K.H. Complete amino acid sequence and *in vitro* expression of rat NF-M, the middle molecular weight neurofilament protein. *The Journal of Neuroscience* 7(8):2590-2599, 1987.

Nixon, R.A., Clarke, J.F., Logvinenko, K.B., Tan, M.K.H., Hoult, M. and Grynspan, F. Aluminum inhibits calpain-mediated proteolysis and induces human neurofilament proteins to form protease-resistant high molecular weight complexes. *Journal of Neurochemistry* 55:1950-1959, 1990.

Nixon, R.A., Lewis, S.E., Mercken, M. and Sihag, R.K. [^{32}P]orthophosphate and [^{35}S]methionine label separate pools of neurofilaments with markedly different axonal transport kinetics in mouse retinal ganglion cells in vivo. *Neurochemical Research* 19(11):1445-1453, 1994.

Nixon, R.A., Paskevich, P.A., Sihag, R.K. and Thayer, C.Y. Phosphorylation on carboxyl terminum domains of neurofilament proteins in retinal ganglion cell neurons in vivo: influences on regional neurofilament accumulation, interneurofilament spacing and axon caliber. *The Journal of Cell Biology* 126(4):1031-1046, 1994.

Nixon, R.A. and Sihag, R.K. Neurofilament phosphorylation: a new look at regulation and function. *Trends in Neurosciences* 14(11):501-506, 1991.

Nona, S.N., Trowell, S.C. and Cronly-Dillon, J.R. Postnatal development profiles of filamentous actin and of 200 kDa neurofilament polypeptide in the visual cortex of light- and dark-reared rats and their relationship to critical period plasticity. *FEBS Letters* 186(1):111-115, 1985.

Nukina, N., Kosik, K.S. and Selkoe, D.J. Recognition of Alzheimer paired helical filaments by monoclonal neurofilament antibodies is due to crossreaction with tau protein. *Proceedings of the National Academy of Sciences* 84:3415-3419, 1987.

Núñez, M.-T., Gaete, V., Watkins, J.A. and Glass, J. Mobilization of iron from endocytotic vesicles. *The Journal of Biological Chemistry* 265(12):6688-6692, 1990.

OOrschot, D.T. Are you using neuronal densities, synaptic densities or neurochemical densities as your definitive data? There is a better way to go. *Progress in Neurobiology* 44:233-247, 1994.

Pachter, J.S. and Liei R.K. The differential appearance of neurofilament triplet polypeptides in the developing rat optic nerve. *Developmental Biology* 103:200-210, 1984.

Palay, S.L. and Palade, G.E. The fine structure of neurons. *Journal of Biophysical and Biochemical Cytology* 1:69-88, 1955.

Palgi, J., Palm, K. and Saarma, M. *Rattus norvegicus NF68 gene for 68kDa neurofilament*, 1990. (UnPub)

Pant, H.C. Dephosphorylation of neurofilament proteins enhances their susceptibility to degradation by calpain. *Biochemical Journal* 256:665-668, 1988.

Papez, J.W. A proposed mechanism of emotion. *Archives of Neurology and Psychiatry* 38:725-743, 1937.

Paxinos, G. *Atlas of the Developing Rat Brain*, New York:Academic Press, 1990.

Paxinos, G. and Watson, C. *The Rat Brain in Stereotaxic Coordinates*, New York:Academic Press, Harcourt Brace Jovanovich, 1986. Ed. 2nd

Perry, M.J., Lawson, S.N. and Robertson, J. Neurofilament immunoreactivity in populations of rat primary afferent neurons: a quantitative study of phosphorylated and non-phosphorylated subunits. *Journal of Neurocytology* 20:746-758, 1991.

Peters, A., Palay, S.L. and Webster, H.deF. *The Fine Structure of the Nervous System: The Neurons and Supporting Cells*, Philadelphia:W.B. Saunders Company, 1976.

Peters, A. and Vaughn, J.E. Microtubules and filaments in the axons and astrocytes of early post-natal rat optic nerves. *Journal of Cell Biology* 32:113-119, 1967.

Phillips, L.L., Autilio-Gambetti, L. and Lasek, R.J. Bodian's silver method reveals molecular variation in the evolution of neurofilament proteins. *Brain Research* 278:219-223, 1983.

Pierson, K.B. and Evenson, M.A. 200 kD neurofilament protein binds Al, Cu and Zn. *Biochemical and Biophysical Research Communications* 152(2):598-604, 1988.

Poltorak, M. and Freed, W.J. Normal neuronal cell bodies of the nucleus tractus mesencephalici nerve trigemini react with antibodies against phosphorylated epitopes on neurofilaments. *Experimental Neurology* 97:735-738, 1987.

Poulos, B.K., Perazzolo, M., Lee, V.M.-Y., Rudelli, R., Wisniewski, H.M. and Soifer, D. Oral aluminum administration during pregnancy and lactation produces gastric and renal lesions in rat mothers and delay in CNS development of their pups. *Molecular and Chemical Neuropathology* 1995.(In Press)

Powell, J.J., Ainley, C.C., Evans, R. and Thompson, R.P.H. Intestinal perfusion of dietary levels of aluminium: association with the mucosa. *Gut* 35:1053-1057, 1994.

Price, R.L., Lasek, R.J. and Katz, M.J. Internal axonal cytoarchitecture is shaped locally by external compressive forces. *Brain Research* 530:205-214, 1990.

Price, R.L., Lasek, R.J. and Katz, M.J. Neurofilaments assume a less random architecture at nodes and in other regions of axonal compression. *Brain Research* 607:125-133, 1993.

Rabe, A., French, J.H., Sinha, B. and Fersko, R. Functional consequences of prenatal exposure to lead in immature rats. *NeuroToxicology* 6(1):43-54, 1985.

Reles, A. and Friede, R.L. Axonal cytoskeleton at the nodes of Ranvier. *Journal of Neurocytology* 20:450-458, 1991.

Ritchie, J.M., Black, J.A., Waxman, S.G. and Angelides, K.J. Sodium channels in the cytoplasm of Schwann cells. *Proceedings of the National Academy of Sciences* 87(23):9290-9294, 1990.

Roder, H.M. and Ingram, V.M. Two novel kinases phosphorylate tau and the KSP site of heavy neurofilament subunits in high stoichiometric ratios. *The Journal of Neuroscience* 11(11):3325-2243, 1991.

Rodriguez, M., Felsenfeld, A.J. and Llach, F. The evolution of osteomalacia in the rat with acute aluminum toxicity. *Journal of Bone and Mineral Research* 4(5):687-696, 1989.

Romeu, A., Alemany, M. and Arola, L. Net transfer of essential metals from mother to fetus in the second half of pregnancy in the rat. *Biology of the Neonate* 49:204-210, 1986.

Roskams, A.J. and Connor, J.R. Aluminum access to the brain: A role for transferrin and its receptor. *Proceedings of the National Academy of Sciences* 87:9024-9027, 1990.

Roy, A.K., Talukder, G. and Sharma, A. Similar effects in vivo of two aluminum salts on the liver, kidney, bone, and brain of Rattus norvegicus. *Bulletin of Environmental Contamination and Toxicology* 47:288-295, 1991.

Sawant, L.A., Hasgekar, N.N. and Vyasarayani, L.S. Developmental expression of neurofilament and glial filament proteins in rat cerebellum. *International Journal of Developmental Biology* 38:429-437, 1994.

Scherp, H.W. and Church, C.F. Neurotoxic action of aluminum salts. *Proceedings of the Society for Experimental Biology and Medicine* 36:851-853, 1937.

Schilling, K., Scherbaum, C. and Pilgrim, C. Developmental changes of neuron-specific enolase and neurofilament proteins in primary neural culture. *Histochemistry* 89:295-299, 1988.

Schlaepfer, W.W. Immunological and ultrastructural studies of neurofilaments isolated from rat peripheral nerve. *The Journal of Cell Biology* 74:226-240, 1977.

Schlaepfer, W.W. and Lynch, R.G. Immunofluorescence studies of neurofilaments in the rat and human peripheral and central nervous system. *The Journal of Cell Biology* 74:241-250, 1977.

Schlaepfer, W.W. and Micko, S. Chemical and structural changes of neurofilaments in transected rat sciatic nerve. *Journal of Cell Biology* 78:369-378, 1978.

Schmitt, F.O. and Geren, B.B. The fibrous structure of the nerve axon in relation to the localization of "neurotubules". *Journal of Experimental Medicine* 91:499-503, 1950.

Scholtz, C.L., Swash, M., Gray, A., Kogeorgos, J. and Marsh, F. Neurofibrillary neuronal degeneration in dialysis dementia: a feature of aluminum toxicity. *Clinical Neuropathology* 6(3):93-97, 1990.

Shaw, G. Neurofilament Proteins. In: *The Neuronal Cytoskeleton*, edited by Burgoyne, R.D. New York: Wiley-Liss,Inc., 1991, p. 185-214.

Shaw, G., Debus, E. and Weber, K. The immunological relatedness of neurofilament proteins of higher vertebrates. *European Journal of Cell Biology* 34:130-136, 1984.

Shaw, G., Osborn, M. and Weber, K. An immunofluorescence microscopical study of the neurofilament triplet proteins, vimentin, and glial fibrillary acidic protein within rat brain. *European Journal of Cell Biology* 26:68-82, 1981.

Shaw, G. and Weber, K. Differential expression of neurofilament triplet proteins in brain development. *Nature* 298:277-279, 1982.

Shaw, G. and Weber, K. The structure and development of the rat retina: An immunofluorescence microscopical study using antibodies specific for intermediate filament proteins. *European Journal of Cell Biology* 30:219-232, 1983.

Shea, T.B., Balikian, P. and Beermann, M.L. Aluminum inhibits neurofilament protein degradation by multiple cytoskeleton-associated proteases. *FEBS Letters* 307(2):195-198, 1992.

Shea, T.B. and Beermann, M.L. Multiple interactions of aluminum with neurofilament subunits: regulation by phosphate-dependent interactions between C-terminal extensions of the high and middle molecular weight subunits. *Journal of Neuroscience Research* 38:160-166, 1994.

Shea, T.B., Beermann, M.L. and Nixon, R.A. Appearance and localization of phosphorylated variants of the high molecular weight neurofilament protein in NB2a/d1 cytoskeletons during differentiation. *Developmental Brain Research* 50:142-146, 1989.

Shea, T.B., Beermann, M.L. and Nixon, R.A. Aluminum alters the electrophoretic properties of neurofilament proteins: role of phosphorylation state. *Journal of Neurochemistry* 58:542-547, 1992.

Sherwood, N.M. and Timeras, P.S. *A Stereotaxic Atlas of the Developing Rat Brain*, Los Angeles:University of California Press, 1970.

Shetty, A.K. and Turner, D.A. Non-phosphorylated neurofilament protein immunoreactivity in adult and developing rat hippocampus: specificity and application in grafting studies. *Brain Research* 676:293-306, 1995.

Shetty, K.T., Guru, V. and Guru, S.C. Phosphatase activity against neurofilament proteins from bovine spinal cord: effect of aluminium and neuropsychoactive drugs. *Neuroscience Letters* 137:83-86, 1992.

Shetty, K.T., Link, W.T. and Pant, H.C. cdc2-like kinase from rat spinal cord specifically phosphorylates KSPXK motifs in neurofilament proteins: Isolation and characterization. *Proceedings of the National Academy of Sciences* 90:6844-6848, 1993.

Siem, P. *Ueber die Wirkung des Aluminiums und des Berylliums auf den thierischen Organismus*, Dorpat:Schnakenburg's Buchdruckerei, 1886.

Singer, R.H., Lawrence, J.B. and Rashtchian, R.N. Toward a rapid and sensitive *in situ* hybridization methodology using isotopic and nonisotopic probes. In: *In Situ Hybridization: applications to neurobiology*, edited by Valentino, K.L., Eberwine, J.H. and Barchas, J.D. New York: Oxford University Press, 1987, p. 71-96.

Smitt, P.A.E.S., van der Loos, C., de Jong, J.M.B.V. and Troost, D. Tissue fixation methods alter the immunhistochemical demonstrability of neurofilament proteins, synpatophysin and glial fibrillary acidic protein in human cerebellum. *Acta Histochemica* 95:13-21, 1993.

Soifer, D., Iqbal, K., Czosnek, H., De Martini, J., Sturman, J.A. and Wisniewski, H.M. The loss of neuron-specific proteins during the course of wallerian degeneration of optic and sciatic nerve. *The Journal of Neuroscience* 1(5):461-470, 1981.

Soifer, D. and Mack, K. Genetic heterogeneity in the neurofilament protein, NF-H. In: *Regulation of Gene Expression in the Nervous System*, New York: Wiley-Liss,Inc., 1990, p. 219-231.

Soifer, D., Nicoletti, V., Cabane, K., Mack, K. and Poulos, B. Expression of the neurofilament protein NF-H in a non-neuronal cell line. *Journal of Neuroscience Research* 30:63-71, 1991.

Srinivasan, Y., Elmer, L., Davis, J., Bennett, V. and Angelides, K. Ankyrin and spectrin associate with voltage-dependent sodium channels in brain. *Nature* 333:177-180, 1988.

Steckhoven, J.H.S., Renkawek, K., Otte-Höller, I. and Stols, A. Exogenous aluminum accumulates in the lysosomes of cultured rat cortical neurons. *Neuroscience Letters* 119(1):71-74, 1990.

Stein, G., Laske, V., Müller, A., Bräunlich, H., Linss, W. and Fleck, C. Aluminium induced damage of the lysosomes in the liver, spleen and kidneys of rats. *Journal of Applied Toxicology* 7(4):253-258, 1987.

Steinert, P.M. and Liem, R.K.H. Intermediate filament dynamics. *Cell* 60:521-523, 1990.

Steinert, P.M. and Roop, D.R. Molecular and cellular biology of intermediate filaments. *Annual Review of Biochemistry* 57:593-625, 1988.

Sternberger, L.A. and Sternberger, N.H. Monoclonal antibodies distinguish phosphorylated and nonphosphorylated forms of neurofilaments in situ. *Proceedings of the National Academy of Sciences* 80:6126-6130, 1983.

Studier, F.W. Analysis of bacteriophage T7 early RNAs and proteins on gel slabs. *Journal of Molecular Biology* 79:237-248, 1973.

Terry, R.D. and Peña, C. Experimental production of neurofibrillary degeneration. 2 Electron microscopy, phosphatase histochemistry and electron probe analysis. *Journal of Neuropathology and Experimental Neurology* 24:200-210, 1965.

Tilney, F. Behavior in its relation to the development of the brain Part II. Correlation between the development of the brain and behavior in the albino rat from embryonic states to maturity. *Bulletin of the Neurological Institute of New York* 3(2):252-358, 1933.

Touam, M., Martinez, F., Lacour, B., et al. Aluminum-induced reversible microcytic anemia in chronic renal failure: Clinical and experimental studies. *Clinical Nephrology* 19:295-298, 1983.

Troncoso, J.C., March, J.L., Häner, M. and Aebi, U. Effect of aluminum and other multivalent cations on neurofilaments *in vitro*: an electron microscopic study. *Journal of Structural Biology* 103:2-12, 1990.

Troncoso, J.C., Sternberger, N.H., Sternberger, L.A., Hoffman, P.N. and Price, D.L. Immunocytochemical studies of neurofilament antigens in the neurofibrillary pathology induced by aluminum. *Brain Research* 364:295-300, 1986.

Troost, D., Smitt, P.A.E.S., de Jong, J.M.B.V. and Swaab, D.F. Neurofilament and glial alterations in the cerebral cortex in amyotrophic lateral sclerosis. *Acta Neuropathologica* 84:664-673, 1992.

Tsukita, S. and Ishikawa, H. The cytoskeleton in myelinated axons: serial section study. *Biomedical Research* 2:424-437, 1981.

van der Voet, G.B., van Ginkel, M.F. and de Wolff, F.A. Intestinal absorption of aluminum in rats: Stimulation by citric acid and inhibition by dinitrophenol. *Toxicology and Applied Pharmacology* 99:90-97, 1989.

Vaughn, J.E. An electron microscopic analysis of gliogenesis in rat optic nerves. *Zeitschrift für Zellforschung und Mikroskopische Anatomie* 94:293-324, 1969.

Vickers, J.C. and Costa, M. Neurofilament protein triplet immunoreactivity in the dorsal root ganglia of the guinea-pig. *Cell Tissue Research* 265:159-167, 1991.

Vitadello, M. and Denis-Donini, S. Expression of neurofilament proteins in granule cells of the cerebellum. *Brain Research* 509:47-54, 1990.

Vorbrodt, A.W., Lossinsky, A.S. and Wisniewski, H.M. Cytochemical localization of oubain-sensitive,K^+-dependent *p*-nitro-phenylphosphatase (transport ATPase) in the mouse central and peripheral nervous system. *Brain Research* 243:225-234, 1982.

Walker, V.R., Sutton, R.A.L., Meirav, O., et al. Tissue disposition of 26aluminum in rats measured by accelerator mass spectrometry. *Clinical Investigative Medicine* 17(5):420-425, 1994.

Waller, A. Experiments on the section of the glossopharyngeal and hypoglossal nerves of the frog, and observations of the alterations produced thereby in the structure of their primitive fibers. *Philosophical Transactions of the Royal Society of London (Biology)* 140:423-429, 1850.

Walton, K.D., Lieberman, D., Llinás, A. and Llinás, R.R. Identification of a critical period for motor development in neonatal rats. *Neuroscience* 51(4):763-767, 1992.

Ward, M.K., Feest, T.G., Ellis, H.A., et al. Osteomalacic dialysis osteodystrophy: Evidence for a water-borne aetiological agent probably aluminum. *The Lancet* 1:841-845, 1978.

Watson, D.F., Griffin, J.W., Fittro, K.P. and Hoffman, P.N. Phosphorylation-dependent immunoreactivity of neurofilaments increases during axonal maturation and β,β'-iminodipropionitrile intoxication. *Journal of Neurochemistry* 53:1818-1829, 1989.

Watson, J.B. *Animal education - an experimental study on the psychical development of the white rat, correlated with the growth of its nervous system*, Chicago:University of Chicago Press, 1903. pp. 5-122.

Waxman, S.G. and Ritchie, J.M. Molecular dissection of the myelinated axon. *Annals of Neurology* 33(2):121-136, 1993.

Weidman, T.A. and Kuwabara, T. Postnatal development of the rat retina. *Archives of Ophthalmology* 79:470-484, 1968.

Weihe, W.H. The laboratory rat. In: *The UFAW Handbook on the Care and Management of Laboratory Animals*, edited by Poole, T.B. Bath: Longman Scientific & Technical, 1987, p. 309-330.

Weiss, P. and Hiscoe, H.B. Experiments on the mechanism of nerve growth. *Journal of Experimental Zoology* 107(3):315-396, 1948.

Wilhelm, M., Jäger, D.E. and Ohnesorge, F.K. Aluminum toxicokinetics. *Pharmacology and Toxicology* 66:4-9, 1990.

Wilhelm, M., Zhang, X.-J., Hafner, D. and Ohnesorge, F.K. Single-dose toxicokinetics of aluminum in the rat. *Archives of Toxicology* 66:700-705, 1992.

Willard, M. and Simon, C. Antibody decoration of neurofilaments. *The Journal of Cell Biology* 89:198-205, 1981.

Willard, M. and Simon, C. Modulations of neurofilament axonal transport during the development of rabbit retinal ganglion cells. *Cell* 35:551-559, 1983.

Willard, M., Simon, C., Baitinger, C., Levine, J. and Skene, P. Association of an axonally transported polypeptide (H) with 100-Å filaments. Use of immunoaffinity electron microscope grids. *The Journal of Cell Biology* 85:587-596, 1980.

Williams, P.L. and Landon, D.N. Paranodal apparatus of peripheral nerve fibres of mammals. *Nature* 198:670-673, 1963.

Wilson, G.F. and Chiu, S.Y. Ion channels in axon and Schwann cell membranes at paranodes of mammalian myelinated fibers studied with patch clamp. *The Journal of Neuroscience* 10(10):3263-3274, 1990.

Wisniewski, H.M., Korthals, J.K., Kopeloff, L.M., Ferszt, R., Chusid, J.C. and Terry, R.D. Neurotoxicity of aluminum. *NeuroToxicology* 313-315, 1977.

Wuerker, R.B. and Palay, S.L. Neurofilaments and microtubules in anterior horn cells of the rat. *Tissue & Cell* 1(3):387-402, 1969.

Xu, Z.-S., Liu, W.-S. and Willard, M.B. Identification of six phosphorylation sites in the COOH-terminal tail region of the rat neurofilament protein M. *The Journal of Biological Chemistry* 267(7):4467-4471, 1992.

Yokel, R.A. Toxicity of aluminum exposure during lactation to the maternal and suckling rabbit. *Toxicology and Applied Pharmacology* 75:35-43, 1984.

Yokel, R.A. Aluminum produces age related behavioral toxicity in the rabbit. *Neurotoxicology and Teratology* 11:237-242, 1989.

Yokel, R.A., Lidums, V., McNamara, P.J. and Ungerstedt, U. Aluminum distribution into brain and liver of rats and rabbits following intravenous aluminum lactate or citrate: a microdialysis study. *Toxicology and Applied Pharmacology* 107:153-163, 1991.

Yokel, R.A. and McNamara, P.J. Influence of renal impairment, chemical form, and serum protein binding on intravenous and oral aluminum kinetics in the rabbit. *Toxicology and Applied Pharmacology* 95(1):32-43, 1988.

Yokel, R.A., Provan, S.D., Meyer, J.J. and Campbell, S.R. Aluminum intoxication and the victim of Alzheimer's disease: similarities and differences. *NeuroToxicology* 9(3):429-442, 1988.

Yokoyama, K., Mori, H. and Kurokawa, M. Astroglial filament and fibroblast intermediate filament proteins in cytoskeletal preparations from spinal cord and optic nerve. *FEBS Letters* 135:25-30, 1981.